Design of an LTE Antenna for Mobile Communication

BY

Yanal Shaher A. AlFaouri

A Thesis Presented to the

DEANSHIP OF GRADUATE STUDIES

KING FAHD UNIVERSITY OF PETROLEUM & MINERALS

DHAHRAN, SAUDI ARABIA

In Partial Fulfillment of the
Requirements for the Degree of

MASTER OF SCIENCE

In

ELECTRICAL ENGINEERING

June 2010

KING FAHD UNIVERSITY OF PETROLEUM & MINERALS
DHAHRAN 31261, SAUDI ARABIA

DEANSHIP OF GRADUATE STUDIES

This thesis, written by **Yanal Shaher AlFaouri** under the supervision of his thesis advisors and approved by his thesis committee, has been presented to and accepted by the Dean of Graduate Studies, in partial fulfillment of the requirements for the degree of

MASTER OF SCIENCE IN ELECTRICAL ENGINEERING

Thesis Committee

Dr. Sheikh Sharif Iqbal
(Chairman)

Dr. Mohammad S. Sharawi
(Co-Chairman)

Dr. Mahmoud M. Dawoud
(Member)

Dr. Husain M. Masoudi
(Member)

Dr. Samir H. Abdul-Jauwad
Department Chairman

Dr. Mohammad A. Alsunaidi
(Member)

Dr. Salam A. Zummo
Dean of Graduate Studies

14/6/10
Date

Dedicated to

My Parents

Whose Prayers and Perseverance led to this accomplishment

ACKNOWLEDGEMENTS

In the name of Allah, the Most Gracious and the Most Merciful

All praises and glory be to Allah (SWT) for blessing me with opportunities abound and showering upon me his mercy and guidance all through the life. I pray that He continues the same the rest of my life. And may his peace and blessings of Allah be upon Prophet Muhammad, a guidance and inspiration to our lives.

I would like to thank my supervisors, ***Dr. Sheikh Sharif Iqbal and Dr. Mohammad S. Sharawi*** for their guidance and expertise throughout this thesis. There were always there when I needed them, and even with their tight schedule, they have always found time for me. I am extremely grateful to them for their prompt replies and their numerous proofreads. I am also very grateful to my thesis committee members, Dr. Mahmoud M. Dawoud, Dr. Husain M. Masoudi and Dr. Mohammad A. Alsunaidi, for their care, cooperation and constructive advice.

Special thanks to my colleagues and friends for their encouragements and various help that they provided throughout my graduate studies at KFUPM. I would like to give my special thanks to my parents, brother and my sister for their support, patience and love. Without their encouragement, motivation and understanding it would have been impossible for me to complete this work.

Table of Contents

LIST OF TABLES

LIST OF FIGURES

THESIS ABSTRACT

Name: Yanal Shaher A. AlFaouri

Title: DESIGN OF an LTE Antenna for Mobile Communications

Major Field: ELECTRICAL ENGINEERING

Date of Degree: June 2010

The fourth generation of cellular networks will use a new high performance air interface for cellular mobile communication systems called Long Term Evolution (LTE). LTE is the evolution of Mobile Telecommunication System and will considerably increase the capacity and speed of mobile telephone networks by employing several enabling technologies including multiple-input-multiple-output (MIMO) systems.

In any wireless device, the performance of radio communications depends on the design of the efficient antennas. The objective of this research work is to design printed antennas suitable for use within LTE mobile terminals. To satisfy the antenna size of LTE devices, meander line technology is used to reduce the resonant length of the antenna. Design equations and professional software (HFSS) are used to design and optimize a 780 MHz single element meander line antenna (MLA) before designing a 2-element MLA for MIMO applications. Novel technique is used to reduce the mutual coupling of the MLA elements to an acceptable level (in

excess of -15 dB at 870 MHz). MATLAB codes are written to investigate the frequency dependency of the correlation coefficient of the MIMO antenna.

In house printed facility is used to fabricate the prototypes of the single and the two element meander line antennas. A Network analyser and an antenna measurement trainer are used to measure the S-parameters and radiation patterns of both the antenna. Due to inaccuracy in the fabrication process, a precent error of 13.09% and 19.17% are observed in the reflection responses of the single element and MIMO antenna.

THESIS ABSTRACT (ARABIC)

ملخص الرسالة

الاســــــــــم: ينال شاهر عبدالفتاح الفاعوري

عنوان الرسالة: تصميم هوائي متطور طويل الأمد لأجهزة الهواتف النقالة

التخصـــــــص: الهندسة الكهربائية

تاريـخ التخـرج: حزيران 2010

الجيل الرابع من الشبكات الخلوية سوف يستخدم تقنية جديدة عالية الأداء في الأوساط الهوائية لأنظمة الاتصالات الخلوية المتنقلة ويدعى التطور على المدى الطويل (التطور طويل الأمد). التطور طويل الأمد هو نسخة مطورة من نظام الاتصالات المتنقلة (UMTS) وسيركز بشكل كبير على زيادة قدرة وسرعة شبكات الهاتف النقال من خلال توظيف التقنيات الحديثة مثل المدخلات والمخرجات المتعددة (MIMO) الخ.

وأداء الاتصالات اللاسلكية في أي جهاز لاسلكي يعتمد على تصميم هوائيات ذات كفاءة. والهدف من هذا البحث هو العمل على تصميم نظام هوائي مطبوع مناسب للاستخدام في الأجهزة النقالة التي ستعمل على هذه التقنية الجديدة. ومن أجل الحصول على حجم الهوائي المناسب لهذا النظام الجديد سوف نقوم باستخدام نوع معين من الهوائيات المطبوعة لتقليل حجم الهوائي ليكون ملائما للاستخدام مع هذه التقنية. سيتم الاستعانة بالقوانين وأحد برامج المحاكاة لتحسين تصميم الهوائي للعمل على التردد المطلوب وهو 780 ميجاهيرتز والتأكد من كفائته قبل البدء بتصميم نظام ثنائي الهوائي لأغراض المدخلات والمخرجات المتعددة. وسوف يتم استخدام الطرق الشائعة من أجل تقليل التأثير بين هذين الهوائيين لأقل من -15 ديسيبل. وسيتم كتابة برنامج لدراسة تأثر وعلاقة هذا العامل بالتردد. وسيتم بناء كل من الهوائي المفرد والهوائيان من خلال الاستفادة

من الأجهزة الموجودة في الجامعة واختبارها باستخدام محلل شبكة النواقل وقياس نظام الانبعاث من خلال أدوات مخصصة للتعامل مع هذه الهوائيات. وبسبب عدم الدقة في بناء هذه الهوائيات فقد لوحظ وجود نسبة خطأ بين الواقع و المصمم باستخدام البرنامج تقدر ب 13.09% في حالة الهوائي الأحادي و 19.17% في حالة الهوائيان الثنائيان.

CHAPTER 1

INTRODUCTION

1.1 Review of Mobile Communication Standard

The mobile communication technology has experienced a significant growth from first-generation (1G) analogue voice-only communication to second-generation (2G) digital voice communication. These 2G technologies became popular worldwide including GSM (Global System for Mobile Communications) in Europe, IS-136 (also known as US-TDMA and Digital AMPS) in the U.S., and PDC (Personal Digital Communications) in Japan. Currently, the third generation (3G) mobile communication technology not only provides digital voice services, also provides video telephony, internet access and video/music download services. Further, the forthcoming fourth-generation (4G) mobile telephone technology aims to provide on-demand high quality video and audio services. [**1**]

This section will address the evolution of mobile communication standards, from its first generation, 1G, to the latest 3G and give a look of on the future of 4G.

1.1.1 Introduction

New mobile generations do not pretend to improve the voice communication experience but try to give the user access to a new global communication reality. The aim is to reach communication ubiquity (every time, everywhere) and to provide users with a new set of services. The growth of the number of mobile subscribers over the last years led to a saturation of voice-oriented wireless telephony. From 214 million subscribers in 1997 to 1162 million in 2002 [**2**], it is predicted that by 2010 there will be 1700 million subscribers worldwide [**3**]. It is now time to explore new demands and to find new ways to extend the mobile concept. The first steps have already been taken by the 2.5G, which gave users access to data networks (e.g. Internet access and MMS - Multimedia Message Service). However, users and applications demanded more communication data rates. In response to this demand a new generation with new standards has been developed - 3G.

In the last years, benefiting from 3G constant delays, many new mobile technologies were deployed with great success e.g. Wi-Fi (Wireless Fidelity). Now, all this new technologies (e.g. UMTS, Wi-Fi, Bluetooth) claim for a convergence that can only be achieved by a new mobile generation. This new mobile generation to be deployed must work with many mobile technologies while being transparent to the final user.

1.1.2 The first mobile generations (1G to 2.5G)

In 1G, a narrow band analogue wireless network is used, with this we can have the voice calls and can send text messages. These services are provided with circuit switching. The 2G narrow band wireless network also uses the circuit switching model but provides more voice clarity as compared to 1G.

Both 1G and 2G deals with voice calls and sending messages i.e. SMS (Short Message Service). The latest technologies such as GPRS (General Packet Radio Service), is not available in these generations. But the greatest disadvantage to 1G is that it can be used only within a particular nation, where in the case of 2G, the roaming facility is a semi-global one.

In between 2G and 3G there is another generation called 2.5G. Initially, this mid generation was introduced mainly for involving latest bandwidth technology with addition to the existing 2G generation. To be frank but this had not brought out any new evolution and so had not clicked to as much to that extend.

1.1.3 Third mobile generation networks (3G)

To overcome the limitations of 2G and 2.5G, 3G was introduced. In 3G a Wide Band Wireless Network is utilized with which the clarity increases and gives the perfection as like that of a real conversation. The data are sent through a technology called Packet Switching .Voice calls are interpreted through Circuit Switching.

With the help of 3G, we can access many new services too. One such service is global roaming. In 3G we can also have several entertainments services such as Fast Communication, Internet, Mobile T.V, Video Conferencing, Video Calls, Multi Media Messaging Service (MMS), 3D gaming, Multi-Gaming etc.

Table 1 shows some specifications for some of the standards used in the first three generations such as data rate, bandwidth and bands.

Table 1: Transport Technologies [**4**], [**5**]

Transport Technology	Description	Data Rate	Band-width	Bands	Pros/cons
TDMA	Time Division Multiple Access is 2G technology	Up to 9.6kbps	-	850 MHz and 1.9 GHz	• Low battery consumption • Transmission is one-way • Speed pales next to 3G technologies
GSM	Global System for Mobile Communications is a 2G digital cell phone technology	Up to 9.6kbps	0.2 MHz	900 MHz or 1800 MHz	• Popular around the globe. • Worldwide roaming in about 180 countries. • GSM's short messaging service (GSM-SMS) only transmits one-way. • Can only deliver messages up to 160 characters long
GPRS	General Packet Radio Service is a 2.5G network that supports data packets	Up to 115kbps	0.2 MHz	900 MHz or 1800 MHz	• Messages not limited to 160 characters, like GSM SMS

EDGE	Enhanced Data GSM Environment is a 3G digital network	Up to 384kbps	0.2 MHz	900 MHz or 1800 MHz	• May be temporary solution for operators • unable to get W-CDMA licenses
CDMA	Code Division Multiple Access is a 2G technology developed by Qualcomm that is transitioning to 3G	Up to 115kbps	1.23 MHz	800-MHz and 1.9-GHz	• Although behind TDMA in number of subscribers, this fast-growing technology has more capacity than TDMA
W-CDMA (UMTS)	Wideband CDMA (also known as Universal Mobile Telecommunications System-UMTS) is 3G technology. On Nov. 6, 2002, NTT DoCoMo, Ericsson, Nokia, and Siemens agreed on licensing arrangements for W-CDMA, which should set a benchmark for royalty rates	Up to 2Mbps initially. Up to 10Mbps by 2005, according to designers	1.25 MHz	850, 900, 1700, 1900, 2100, MHz	• Likely to be dominant outside the United States. • Good for roaming globally • Commitments from U.S. operators are currently lacking, though AT&T Wireless performed UMTS tests in 2002. • Primarily to be implemented in Asia-Pacific region
CDMA2000 1xRTT	A 3G technology, 1xRTT is the first phase of CDMA2000	Up to 144kbps	1.25 MHz	850, 900, 1700, 1900, 2100, MHz	• Proponents say migration from TDMA is simpler with CDMA2000 than W-CDMA • Spectrum use is more efficient • W-CDMA will likely be more common in Europe

CDMA 2000 1xEV-DO	Delivers data on a separate channel	Up to 2.4Mbps	1.25 MHz	850, 900, 1700, 1900, 2100, MHz	• (see CDMA2000 1xRTT above)
CDMA 2000 1xEV-DV	Integrates voice and data on the same channel	Up to 2.4Mbps	1.25, 3.75 MHz		• (see CDMA2000 1xRTT above)

1.1.4 Future mobile generation networks (4G)

The objective of 3G was to develop a new protocol and new technologies to further enhance the mobile experience. In contrast, the new 4G framework to be established will try to accomplish new levels of user experience and multi-service capacity by also integrating all the mobile technologies that exist (e.g. GSM - Global System for Mobile Communications, GPRS, IMT-2000 - International Mobile Communications, Wi-Fi, and Bluetooth). [**6**]

In addition to the services of 3G, 4 G will have some additional features such as Multi-Media Newspapers and T.V programs with the clarity as to that of an ordinary T.V. In addition, we can send Data much faster than that of the previous generations. Due to some key enabling technologies 4G systems are given the standard name Long Term Evolution (LTE)

1.2 Long Term Evolution (LTE)

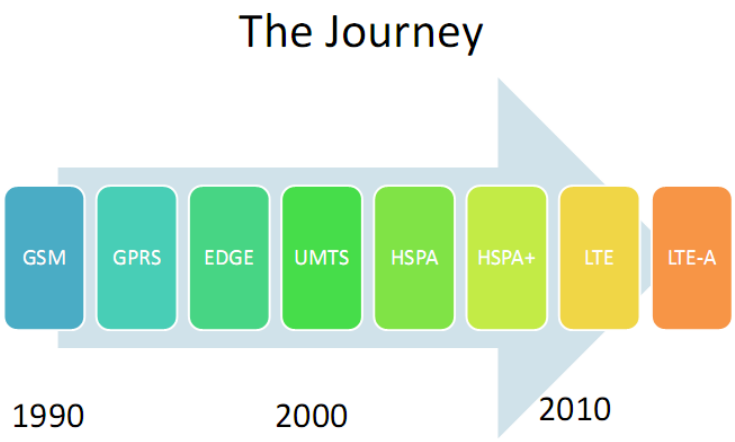

Figure 1: The Evolution of Wireless Communication Standards [7]

Figure 1 shows the evolution of wireless communication standards from 1990 to 2010. Mobile networks continue to develop at an exciting pace. In ten years, mobile networks may well support services beyond that of today's multi-megabit fixed connections, while the amount of data traffic on mobile networks could surpass that of today's broadband connections in the next decade. As consumer demand grows for ever-richer services and connected lifestyles, mobile networks will evolve, and the mobile industry is already hard at work defining the technical solution that will allow mobile networks to meet the growing demand for wireless broadband services. The radio access technologies enabling these networks have been given the name Long Term Evolution of Universal Terrestrial Radio Access Network – or LTE for short.

LTE will be used for mobile, fixed and portable wireless broadband access, and will offer a number of benefits to operators, aimed at increasing capacity, reducing

network complexity and thus lowering deployment and operational costs. It will enable operators to meet the growing demand for mobile data solutions, making it possible for richer services to be delivered to consumers more cost effectively. [**8**]

1.2.1 What is LTE?

LTE (Long Term Evolution) is the trademarked project name of a high performance air interface for cellular mobile telephony. It is a project of the 3rd Generation Partnership Project (3GPP), operating under a named trademarked by one of the associations within the partnership, the European Telecommunications Standards Institute

The recent increase of mobile data usage and emergence of new applications such as mobile TV, MMOG (Multimedia Online Gaming) and streaming contents have motivated the use of (LTE) standards. LTE is the latest in the mobile network technology that ensures competitive edge over its existing standards: GSM/EDGE and UMTS/HSxPA [**9**], where HSPA means High Speed Packet Access is a collection of two mobile telephony protocols, High Speed Downlink Packet Access (HSDPA) and High Speed Uplink Packet Access (HSUPA), that extends and improves the performance of existing WCDMA protocols.

LTE, whose radio access is called "Evolved UMTS Terrestrial Radio Access Network (E-UTRAN)", is expected to substantially improve end-user throughputs, sector capacity and reduce user plane latency, bringing significantly improved user experience

with full mobility. With the emergence of Internet Protocol (IP) for carrying all types of traffic, LTE is scheduled to provide support for IP-based traffic with end-to-end Quality of service (QoS). Voice traffic will be supported mainly as Voice over IP (VoIP) enabling better integration with other multimedia services. Initial deployments of LTE are expected by 2010 and commercial availability on a larger scale are expected 1-2 years later [**9**].

LTE uses Evolved Packet Core (EPC) network architecture to support the E-UTRAN which reduces the number of network elements, simplifies functionality, improves redundancy, but most importantly allows for connections and hand-over to other fixed line and wireless access technologies in a flawless manner. The aggressive performance of LTE rely on physical layer technologies, such as, Orthogonal Frequency Division Multiplexing (OFDM), Multiple-Input Multiple-Output (MIMO) systems and Smart Antennas to achieve these targets. The main objective of LTE is to minimize the system and user-equipment complexities for high data throughput and reduced latency.

1.2.2 LTE Bands

There are a large number of allocations or radio spectrum that has been reserved for FDD (Frequency Division Duplex) LTE use. Table 2 shows the 14 E-UTRAN band used by the LTE standard for each downlink and uplink for both UE (User Equipment) and eNB (evolved NodeB) with the minimum and maximum frequencies for downlink and uplink for every band. Also it shows more than 18000 channels divided to these bands.

Table 2: LTE FDD Frequency Bands and Channel Numbers [**5**]

E-UTRAN Band	Downlink (DL) (UE Receive, eNB Transmit)		Channel Numbers (N_{DL})	Uplink (DL) (UE Transmit, eNB Receive)		Channel Numbers (N_{UL})
	f_{DL_Low} (MHZ)	f_{DL_High} (MHZ)		F_{UL_Low} (MHZ)	F_{UL_High} (MHZ)	
1	2110	2170	0-599	1920	1980	13000-13599
2	1930	1990	600-1199	1850	1910	13600-14199
3	1805	1880	1200-1949	1710	1785	14200-14949
4	2110	2155	1950-2399	1710	1755	14950-15399
5	869	894	2400-2649	824	849	15400-15649
6	875	885	2650-2749	830	840	15650-15749
7	2620	2690	2750-3449	2500	2570	15750-16449
8	925	960	3450-3799	880	915	16450-16799
9	1844.9	1879.9	3800-4149	1749.9	1784.9	16800-17149
10	2110	2170	4150-4749	1710	1770	17150-17749
11	1475.9	1500.9	4750-4999	1427.9	1452.9	17750-17999
12	728	746	5000-5179	698	716	18000-18179
13	746	756	5180-5279	777	787	18180-18279
14	758	768	5280-5379	788	798	18280-18379

1.2.4 Performance Goals for LTE

E-UTRA is expected to support different types of services including web browsing, FTP (File Transfer Protocol), video streaming, VoIP (Voice over Internet Protocol), online gaming, real time video, push-to-talk and push-to-view. Therefore, LTE is being designed to be a high data rate and low latency system as indicated by the key performance criteria shown in Table 3. The bandwidth capability of a UE is expected to be up to 20 MHz for both transmission and reception. The service provider can however deploy cells with any of the bandwidths listed in Table 3. This gives flexibility to service providers to tailor their offering dependent on the amount of available spectrum or the ability to start with limited spectrum for lower upfront cost and grow the spectrum for extra capacity.

Table 3: LTE Performance Requirements [**9**]

Metric	Requirements
Peak Data Rate	DL: 100Mbps UL: 50Mbps (For 20MHz Spectrum)
Mobility Support	Up to 500Kmph but optimized for low speeds from 0-15kmph
Control Plane Latency (Transition Time to Active State)	<100ms (For Idle to Active)
User Plane Latency	<5ms

Control Plane Capacity	>200 users per cell (For 5MHz spectrum)
Coverage (Cell Size)	5-100Km with slight degradation after 30Km
Spectrum Flexibility	1.25, 2.5, 5, 10, 15 and 20

LTE has instantaneous downlink peak data rate (DL) of 100 Mbps within a 20 MHz downlink spectrum allocation (5 bps/Hz) and instantaneous uplink peak data rate (UL) of 50 Mb/s (2.5 bps/Hz) within a 20 MHz uplink spectrum allocation**.** The Control plane latency has a transition time of less than 100 ms from a camped state to an active state and less than 50 ms from a dormant state and an active state. The control plane capacity is at least 200 users per cell and is supported in the active state for spectrum allocations up to 5 MHz. The user plane latency is of less than 5ms in unloading condition (i.e. single user with single data stream) for small IP packet.

The downlink average user throughput per MHz for 4G networks is 3 to 4 times larger and the uplink average user throughput per MHz is 2 to 3 times larger as compared to 3G networks**.** The target for spectrum efficiency (bits/sec/Hz/site) of downlink in a loaded network is 3 to 4 times larger and for uplink it is 2 to 3 times larger. E-UTRAN should be optimized for low mobile speed from 0 to 15 km/h**.** The higher mobile speed between 15 and 120 km/h should be supported with high performance and mobility across the cellular network shall be maintained at speeds from 120 km/h to 350 km/h (or even up to 500 km/h depending on the frequency band).Throughput, spectrum efficiency and mobility targets above should be met for 5 km cells, and with a slight degradation for 30 km cells and the cells in a range up to 100 km should not be precluded.

Co-existence in the same geographical area and co-location with GERAN/UTRAN on adjacent channels is also accounted for. GERAN is an abbreviation for GSMEDGE Radio Access Network. The standards for GERAN are maintained by the 3GPP (Third Generation Partnership Project). GERAN is a key part of GSM, and also of combined UMTS/GSM networks. GERAN is the radio part of GSM/EDGE together with the network that joins the base stations and the base station controllers. The network represents the core of a GSM network, through which phone calls and packet data are routed from and to the PSTN and Internet to and from subscriber handsets. A mobile phone operator's network comprises one or more GERANs, coupled with UTRANs in the case of a UMTS/GSM network.

A GERAN network without EDGE is a GRAN, but is otherwise identical in concept.
A GERAN network without GSM is an ERAN

1.2.5 Enabling Technologies in LTE

A) MIMO

The Shannon-Hartley capacity theorem predicts that the capacity of the error free channel for a single-input-single-output (SISO) system is given by:

$$C = B\log_2(1+SNR) \qquad (1.1)$$

where, C is the capacity in bits/second, B is the channel bandwidth and SNR is the linear signal-to-noise ratio value. In a MIMO system, the cross-coupling between the signals

from the transmit antennas to the receive antennas introduces a path dependency through the radio channel. This will impact the overall capacity of the system as [**10**]:

$$C = B\log_2\left|\mathbf{I} + \frac{\mathbf{R}}{k}SNR\right| \qquad (1.2)$$

where, C is the channel capacity in bit/second, **I** is the identity matrix, **R** is the channel and antenna correlation matrix, k is rank of **R** (i.e. number of transmit antennas). Equation (1.2) can also be written as

$$C \approx B\log_2\left(1 + M_T * N_R * SNR\right) \qquad (1.3)$$

where, M_T is the number of transmit antennas, N_R is the number of receive antennas.

For diversity and MIMO applications, the correlation between signals received by the involved antennas at the same side of a wireless link is an important figure of merit of the whole system. Usually, the envelope correlation is presented to evaluate the diversity capabilities of a multi-antenna system [**11**]. It can be measured directly in a representative scattering environment, or calculated from the full-sphere radiation patterns. Both methods require special measurement equipment and are time-consuming. [**12**]

For isotropic signal environments the received signal correlation can be found from a simpler and faster method than the one previously described. The method derives the correlation coefficient from the S-parameters of the antennas, i.e., the port reflection coefficients S_{11} and S_{22} of the two antennas, and the coupling S_{21}=S_{12}. Several publications present the relation between the S-parameters and the correlation coefficient

[**13**] [**14**] [**15**]. What are missing in these relations are the radiation efficiencies of the two antennas.

This parameter (Correlation Coefficient) should be preferably computed from 3D radiation patterns but this method requires a lot of work [**13**] and may suffer from errors if no sufficient pattern cuts are taken into account in the computation.

The Total radiated powers for the two antennas can be expressed as;

$$P_{rad\,1} = \left(1 - |S_{11}|^2 - |S_{21}|^2\right)\eta_1 \qquad (1.4)$$

$$P_{rad\,2} = \left(1 - |S_{22}|^2 - |S_{12}|^2\right)\eta_2 \qquad (1.5)$$

from which the definition of radiation efficiencies η_1 and η_2 are clear, and the internal losses for the two antennas are given by

$$P_{loss\,1} = \left(1 - |S_{11}|^2 - |S_{21}|^2\right)(1 - \eta_1) \qquad (1.6)$$

$$P_{loss\,2} = \left(1 - |S_{22}|^2 - |S_{12}|^2\right)(1 - \eta_2) \qquad (1.7)$$

The relation for the correlation coefficient is derived on the basis of orthogonality between two signals of separate independent sources. This is the fundamental principle and is described in most microwave books as a requirement of zero correlation between two columns in an S-matrix [**16**]. Generalized S-parameters should be used when ports have different impedances [**17**], which means that S-parameters are adjusted so that each signal's amplitude is proportional to the square root of the corresponding power. The requirement of zero correlation is valid for lossless S-matrices, but internal losses are easily incorporated by treating the losses as additional ports where power is terminated.

Generally, the S-matrix is an applicable tool to model the signal flow of any device. To derive a general relation for orthogonality, assume that the amplitudes of the complex signals from two sources are denoted by E_1 and E_2, respectively, both being functions over volume. These functions E_1 and E_2 are vectors of S-parameters according to eq. 1.8

$$E_k = \left[S_{1k} \quad ... \quad S_{Nk} \right]^T \qquad (1.8)$$

where N is the number of ports. The impedance function Z is also introduced for the purpose of making E_1 and E_2 correspond to generalize S-parameters. The orthogonality between the signals is then simply

$$ort(1,2) = \frac{1}{P_{tot}} \int_{Ptot} \frac{E_1 E_2^*}{Z} dP \qquad (1.9)$$

where P_{tot} is the total power. The amplitudes E_1 and E_2 should be normalized so that dividing by P_{tot} results in an orthogonality with a magnitude between zero and unity. Using the analogy in (1.8) in conjunction with the requirement of orthogonality between two columns of the S-matrix renders the conclusion that ort(1,2) should be zero.

Now consider a pair of antennas, and let E_1 and E_2 be the signals scattered at the ports and over the sphere. The total S-matrix can be divided into one S-matrix for the antenna ports and one for the radiation functions, after which orthogonality is applied to the sum of the two [**13**]. A third S-matrix is introduced to account for the losses, and orthogonality then applies to the sum of all three. With the antennas described by their S-parameters and relative powers according to (1.4)–(1.7), the requirement for orthogonality takes the form

$$S_{11}^{*}S_{12}+S_{21}^{*}S_{22}+\rho_{rec}\sqrt{P_{rad1}P_{rad2}}+\rho_{loss}\sqrt{P_{loss1}P_{loss2}}=0 \qquad (1.10)$$

where ρ_{rec} and ρ_{loss} are the normalized complex correlation coefficients of the radiation patterns and the internal losses, respectively. Multiplying by the square root of the powers in the two last terms in (1.10) is done for the purpose of making the terms correspond to generalize S-parameters. The first two terms also need such normalization, but because all powers (P_{rad} and P_{loss}) are relative to these powers, they are in effect unity.

Substituting (1.4)–(1.7) into (1.10) gives the expression relating correlation coefficients to S-parameters and radiation efficiencies

$$\frac{S_{11}^{*}S_{12}+S_{21}^{*}S_{22}}{\sqrt{\left(1-|S_{11}|^2-|S_{21}|^2\right)\left(1-|S_{22}|^2-|S_{12}|^2\right)}}+\rho_{rec}\sqrt{\eta_1\eta_2}+\rho_{loss}\sqrt{(1-\eta_1)(1-\eta_2)}=0 \qquad (1.11)$$

Since the expression on the left-hand side in (1.11) is zero, one unknown term can be calculated if the other terms are known. The principle of calculating received signal correlation from S-parameters is to measure the first term and take the second term to be the negative of this value. The last term in (1.11) is then omitted or assumed to be zero.

Assuming that the antennas will operate in a uniform multi-path environment, an alternative consists in computing this parameter from its scattering parameters definition [**13**]. The envelope correlation of two antennas is given by Eq. 1.12

$$\left|\rho_{12}\right|_{max}=\frac{-S_{11}^{*}S_{12}-S_{21}^{*}S_{22}}{\sqrt{\left(1-|S_{11}|^2-|S_{21}|^2\right)\left(1-|S_{22}|^2-|S_{12}|^2\right)\eta_1\eta_2}}+\sqrt{\left(\frac{1}{\eta_1}-1\right)\left(\frac{1}{\eta_2}-1\right)} \qquad (1.12)$$

Where, $|\rho_{12}|_{max}$: is the upper bound of the signal correlation coefficient between antenna 1 and antenna 2, $S_{11}$is is the reflection coefficient of the antenna number 1, S_{22} is the reflection coefficient of the antenna number 2, S_{21}, S_{12}: are the transmission parameters between the two antennas, $(.)^*$ means the conjugate complex value, η_1, η_2 are the radiation efficiencies of antennas 1 and 2, respectively.

Figure 2 shows a diagram that describes a MIMO system with M_T transmit antennas and N_R receives antennas.

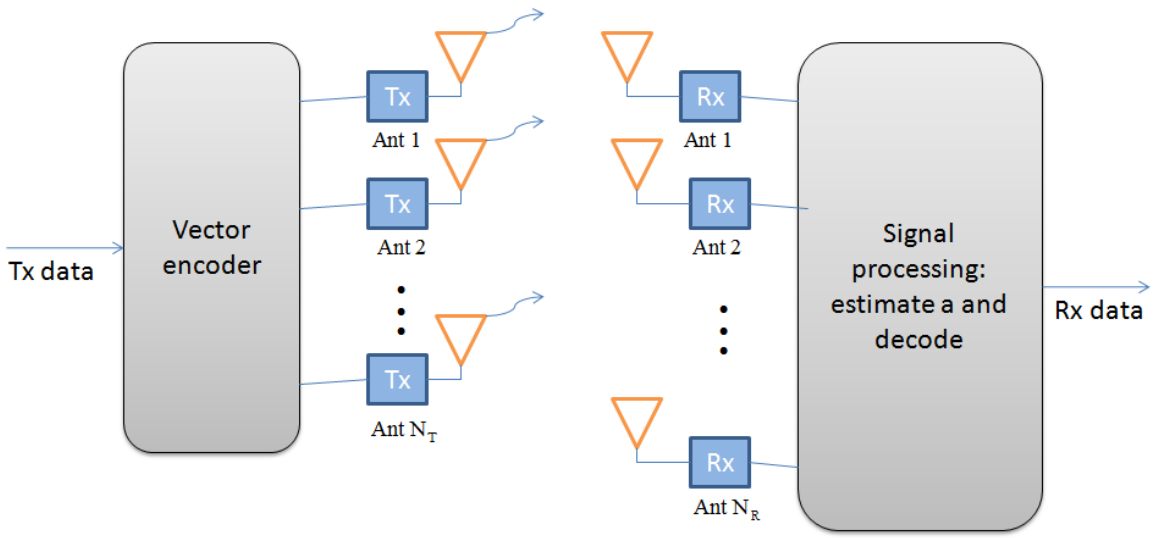

Figure 2: MIMO System Diagram

B) Orthogonal Frequency Division Multiplexing (OFDM)

One of the key elements of LTE is the use of OFDM (Orthogonal Frequency Division Multiplex) as the signal bearer and the associated access schemes. OFDM has many advantages including its robustness to multipath fading and interference. In

addition to this, even though, it may appear to be a particularly complicated form of modulation, it lends itself to digital signal processing techniques.

One of the key parameters associated with the use of OFDM within LTE is the choice of bandwidth. The available bandwidth influences a variety of decisions including the number of carriers that can be accommodated in the OFDM signal and in turn this influences elements including the symbol length and so forth.

LTE defines a number of channel bandwidths. Obviously the greater the bandwidth, the greater the channel capacity.

1.2.6 LTE Antennas

Small and conformal antennas are fundamental to the development of mobile communication devices. Printed antennas are always used in mobile terminals, but for 780 MHz it will be a challenge using conventional ways. Recently, meander line technology is adopted to design small but wideband antennas, were size of the radiating element at a given frequency is reduced by a factor that is proportional to the number of turns. Due to the small size of printed meander line antenna (MLA), they are directly embedded within the mobile handsets. In addition, they feature an improvement in efficiency, resulting in longer battery life than other handsets currently available on the market today. Furthermore, MLA technology allows engineers to design ultra-broadband antennas capable of operating at multiple frequencies and in a variety of modes.

Some of the LTE bands associated with its adopted countries are shown in Figure 3.

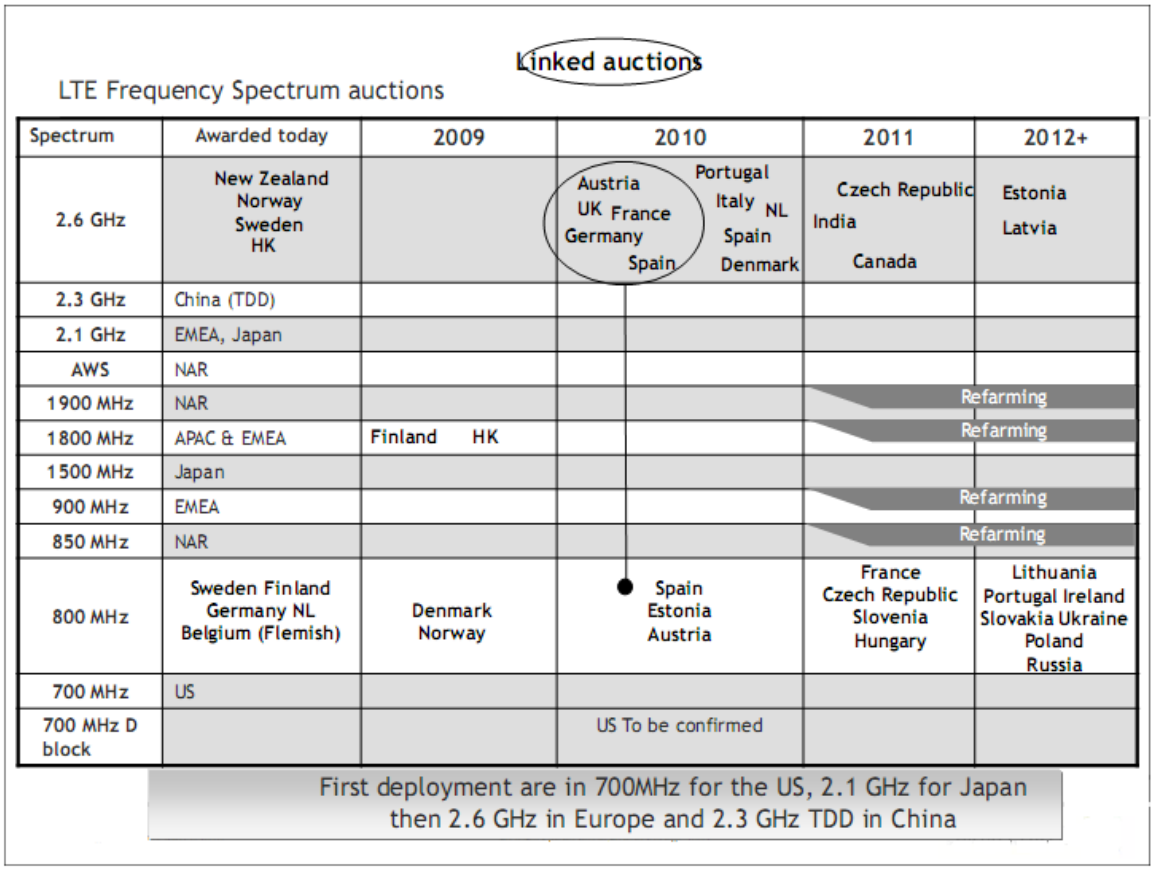

Figure 3: LTE Frequency Spectrum Auctions [7]

The United States 700 MHz wireless spectrum auction, officially known as Auction 73, was started by the Federal Communications Commission (FCC) on January 24, 2008 for the rights to use the 700 MHz frequency band in the United States. The details of process were the subject of debate among several telecommunications companies, including Verizon Wireless and AT&T.

The last transmissions by the incumbent television broadcasters using this spectrum ceased on June 12, 2009 except for LPTV (Low Power TV) stations, which can stay on the air with an analog signal until the winning bidders start operations. Full power TV stations ceased analog broadcasting on June 12, 2009.

The 700 MHz spectrum was previously used for analog television broadcasting. The FCC has ruled that the switch to digital television has made these frequencies no longer necessary for broadcasters, due to the improved spectral efficiency of digital broadcasts. Thus, all broadcasters will be required to move to newer channels as part of the digital TV transition. Some of the 700 MHz spectrum was already in some areas are already being used for broadcasting and Internet access. For example Qualcomm MediaFLO in 2007 started using Channel 55 for broadcasting TV to cell phones in New York City, San Diego and elsewhere. [**18**]

1.3 Thesis Motivation

In the recent years, there has been rapid growth in wireless communication. With the increasing number of users and limited bandwidth available, operators are trying hard to optimize the network for larger capacity and improved quality coverage. This has led to the field of antenna engineering to constantly evolve and accommodate the need for wideband, low-cost, miniaturized and easily integrated antennas [**19**].

Since LTE will be the technology used for the next generation of mobile communication which will be implemented by the end of this year and will be commercialized by the coming years, there will be a huge demand for it. Because of these reasons, mobile phones should be compatible with the technology mentioned above and in order to achieve this, mobile antennas should be properly designed according to the new LTE standards.

In this thesis, we propose a 2 element MIMO antenna system operating in 700 MHz band which is one of the newest and the most challenging bands for designing an antenna within the LTE specifications.

1.4 Thesis Objectives

The objectives for this work are the following:

1. Design and optimize a single element and a 2-element (MIMO) meander line antenna system for LTE standards. The design should fit within a cellular phone handset size and satisfy the following requirements.

(a) Operating frequency of 780 MHz with a bandwidth greater than 40 MHz

(b) Isolation between the two elements MIMO antenna should be less than -15 dB

(c) Size of the 2-element MIMO antenna should fit with an area of 40x50 mm^2

2. To study the correlation coefficient for the 2-element MIMO antenna for this band and come up with a novel technique to reduce it to a value less than 0.3

4. Fabricate a single and 2-element Meander line antenna and experimentally observe their characteristics using a “network analyzer” and the “Antenna Test and Measurement System”.

5. Compare and comment on the simulated and experimentally obtained reflection and radiation responses of the single and 2 element MIMO antennas.

1.5 Thesis Overview

The thesis is organized in six chapters as follows:

Chapter 2 of this thesis starts with an introduction of the types of mobile printed antennas and electrically small antennas and it summarizes the reviewed literature. In Chapter 3, the design of electrically small antenna (ESA) is described, where the first part describes the designing of a Meander Line Antenna (MLA), second part is dedicated to introduce PIFA antenna and to compare between these two designs, the simulation results of the two proposed antennas will be discussed as well. Chapter 4 discusses all the design of a dual element MIMO antenna system using ESA then study the correlation coefficient that will arise from this system then modify the design to reduce its effect. The simulated (HFSS) radiation characteristics associated with the designed antenna will be discussed in this chapter also. In Chapter 5, the experimentally observed results for single antenna and 2-element MIMO antenna are then presented and analyzed. Comparisons between the experimental and simulated results for both single and dual element MIMO antenna are also tabulated in this chapter. Finally chapter 6 describes the conclusions drawn from this research work and recommendations on future work to be carried on this subject.

CHAPTER 2

LITERATURE REVIEW

2.1 Introduction

The development of small integrated printed antennas plays a significant role in the progress of rapidly expanding wireless communication applications. They are increasingly used in wireless communication systems due to advantages of being lightweight, compact and conformal. Recent evolution of mobile phones and RF/microwave networks demanded miniaturized version of printed antennas, which often employs: (i) High permittivity substrate. (ii) Shorting pins. (iii) Meandering or combination of these and other approaches. [**20**]

In mobile communication, Meander line antennas are recently favored over other printed antennas due to its simplicity and ease in integration. The following sections briefly discuss the evolution and characteristics of Meander line antennas (MLA).

The design process of 1.025 GHz meander line antenna, described in the literature [**21**], a design a meander line antenna operating at 1025MHz using empirical equations is discussed that give a certain dimensions for the width, length, number of turns and

spacing at a certain frequency, and then they test their design to check the validity of these equations. The value so obtained by two methods one by empirical relation and other by design equation are compared. It is found that the dimension obtained by both methods matched. Thus one can use these empirical relations for designing the meander line antenna, but the problem of this design that the dimensions of this antenna is too big (as will be shown in results section) but it give us an idea how the meander works and how it resonate at that frequency.

A more compact design of a meander line antenna, available in the literature [**22**], was designed to operate at 2.4-GHz for WLAN application. The paper described two different designs of meander line antenna with and without conductor line. The designed antennas were fabricated on a double-sided FR-4 printed circuit board using standard PCB technique and tested with a Network Analyzer. A bandwidth of 152MHz and return loss of -37.7dB were obtained at the operating center frequency of 2.4GHz. The effect on the antenna radiation and reflection properties with varying the MLA length, width, number of turns and conductor dimensions are also discussed in this paper.

In reference [**23**], a meander line antenna with smaller dimensions (40 by 40 cm) are presented. The designed antenna exhibited a bandwidth of 274 MHz and return loss of -25 dB at a center frequency of 1.575 GHz. This design is of importance to this research work due to the similarity of the antenna dimensions and will be carefully investigated.

Reference [**24**], discusses the design process of two electrically small printed antennas, suitable for mobile communication handsets. In this design, the resonant frequency of the antenna is significantly reduced by employing shorted patches, which

maximizes the length of the current path for a given area. In the literature, reductions in operating frequencies are also achieved using different methods, such as; shorting posts [**25**], high dielectric constant material [**26**], resistive loads [**27**], and deformation of the conductor shape (in addition to using a shorting post) [**28**], each with their relative merits and disadvantages.

It is evident from the literature review that most of the designed antenna with reduced element size have the trend to use higher frequency bands (i.e. 2.4 GHz and 5.5 GHz) [**25**], [**27**]- [**29**]. But little references are available for designing low frequency antennas with limited size. This is particularly important for the most recent initiative to adopt the 700 MHz band for 4_{th} generation (LTE) of cellular phones by AT&T, Verizon and other world leaders in wireless technologies. In this research work, a 700 MHz antenna with limited dimensions will be designed for LTE applications. Although similar antenna is available in the literature [**30**], but needs to be improved in terms of antenna efficiency and cost-effectiveness.

Reference [**31**] describes the design process of a PIFA antenna with two separate patches of different sizes for operating in two different bands. The larger and smaller patches have separate shorting points and are operated, respectively, in the 900 and 1800 MHz bands as quarter-wavelength resonant structures. A dual feed (feed point 1 for the larger patch and feed point 2 for the smaller patch) is also utilized in the design, which can find application where mobile phones have receivers with dual front ends. In addition, to achieve a compact antenna size, a portion of the larger patch is removed to accommodate the smaller patch. A compact 900/1800 MHz dual-frequency PIFA with an area of 25x26 mm^2 and a height of 4 mm has been presented in [**32**], This design has a

capacitive load, fed by a capacitive feed and uses a substrate with a relative permittivity of 2.1 between the two top patches and the ground plane.

Instead of using a simple flat ground plane, a PIFA with an L-shaped ground plane has also been studied in literature. It has been found that such a PIFA can have decreased backward radiation and enhanced antenna gain. A related study is reported in Reference [**33**]. An additional vertical ground is added to the edge of the horizontal ground plane in the proposed design to enhance the antenna performance. This shape will be thoroughly studied in this research work to fabricate a similar 700 MHz PIFA antenna. The radiation and reflection performances of the PIFA and meander-line antenna will then be compared.

2.2 Printed Antenna for Mobile Devices

Planner antennas are low profile, cost-effective and flat in appearance which makes them suitable for recent communication systems, such as the Global System for Mobile (GSM; 890-960 MHz), the Digital Communication System (DCS; 1710-1880 MHz), the Personal Communication System (PCS; 1850-1990 MHz), the Universal Mobile Telecommunication System (UMTS; 1920-2170), the Wireless Local Area Networks (WLANs) in the 2.4 GHz (2400-2484 MHz) and 5.2 GHz (5150-5350 MHz) bands [**30**] and Long Term Evolution (LTE) in the 700 MHz (758-798 MHz). LTE is a new standard for wireless communication that FCC has recently agreed to adopt for the 4^{th} generation cellular phones. Before LTE antennas can be designed with confidence, basic characteristics of antennas in general needs to be understood.

2.2.1 Antenna Basics

According to the IEEE Standard Definitions, the antenna or aerial is defined as “a means of radiating or receiving radio waves" [**19**]. In other words, antennas act as an interface for electromagnetic energy, propagating between free space and guided medium. Amongst the various types of antennas that include wire antennas, aperture antennas, reflector antennas, lens antennas etc., microstrip patches are one of the most versatile, conformal and easy to fabricate antennas.

Good antenna design is a critical factor in obtaining good range and stable throughput in a wireless application. This is especially true in low power and compact designs where antenna space is less than optimal. To obtain the desired performance, it is required that users have at least a basic knowledge about how antennas function and the design parameters involved. These parameters include selecting the correct antenna, antenna tuning, matching, gain/loss, and knowing the required radiation pattern.

2.2.1.1 Basic Antenna Parameters: Some of the basic antenna characteristics that a designer should be familiar with before starting the design process are briefly described below:

Antenna gain

Relates the intensity of an antenna in a given direction to the intensity that would be produced by a hypothetical ideal antenna that radiates equally in all directions (isotropically) and has no losses.

Gain is 4π times the ratio of an antenna's radiation intensity in a given direction to the total power accepted by the antenna. Peak gain, in turn, is the maximum gain over all the user-specified directions of the far-field infinite sphere.

The following equation is used to calculate the gain

$$Gain = 4\pi \frac{U}{P_{acc}} \qquad (2.1)$$

where, $\{U\}$ is the radiation intensity in watts per steradian in the direction specified and $\{P_{\text{acc}}\}$ is the accepted power in watts entering the antenna.

Gain can be confused with directivity, since they are equivalent for lossless antennas. Gain is related to directivity by the radiation efficiency of the antenna. If the radiation efficiency is 100%, they are equal.

Peak Realized Gain

Realized gain is 4π times the ratio of an antenna's radiation intensity in a given direction to the total power incident upon the antenna port(s). Peak realized gain, in turn, is the maximum realized gain over all the user-specified directions of the far-field infinite sphere.

The following equation is used to calculate realized gain [**34**]

$$\text{Realized } Gain = 4\pi \frac{U}{P_{incident}} \qquad (2.2)$$

Where, $\{U\}$ is the radiation intensity in watts per steradian in the direction specified, and $\{P_{\text{incident}}\}$ is the incident power in watts.

Antenna Directivity

It is defined by direction to the radiation intensity averaged over all directions.

$$D = D_{\max}(\theta,\phi) = \mathcal{P}_{\max} / \mathcal{P}_{ave} = U_{\max}/U_{ave} \qquad (2.3)$$

Peak Directivity

Directivity is defined as the ratio of an antenna's radiation intensity in a given direction to the radiation intensity averaged over all directions. Peak directivity, in turn, is the maximum directivity over all the user-specified directions of the far-field infinite sphere. [**34**]

Directivity is a dimensionless quantity represented by

$$Directivity = 4\pi \frac{U}{P_{rad}} \qquad (2.4)$$

where, $\{U\}$ is the radiation intensity in watts per steradian in the direction specified and $\{P_{\text{rad}}\}$ is the radiated power in watts.

• For a lossless antenna, the directivity will be equal to the gain. However, if the antenna has inherent losses, the directivity is related to the gain by the radiation efficiency of the antenna.

Antenna Bandwidth

It is defined as the range of frequencies within which the performance of the antenna, with respect to some characteristics, conforms to a specified standard [**19**].

Antenna Radiation Patterns

An antenna radiation pattern is a 3-D plot of its radiation far from the source. Antenna radiation patterns usually take two forms, the elevation pattern and the azimuth pattern. The elevation pattern is a graph of the energy radiated from the antenna looking at it from the side (E-Plane). The azimuth pattern is a graph of the energy radiated from the antenna as if you were looking at it from directly above the antenna (H-Plane).

Maximum intensity (Max U)

The radiation intensity $\{U\}$ is the power radiated from an antenna per unit solid angle. The maximum intensity of the radiation is measured in watts per steradian and is calculated by [**34**]

$$U(\theta, \emptyset) = \frac{|E|}{\eta_0} r \qquad (2.5)$$

where, $\{U(\theta,\phi)\}$ is the radiation intensity in watts per steradian, $\{|E|\}$ is the magnitude of the E-field, $\{\eta_0\}$ is the intrinsic impedance of free space and it is equal to 376.7 ohms, $\{r\}$ is the distance from the antenna, in meters.

Radiated Power

Radiated power is the amount of time-averaged power (in watts) exiting a radiating antenna structure through a radiation boundary.

For a general radiating structure, radiated power is computed as [**34**]

$$P_{rad} = Re\left\{\int_s E \times H^* . ds\right\} \qquad (2.6)$$

where, $\{P_{rad}\}$ is the radiated power in watts; {Re} is the real part of a complex number, $\{s\}$ represents the radiation boundary surfaces, $\{E\}$ is the radiated electric field, $\{H^*\}$ is the conjugate of **H** and $\{ds\}$ is the local radiation-boundary unit normal directed out of the 3D model.

Accepted Power

The accepted power is the amount of time-averaged power (in watts) entering a radiating antenna structure through one or more ports. For antennas with a single port, accepted power is a measure of the incident power reduced by the mismatch loss at the port plane. [**34**]

For a general radiating structure, accepted power is computed as

$$P_{acc} = Re\left\{\int_A E \times H^* . ds\right\} \qquad (2.7)$$

where, $\{P_{acc}\}$ is the accepted power in watts, {Re} is the real part of a complex number, $\{A\}$ is the union of all port boundaries in the model, $\{E\}$ is the radiated electric field, $\{H^*\}$ is the conjugate of **H** and $\{ds\}$ is the local port-boundary unit normal directed into the model.

For the simple case of an antenna with one lossless port containing a single propagating mode, the above expression reduces to [**34**]

$$P_{acc} = |a|^2(1 - |s_{11}|^2) \qquad (2.8)$$

where, $\{a\}$ is the complex modal excitation specified, $\{s_{11}\}$ is the reflection coefficient of the antenna.

Incident Power

Incident power is the total amount of time-averaged power (in watts) incident upon all port boundaries of an antenna structure.

For the simple case of an antenna with one lossless port containing a single propagating mode, the incident power $P_{incident}$ is given by [**34**]

$$P_{incident} = |a|^2 \qquad (2.9)$$

where, $\{a\}$ is the complex modal excitation specified.

Radiation Efficiency

The radiation efficiency is the ratio of the radiated power to the accepted power given by [**34**]

$$e = \frac{P_{rad}}{P_{acc}} \qquad (2.10)$$

where, $\{P_{\text{rad}}\}$ is the radiated power in watts, $\{P_{\text{acc}}\}$ is the accepted power in watts.

2.2.1.2 Miniaturization Trade-offs

To satisfy the object of this project, an LTE printed antenna needs to be designed with pre-specified dimensions. Since these dimensions are small, size of the existing printed antennas needs to be reduced. But reducing the size of the antenna results in reduced performance. Some of the parameters that suffer in this process are:

• Reduced efficiency (or gain)

• Shorter range

• Smaller useful bandwidth

• More critical tuning

• Increased sensitivity to component and PCB spread

• Increased sensitivity to external factors

Several performance factors deteriorate with miniaturization, but some antenna types tolerate miniaturization better than others. How much a given antenna can be reduced in size depends on the actual requirements for range, bandwidth, and repeatability. In general, an antenna can be reduced to half its natural size with moderate impact on performance. However, after a 1/2 reduction, performance becomes progressively worse as the radiation resistance drops off rapidly. As loading and antenna losses often increase with reduced size, it is clear that efficiency drops off quite rapidly [**35**].

2.2.2 Printed Antennas

The leading printed antennas commonly used in embedded applications are: Microstrip Lines/Patch, Planar Inverted 'F' (PIFA), Meander Line (MLA) etc. Microstrip lines are an extension of the monopole. They can be easily fabricated by etching a copper strip of the radio circuit board. While very inexpensive to make, its performance is limited by surrounding electronics on the circuit board. Microstrip monopole is also only a single-frequency solution. Patch antennas are a good choice for a system that requires a beam pattern focused in a certain direction. Patches are fabricated out of square or round copper clad on the top surface of a circuit board. Their radiation beam is normal to the surface of the board. One antenna type becoming increasingly popular is planar inverted-F antenna (PIFA). The PIFA antenna literally looks like the letter 'F' lying on its side with the two shorter sections providing feed and ground points and the 'tail' providing the

radiating surface. PIFAs make good embedded antennas in that they exhibit a somewhat omnidirectional pattern and can be made to radiate in more than one frequency band. PIFA has a low profile, and it can easily be incorporated into wireless handsets. PIFA antennas are generally used with a ground plane, which is generally the cellular phone circuit board ground plane. The Meander Line Antenna (MLA) is a new type of radiating element, made from a combination of a loop antenna and frequency tuning meander lines. The electrical length of the MLA is made up mostly by the delay characteristic of the meander line rather than the length of the radiating structure itself. MLAs can be designed to exhibit broadband capabilities that allow operation on several frequency bands. For the base stations classical dipoles are very common. The common dipole has long been recognized as an efficient radiator when cut to the appropriate frequency length. It is made from bending the end of an open circuit two-wire transmission line into a 'T' shape, where the top of the 'T' is the radiating section of the antenna. The length of the top is lambda, the wavelength of the signal. In some applications also monopole antennas with $\lambda/2$ or $\lambda/4$ length mounted over ground plane are used. There are also special antenna constructions for special applications. When you need to flood a wide but defined area with RF energy, such as for perimeter security systems, tunnels, and cellular- or 802.11-system interior zones, one approach is to use an RF-leaky feeder cable to provide controlled radiation.

2.2.2.1 Microstrip Patch Antenna

In its simplest form a microstrip antenna consists of a dielectric substrate sandwiched between two conducting surfaces: the antenna plane and the ground plane. The simplified microstrip patch antenna is shown in Figure 4.

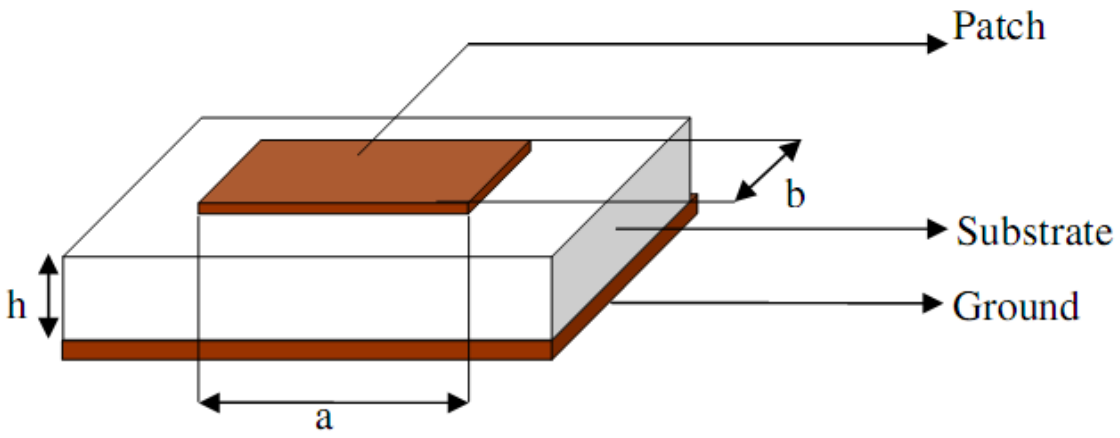

Figure 4: Basic rectangular microstrip patch antenna construction

Microstrip patch antennas radiate primarily because of the fringing fields between the patch edge and the ground plane. Since the propagating EM fields lay, both in the substrate and in free space, a quasi-TEM mode is generated. The length and width of the patch are given by (a) and (b) respectively. The substrate thickness is given by h. Microstrip antennas are often feed using; Microstrip Line feed [**36**], Coaxial feed [**37**], Proximity coupled [**38**] and Aperture coupled [**38**] techniques, each with their own advantages and disadvantages [**19**]. The substrate thickness is given by h.

Along with a number of advantages [**39**] microstrip antennas also suffer from some disadvantages [**36**] [**37**] like narrow bandwidth, low efficiency, low Gain, spurious

radiation and surface wave excitation. While spurious radiation and surface waves can be eliminated by using the right feed mechanisms and substrate thickness [**36**], the issues of major concern are poor bandwidth and low radiation efficiency. Microstrip antennas inherently suffer from Ohmic losses and dielectric losses making it a high Q device [**36**]. In order to achieve greater bandwidth and gain we must increase substrate thickness but this could result in surface waves [**37**].

2.2.2.2 Meander Line Antenna

Meander Line Antenna is a type of printed antenna that achieves miniaturization in size by embedding the wire structure on a dielectric substrate. MLA technology was originally developed by BAE SYSTEMS (a former Lockheed Martin Company) [**40**], for the Information and Electronic Warfare Systems (IEWS), which require high performance antennas for both satellite and terrestrial communications. Recently, this class of antennas are found to be suitable for application mobile handsets; wireless data networking for laptops, PC cards and access points. In basic form meander line antenna is a combination of conventional wire and planer strip line. Benefits include configuration simplicity, easy integration to a wireless device, inexpensive and potential for low Specific Absorption Rate (SAR) features. **SAR** is a measure of the rate at which energy is absorbed by the body when exposed to a radio frequency (RF) electromagnetic field. It is defined as the power absorbed per mass of tissue and has units of watts per kilogram.

DESIGNING OF MEANDER LINE ANTENNA

In a meander line antenna (also called rampart line antenna), the radiating element consists of a meandering microstrip line formed by a series of sets of right angled compensated bends, as shown in Figure 5. The fundamental element in this case is formed by four right angled bends and the radiation mainly occurs from the discontinuities (bend) of the structure. The right angle bends are chamfered or compensated to reduce the right angled discontinuity susceptance for impedance matching. The current directions are changing in every half wavelength and there are more than four half wavelength changes in this design. The radiations from the bend add up to produce the desired polarization depending on the dimensions of the meander line antenna. Detail description of the design process of this class of antenna is presented in chapter 3.

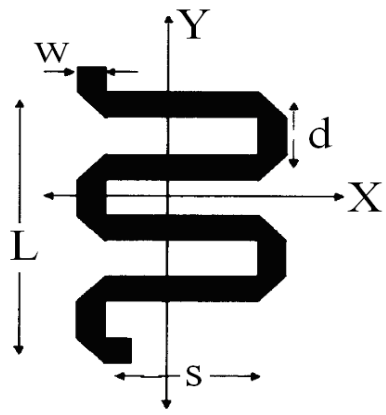

Figure 5: The Fundamental Section of the Meander Line Antenna

2.2.2.3 Planar Inverted F Antenna

The planar inverted –F antenna is popular for portable wireless devices because of its low profile, small size, and built-in structure [**41**]. The other major advantages are easy fabrication, low manufacturing cost, and simple structure [**42**]. Conventional PIFA has limited bandwidth of 4 % to 12 % for a -10 dB return loss [**32**]. Also, PIFA's inherent bandwidth is higher than the bandwidth of the conventional patch antenna (since a thick air substrate is used). The basic PIFA is a "grounded" patch antenna with λ/4 patch lengths instead of the conventional λ/2. As shown in Figure 6, a PIFA consists of a ground plane, a top plate element, a feed wire feeding the resonating top plate, and a DC-shorting plate that is connecting the ground and the top plate at one end of the resonating patch.

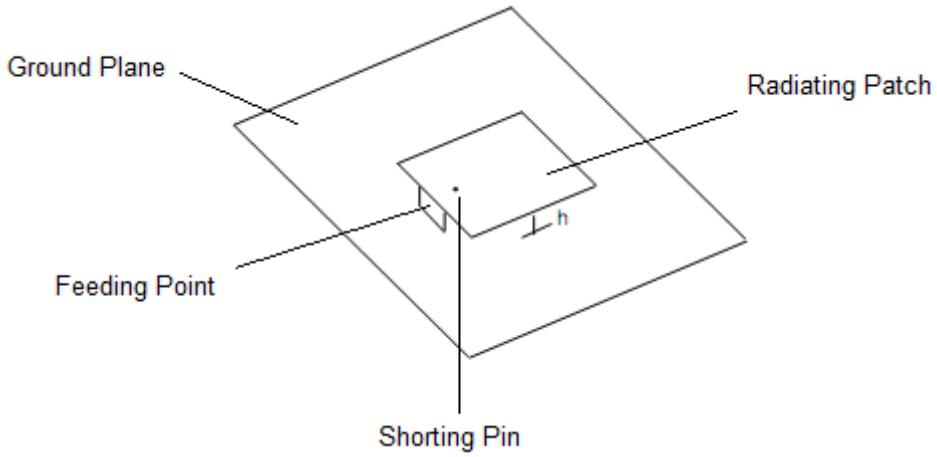

Figure 6: Planar Inverted F Antenna

PIFA creates an exceptionally uniform 3D signal sphere through its inverted-F design, which generates an Omni-directional signal field. In comparison to other popular two-dimensional antenna types, such as IFA (Inverted-F Antenna) and MLA (Meander Line Antenna), the 3D signal generated by the cubic structure of PIFA-type antennae offers double the surface area of other antennas guaranteeing the highest levels of antenna efficiency for enhanced transmission and reception. In this research the antenna properties of the proposed MLA LTE antenna will be compared with a 2nd design of PIFA configuration.

2.3 Electrically Small Antenna

2.3.1 Fundamental Limitations

The fundamental limits on small antenna performance are available in the literature. In 1947 [**43**], Wheeler investigated the effects of antenna effective volume on radiation efficiency and bandwidth. Wheeler described an electrically small antenna as one with a maximum geometrical dimension much less than the radian length. The radian length is a distance measurement equal to $\frac{\lambda}{2\pi}$. This is a convenient definition because a sphere with diameter equal to the radian length contains most of the stored near-field energy of the electrically small antenna. A year later, Chu derived an approximate lower limit for the radiation Q of an electrically small antenna [**44**] Recently, McLean derived an exact lower limit and corrected apparent errors in the derivation of Q. [**45**]. In 1987 the

monograph Small Antennas by Fujimoto, Henderson, Hirasawa and James summarized the approaches used to design electrically small antennas (ESA) [**46**].

Since an ESA is contained within a given volume it has an inherent minimum value of Q thus there exists a limit on the attainable maximum impedance bandwidth of an ESA [**23**]. Note that antennas operating at frequencies outside their normal operating range of Q-factor (also called Quality Factor) are of little practical utility. Electrically small and low-profile antennas are both subject to performance limitations due to size reduction. These classes of antennas have low efficiencies, and are difficult to match to a transmission line due to low input resistance and high input reactance. In addition, ESAs typically exhibit narrow impedance bandwidth, which is an important parameter in the antenna design process.

2.3.2 Limit on Radiation Efficiency

Generally *Q* is defined in terms of the ratio of the energy stored in the resonator to the energy being lost in one cycle:

$$Q = 2\pi \frac{Energy\ \ Stored}{\text{Enrgy Dissipated Per Cycle}} \qquad (2.11)$$

The Q factor is commonly used to describe the ratio of the reactance to the resistance in a device. So equation (2.11) can be written as

$$Q = \frac{2\pi X}{R} \qquad (2.12)$$

where X is the reactance or stored energy, and R is the ohmic resistance. Analogously, Chu defines the radiation Q for an antenna as

$$Q = \frac{2\omega W}{P_{rad}} \qquad (2.13)$$

where ω is the radian frequency, P_{rad} is the radiated power, and W is the time-averaged, non-propagating, stored electric or magnetic energy, whichever is greater [**47**]

Electrically small antennas have high input reactance and low input resistance. Therefore, they have high Q and low frequency bandwidth. ESAs also have low radiation efficiency. The radiation efficiency of an antenna is defined by

$$\eta_a = \frac{R_r}{R_r + R_m} \qquad (2.14)$$

Where R_r is the radiation resistance of the antenna and R_m refers to the ohmic losses in the antenna structure and any matching device. The radiation efficiency (η_a) of a receiving antenna is the fraction of energy delivered by the antenna from free space to a load representing the receiver [**48**]. Every small antenna can be made to perform like a lumped reactance, specifically, a capacitor, inductor, or some combination of the two. An electric dipole, or dipole antenna, behaves like a capacitor. A magnetic dipole, or loop antenna, behaves like an inductor. Either antenna can be represented by some combination of a reactive and a resistive lumped element. The reactance in the equivalent circuit describes the portion of the input energy that is stored in the near-field of the antenna. The resistive element represents the radiation resistance of the antenna. Wheeler models the magnetic dipole as a series inductance and resistance and the electric dipole as

a shunt capacitance and susceptance [**48**]. This representation is consistent with circuit duality. Both equivalent circuits are illustrated in Figure 7.

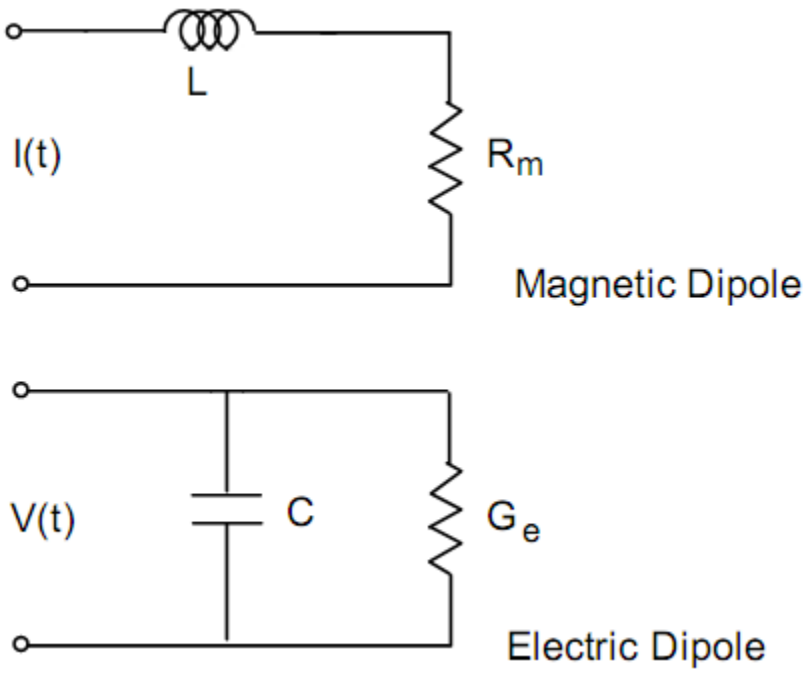

Figure 7: Equivalent circuits of a magnetic and electric dipole

2.4 MIMO Antenna

Antennas for recent wireless communication devices based on MIMO systems require multiple antennas to achieve high date rate without any need to increase transmitted power. High data rate wireless communication has improved by a factor of four, by migrating to the next generation standards. [**49**]

2.4.1 Multiple Antennas

Recent research on wireless communication systems has shown that using multiple antennas at both the transmitter and the receiver offers the possibility of higher data rates compared to single antenna-systems. The information-theoretic capacity of MIMO channels was shown to grow linearly with the minimum number of transmits and receives antennas in rich scattering environments and at sufficiently high signal-to-noise (SNR) ratios [**50**]. However, for single-input single-output (SISO) channels, the capacity increases logarithmically with SNR. Thus, a significant capacity increase can be achieved using MIMO systems without any increase in transmit power or expansion in the bandwidth [**51**]. The earliest ideas in this field go back to work by A.R. Kaye and D.A. George (1970) and W. van Etten (1975, 1976). Jack Winters and Jack Salz at Bell Laboratories published several papers on beamforming related applications in 1984 and 1986 [**52**].

MIMO Techniques

1. **Beamforming**
2. **Diversity**
3. **Multiplexing**

The important techniques used in MIMO technology to enhance the data transfer process are: Beamforming, Diversity and Multiplexing. Brief description of each technique is as follows:

1. **Beamforming**

   It is an effective technique for reducing the multiple-access interference, where the antenna gain is increased in the direction of the desired user, whilst reducing the gain towards the interfering users [**53**]. If the directions of the different propagation paths are known at the transmitter or the receiver, then beamforming techniques can be employed in order to direct the received beam pattern in the direction of the specified antenna or user [**54**] [**55**]. Hence, significant SNR gains can be achieved in comparison to a single-antenna system. On the transmitter side, when the direction of arrival (DOA) of the dominant paths at the receiver is known for the transmitter, then the transmit power is concentrated in the direction of the target user, and less power is wasted in the other directions. On the other hand, beamforming can be used in order to reduce the co-channel interference or multi-user interference [**53**]. When using beamforming, each user adjusts their beam pattern to ensure that there are nulls in the directions of the other users, while there is a high directivity in the direction of the desired receiver. Hence, the system attains an SNR gain.

There are many methods to achieve beamforming, such of these methods are:

a) Phased Array Antenna

A phased array antenna is composed of many radiating elements each with a phase shifter. Beams are formed by shifting the phase of the signal emitted from each radiating element, to provide constructive/destructive interference so as to steer the beams in the desired direction. [**56**]

The main beam always points in the direction of the increasing phase shift. Well, the beam direction can be electronically adjusted if the signal to be radiated is delivered through an electronic phase shifter giving a continuous phase shift. However, this cannot be extended unlimitedly. The highest value, which can be achieved for the Field of View (FOV) of a phased array antenna is 120° (60° left and 60° right). With the sine theorem the necessary phase moving can be calculated. [**56**]

Frequency Scanning Array

Frequency scanning is a special case of the phased array antenna where the main beam steering occurs by the frequency scanning of the exciter. The beam steering is a function of the transmitted frequency. This type of antenna is called a frequency scanning array. The normal arrangement is to feed the different radiating elements from one folded waveguide. The frequency scanning array is a special case of serial feeding type of a phased array antenna and is based on a particular property of wave propagation in waveguides. The phase difference between two radiating elements is n·360° at the normal frequency. [**56**]

By varying the frequency, the angle between the axis of the main beam and the normal on the array antenna changes. Height information is generated using the following philosophy:

- If the transmitted frequency rises then the beam travels up the face of the antenna;
- If the transmitted frequency falls then the beam travels down the face of the antenna.

b) Adaptive Antennas

In adaptive antenna systems multiple antennas are used to receive (or transmit) the same information. Instead of using only one antenna to receive (or transmit) the radio signal, combinations of multiple antennas output (or input) are used to focus the energy towards one direction. The adequate combination of the signals received by the different antennas results in a better link quality for a given transmitted power, or a lower transmitted power required for a given link quality [**57**]. The same concept of adaptive antennas can be found under different names such as smart antennas, or adaptive beamforming [**58**]. The basic concept behind adaptive antennas is to change the standard antenna that has an omnidirectional radiation pattern for a new one with a directive radiation pattern that is continuously adapted to the environment [**57**], by changing the amplitudes and phases from different array elements according to a real time criteria to focus the beam towards a specific spatial direction.

c) Null Steering Techniques

The objective of steering nulls in the antenna array pattern in a particular direction is to reduce the interference arriving in that direction. This can be achieved by controlling the amplitude and/or phase of the current induced on the elements of the array or by controlling the position of the elements of the array such that the array factor in that direction is zero (practically to a required depth e.g. -60 dB with respect to the normalized maximum array factor of 0 dB). This reduction is necessary in today's mobile communication environment in order to face the various sources of interferences like Co-Channel interference, Adjacent channel interference etc. Null steering involving the above mentioned controllable variables is briefed below.

i) Element positive perturbation method

This technique was developed by Ismail and Dawoud [**59**], where null steering is carried out by controlling the positions of the antenna array elements. This avoids the complicated use of amplitude and/or phase control systems and frees the phase shifters merely for steering the main beam towards the direction of the desired signal. An experimental verification was done in [**60**] wherein, null steering was achieved for an eight-element monopole over a ground plane. Single and double nulls were realized in the side lobe region. Dawoud et al [**61**] applied genetic algorithm and compared the results with analytical solution for array pattern nulling by element position perturbation. Null steering in scanned arrays by using position perturbations was carried out in [**62**].

ii) Amplitude Only Control Method

In this method the amplitude of the induced currents are controlled to achieve Null Steering. Mismer and Ismail [**63**] employed the method of amplitude only control to perform null steering by a linear programming technique using minmax approximation. Liao and Chu [**64**] investigated the technique to steer the array nulls for planar arrays by controlling only the excitation current amplitudes based on genetic algorithms. Implementation was done in rectangular and circular planar mays.

iii) Phase only control method

In this method, only the phases of the currents induced on the elements are varied. Liao and Chu [**65**] used phase only null steering in hear arrays using a modified genetic algorithm to speed up the convergence rate. Numerical results for 20-element linear array with one to four imposed interferences were demonstrated. Ismail and Mismer [**66**] presented a new antenna configuration of dual phase shifters to steer multiple nulls by controlling the arbitrary phase perturbations. Steyskal demonstrated pattern nulling by phase perturbations in [**67**]. Complex weight control method. Here pattern synthesis is carried out by perturbing both phase and amplitude of the array elements. This is much efficient technique. The number of degrees of freedom in this case is twice the number of array elements resulting in better control of null steering. Mitchell et al [58] carried out array pattern synthesis with performance constraints in complex plane where genetic

algorithm was applied on the roots of the array polynomial. Also, Compton et a1 [55] presented a numerical technique to arrive at the complex weights, which gives a desired side lobe level in linear arrays.

2. **Diversity Coding**

Techniques are used when there is no channel knowledge at the transmitter. In diversity methods a single stream is transmitted, but the signal is coded using techniques called space-time coding. The signal is emitted from each of the transmit antennas with full or near orthogonal coding. Diversity coding exploits the independent fading in the multiple antenna links to enhance signal diversity. Because there is no channel knowledge, there is no beamforming or array gain from diversity coding.

3. **Spatial multiplexing**

Spatial multiplexing requires MIMO antenna configuration. In spatial multiplexing, a high rate signal is split into multiple lower rate streams and each stream is transmitted from a different transmit antenna in the same frequency channel. If these signals arrive at the receiver antenna array with sufficiently different spatial signatures, the receiver can separate these streams, re-creating parallel channels. Spatial multiplexing is a very powerful technique for increasing channel capacity at higher signal-to-noise ratios

(SNR). The maximum number of spatial streams is limited by the number of antennas at the transmitter or receiver. Spatial multiplexing can be used with or without transmit channel knowledge.

Diversity MIMO vs. Multiplexing MIMO

The spatial freedom introduced by a MIMO system can be used in two distinct ways [**68**] [**69**], i.e., either to improve link quality (diversity MIMO) or to enhance throughput (multiplexing MIMO). Diversity MIMO schemes in general can increase the performance by exploit array gain and/or diversity gain, but it will have the same data rate as the SISO system, e.g. Space-time coding. On the other hand, multiplexing MIMO can increase the symbol data rate at no cost of extra spectrum. So, there are two methods widely used for transmitting MIMO data. If the channel has a negligible error rate, we can send several data simultaneously over multiple antennas. This is known as spatial multiplexing, which utilizes the spectrum very efficiently. In contrast, if the environment has high error rate, we transmit the same data over multiple antennas. This is called as space-time coding. The purpose of this approach is to increase the diversity of MIMO to combat signal fading.

2.4.2 Antenna Array

Often in wireless devices with single element antennas are unable to meet the gain or radiation pattern requirements. Combining several single antenna elements in an array can be a possible solution.

Definition

An array of antenna elements is a spatially extended collection of N similar radiators or elements, where N is a countable number bigger than 1, and the term "similar radiators" means that all the elements have the same polar radiation patterns, orientated in the same direction in 3-d space. Typically, the elements are spaced on a regular grid and fed with the same frequency and same or progressed amplitude and phase angle.

Types of Antenna Arrays

There are a few different general types of antenna arrays. When the array is arranged in a straight line this is called a ***linear array***. Antennas are arranged in parallel lines on one plane has a ***plane array*** in two dimensions. Many planes in a group of arrays or antennas results in a ***three dimensional array***. An antenna array may consist of a group of Omni-directional radiators. Or, the array may have a group of radiators that are identical. In a group of identical radiators all the antennas must be share the same orientation in space. The same orientation results in the desired effect of reinforcement or cancellation of the electric field intensity. The same orientation ensures polarization in the same direction in space. [**70**]

Antenna arrays, radiation pattern and array factor

The antenna elements can be arranged to form a 1 or 2 dimensional antenna array. A number of antenna array specific aspects will be outlined; We used 1-dimensional arrays for simplicity reasons. Antennas exhibit a specific radiation pattern. The overall radiation pattern changes when several antenna elements are combined in an array. This is due to the so called array factor: this factor quantifies the effect of combining radiating elements in an array without the element specific radiation pattern taken into account. The overall radiation pattern of an array is determined by this array factor combined with the radiation pattern of the antenna element. The overall radiation pattern results in a certain directivity and thus gain linked through the efficiency with the directivity. Directivity and gain are equal if the efficiency is 100%.

Broadside vs. end fire arrays

Arrays can be designed to radiate in either **Broadside** i.e. Radiation perpendicular to array orientation or **End Fire** i.e. Radiation in the same direction as the array orientation. The array factor depends on the number of elements, the element spacing, amplitude and phase of the applied signal to each element. The number of elements and the element spacing determine the surface area of the overall radiating structure. This

surface area is called aperture. A larger aperture results in a higher gain. The aperture efficiency quantifies how efficient the aperture is used.

Feed network of the array

The individual antenna elements in an array are fed using a feed network. The complexity of the feed network depends on the number of elements, the amplitude and/or phase distribution between the elements, the ability to do beam steering. It is important to realize that the feed network is the most complex part of the array. A detailed design process of a linear 2-element array for MIMO application is described in chapter 4.

CHAPTER 3

Design of an Electrically Small Antenna

As previously mentioned, meander line technology is adopted for the single element antenna because this type of antennas could have much smaller area than other types of antennas listed in Table 4. In this section we will present the design of an antenna element that will fit a size of 20x40 mm^2 with a resonant frequency of 780 MHz, and at least 40 MHz of bandwidth and 0 dB of gain with a radiation pattern that covers around a cell phone.

3.1 Empirical Design of a Meander Line Antenna

One way of designing a meander line antenna is by using the empirical equation mentioned in [**21**], which represents every dimension needed in the design in term of the wavelength and actually the effective wavelength

The design procedure of a meander antenna using empirical formulas can be summarized as:

1. First determine the type and dielectric constant of the substrate and the operating frequency that you want your antenna to work on.
2. Find the dimensions of your MLA using these equations, see Figure 8:

$$d = 0.16 * \lambda_{\text{eff}} \quad (3.1)$$

$$s = 0.42 * \lambda_{\text{eff}} \quad (3.2)$$

$$l = 0.70 * \lambda_{\text{eff}} \quad (3.3)$$

$$w = 0.05 * \lambda_{\text{eff}} \quad (3.4)$$

where, d is the width of the meander line arm, s is the length of the meander line arm, l is the length of the meander line, w is the width of the meander line, λ_{eff} is the effective wavelength of the substrate and is given by

$$\lambda_{\text{eff}} = \frac{\lambda_0}{\sqrt{\varepsilon_{reff}}} \quad (3.5)$$

Where, λ_0 is the free space wavelength and is the effective dielectric constant

3. Find ε_{reff} using:

$$\varepsilon_{reff} = \frac{\varepsilon_r + 1}{2} + \frac{\varepsilon_r - 1}{2}\left[1 + 10\frac{h}{w}\right]^{-\frac{1}{2}} \quad (3.6)$$

Where, h is the height of substrate, ε_r is the dielectric constant of given material, w is the width of meander line antenna.

Applying 3.1-3.6, and using a resonant frequency of 780 MHz, FR-4 material ($\varepsilon_r = 4.4$) and substrate thickness of 1.6 mm, we get

$$\lambda_0 = \frac{3*10^8}{780*10^6} = 384.6\ mm$$

$$\varepsilon_{reff} = 3.31$$

$$\lambda_{eff} = \frac{\lambda_0}{\sqrt{\varepsilon_{reff}}} = \frac{384.6}{\sqrt{3.31}} = 211.4mm$$

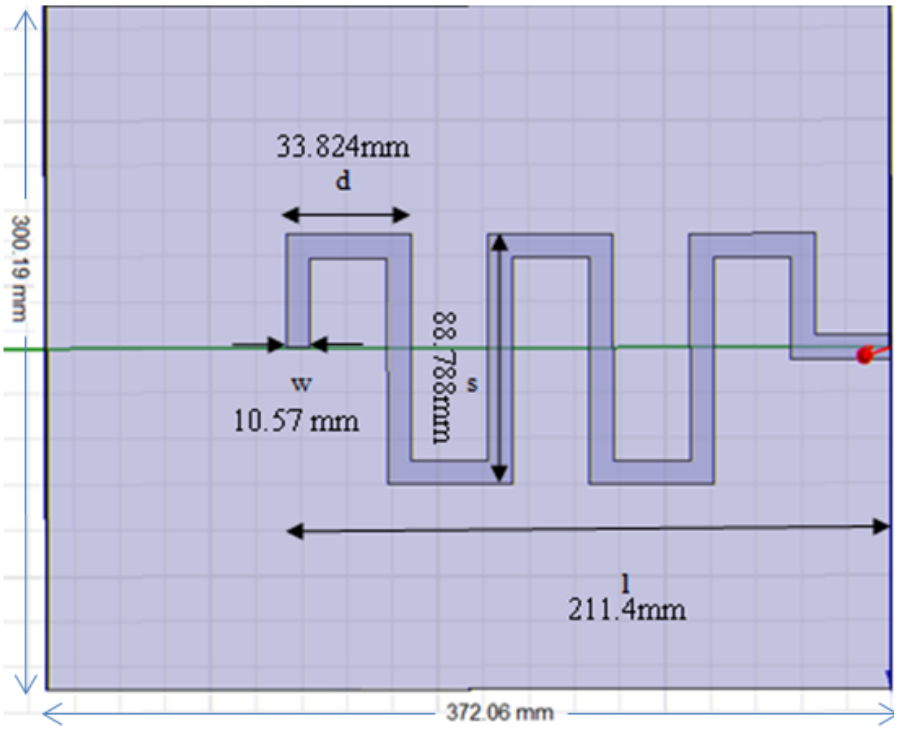

Figure 8: HFSS Model for a MLA Based on Empirical Equations

$$d = 33.824\ mm$$

$$s = 88.788\ mm$$

$$l = 147.98\ mm$$

$$w = 10.57\ mm$$

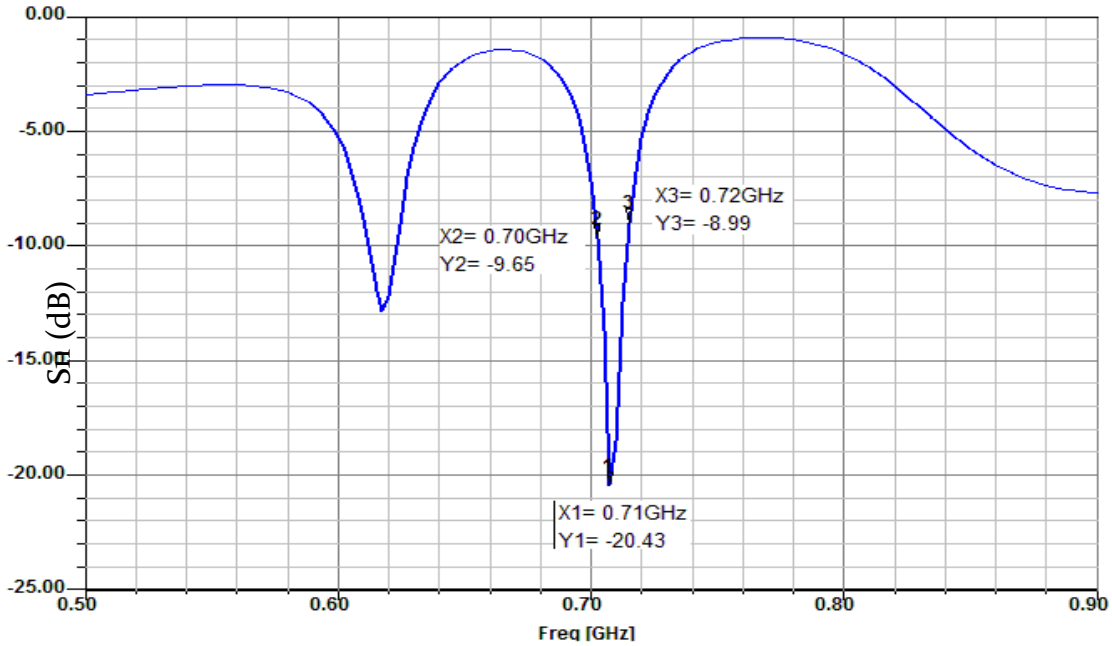

Figure 9: Reflection Coefficient of the Empirical Design

Figure 8 shows the HFSS model of the meander line antenna based on the empirical equations (3.1-3.6); the dimensions of the meander antenna are indicated on the figure as well as the dimension of the substrate. We notice that the dimensions of the substrate are too large and will not fit a small size mobile phone.

The reflection coefficient of the antenna is presented in Figure 9. $|S_{11}|$ had a value of -20.43 dB at 710 MHz which is an acceptable value for the reflection since it less than -10 dB and the bandwidth is 20MHz.

3.2 Design of an Electrical Small Antenna

Since the empirical relation will yield a bulky antenna, we have to find another antenna that would satisfy the design requirements of an electrically small antenna will solve the problem.

According to Wheeler [**43**]; an antenna is considered to be electrically small if it fit inside a sphere of radius (a) such that;

$$ka < 1$$

Where, $k = \frac{2\pi}{\lambda}$ (radians/meter) is the wave number, λ is the free space wavelength (meters), and (a) is the radius of sphere enclosing the maximum dimension of the antenna (meters)

The situation described by Wheeler is illustrated in Figure 10. The electrically small antenna (ESA) is in free space and may be enclosed in a sphere of radius a.

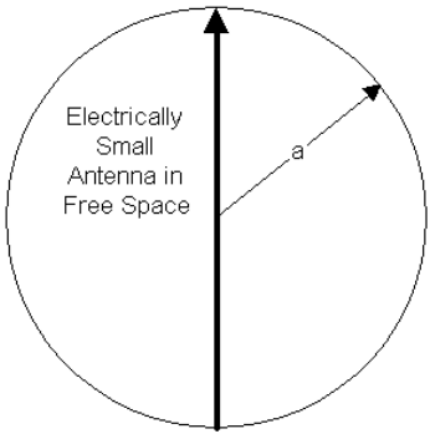

Figure 10: Sphere enclosing an electrically small radiating element

There are several types of ESA. In this work we use a meander line ESA. This design is based on that presented in [**23**] but that design has an operating frequency of 1.575 GHz which is almost double the operating frequency that we need, so we need to re-design the antenna to operate at 780 MHz with a size that satisfies the dimension constraints of our design.

Since MLAs do not have a specific design procedure, a study on the variation of the parameters is conducted to determine the antenna dimensions. First we determine the size of the substrate we need, then we model the meander line antenna on the top of the substrate with the ground plane on the bottom face of it and start vary the parameters to know its effect on the operating frequency, these parameters are thickness of the substrate, dielectric constant, width and length of the meander antenna arms, spacing between these arms, number of turns, width of the matching line, length of the ground plane, width of the meander line and the distance between the last arm and the edge of the substrate and section 3.3 investigate some of these parameters with more details.

Figure 11 shows the schematic diagram of the designed meander line ESA with parameter values given in the Table 4.

Table 4: Specifications of our Designed Antenna

Frequency	Dielectric Constant	NO. of Turns	Substrate Thickness	Substrate Length	Substrate Width
780 MHz	4.4	4	1.6 mm	40 mm	20 mm

W2	W3	W4	W5	Lg	L1	L2	S
1.651 mm	1 mm	1 mm	1 mm	16.4 mm	12.27 mm	5.925 mm	15.5 mm

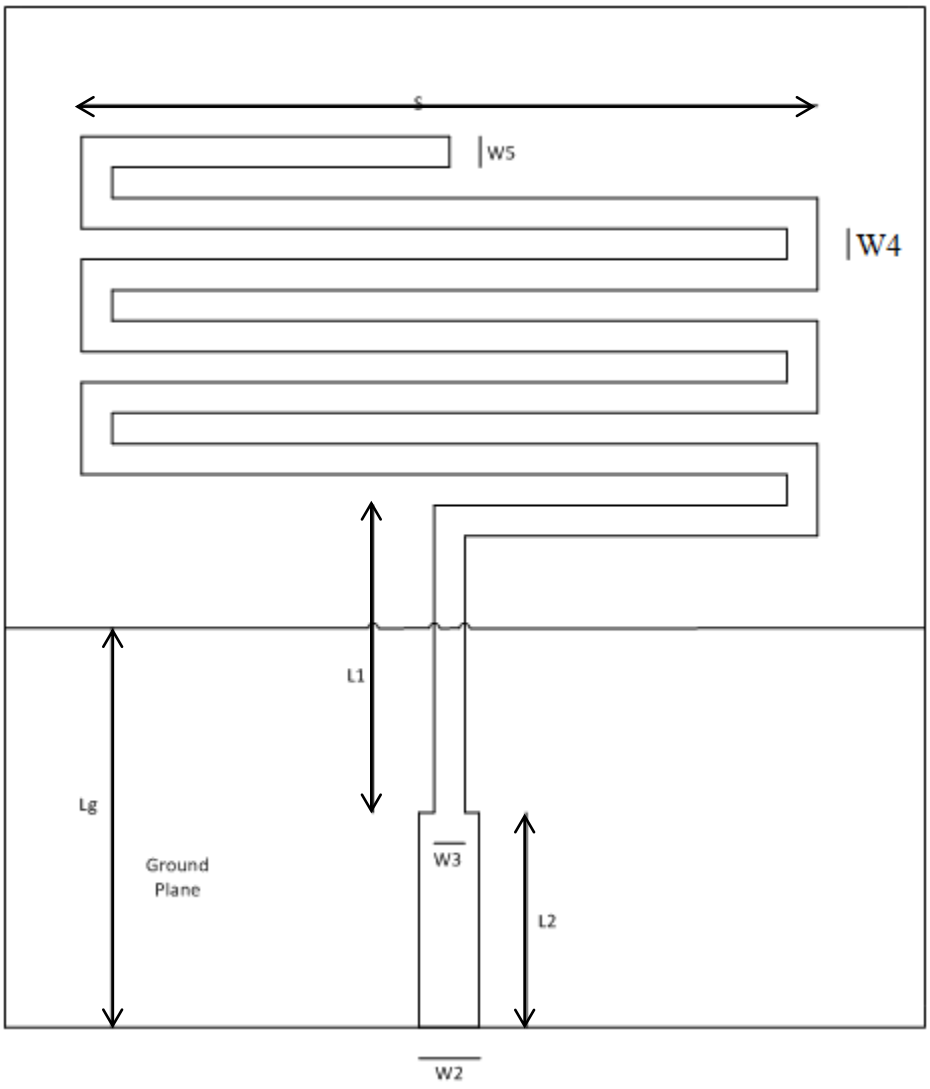

Figure 11: Schematic Diagram of the Proposed Design

Figure 12 shows the reflection coefficient $|S_{11}|$ of the antenna starting from 250 MHz and ending at 2 GHz and it has a value of -36.46 dB at 780 MHz which is a very good value for the reflection since it is less than -10 dB with a 10 dB bandwidth of 260MHz.

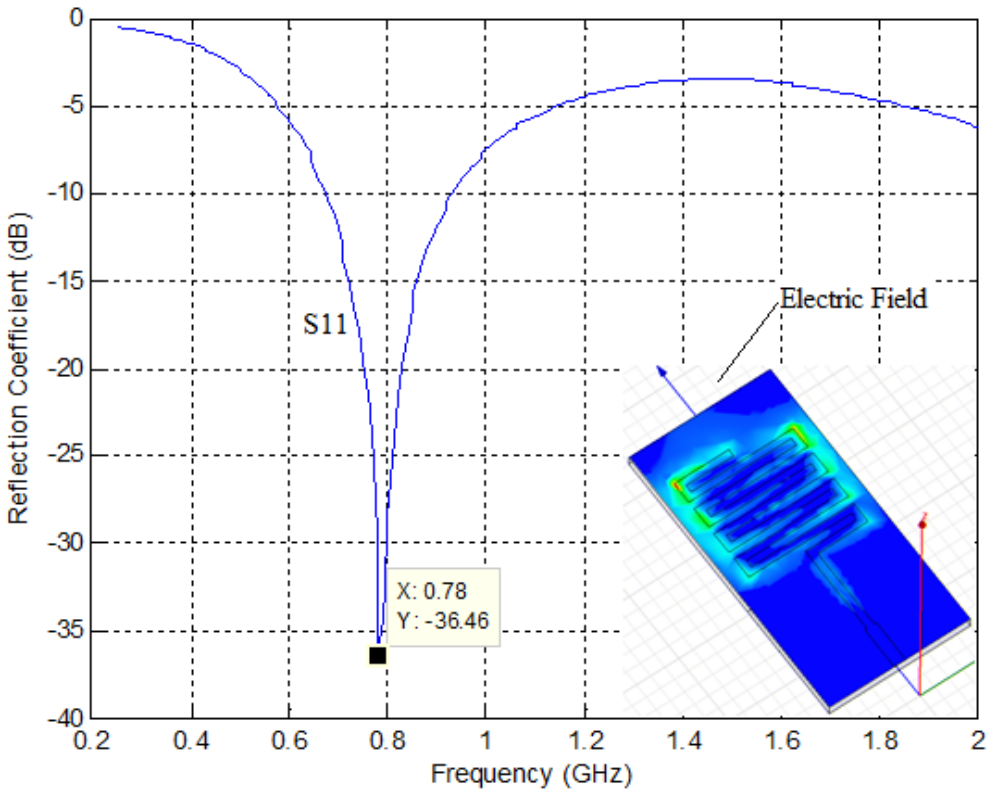

Figure 12: Reflection Coefficient for the Designed MLA

Figure 13a shows the 3D radiation Pattern of the designed antenna where the antenna is placed on X-Y plane. Where Figure 13b shows the elevation plane pattern and 13c shows the azimuth plane pattern for the radiation pattern of the meander line antenna and the scale below the figure shows that the maximum value is 5 dB and the lowest one is -16dB.

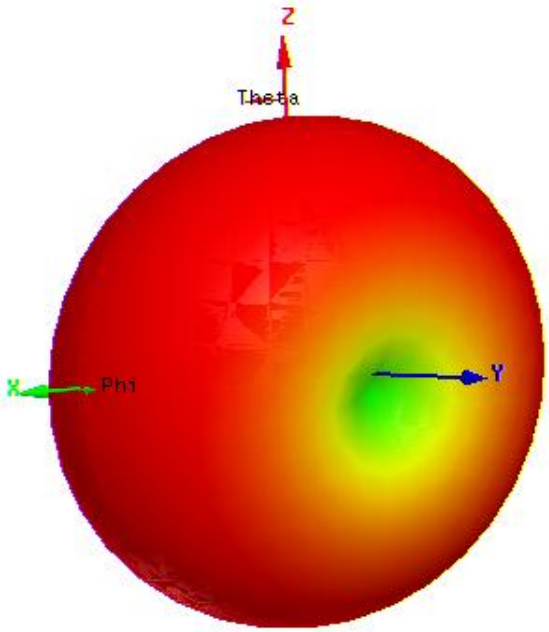

(a)

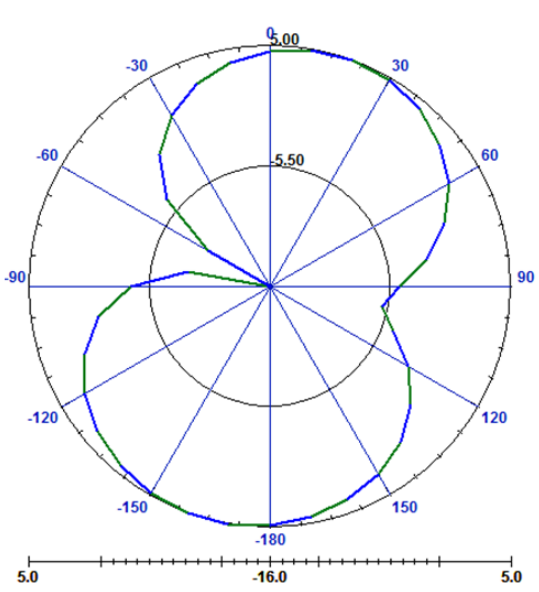

(b)

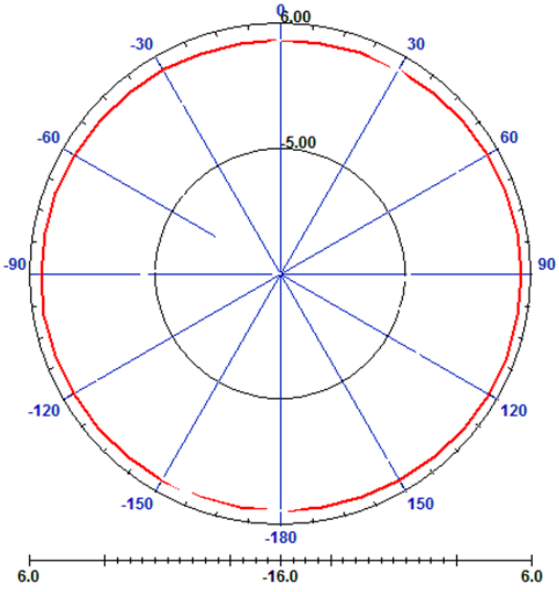

(c)

Figure 13: MLA (a) 3D Radiation Pattern (b) Azimuth (theta=90^0) Plane Pattern and (c) Elevation (phi=90^0)

The elevation plane pattern is formed by slicing the 3D pattern through an orthogonal plane (the y-z plane in this case). From the elevation plane pattern we see that the meander line antenna has an elevation plane beamwidth of around 90-degrees as an approximate value that we can extracted it from the pattern in Figure 13b. The elevation plane beamwidth is the total angular width between the two 3-dB points on the curve.

The azimuth plane pattern is formed by slicing through the 3D pattern in the vertical plane, the x-z plane in this case. Notice that the azimuth plane pattern is non-directional, that is, the antenna radiates its energy equally in all directions in the azimuth plane. So the azimuth plane pattern is a circle, passing through the peaks at all angles, shown in Figure 13c.

Figure 14 below shows the HFSS Model of the meander line antenna in its final design.

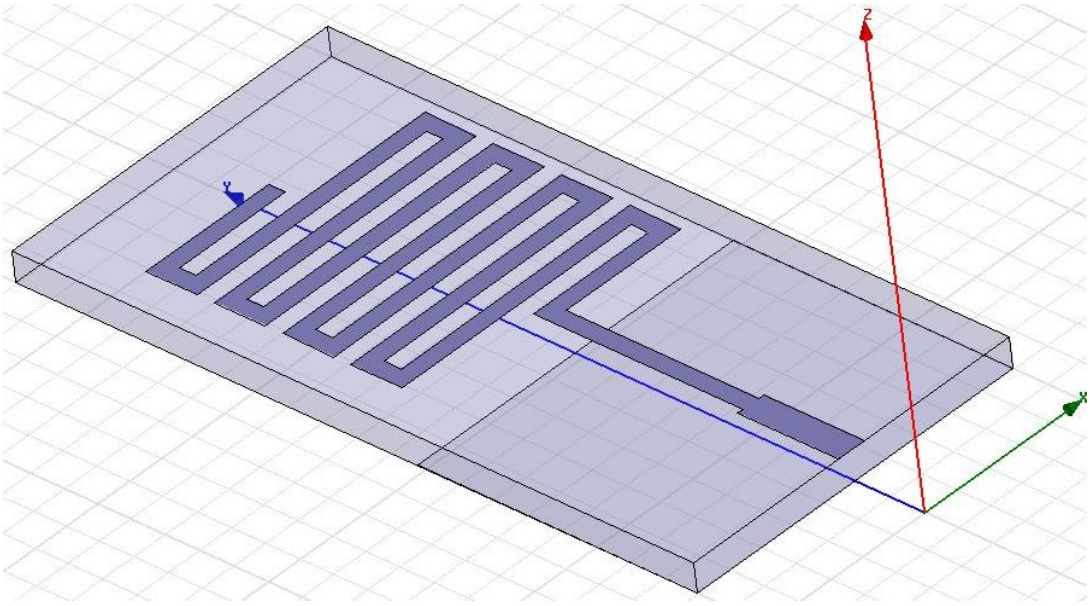

Figure 14: MLA HFSS Model

Now we need to prove that our antenna is indeed an electrically small antenna.

First condition for antenna to be considered as ESA is (ka<1)

$$ka < 1$$
$$\lambda = 211.4\ mm$$
$$k = \frac{2\pi}{\lambda} = 0.0297\ rad/mm$$
$$a < \frac{1}{k} = 33.645\ mm$$

According to our antenna it can be fit inside a sphere of radius $a = 22.36\ mm$

$$ka = 0.0297 * 22.36 = 0.665$$

We can see that (ka) is less than one and this 0.78 GHz meander line antenna is by definition an electrically small antenna. This antenna is known to be linear and polarized vertical to the ground plane so we easily calculate the radiation Q [**71**]

$$Q_L = \left(\frac{1}{ka}\right)^3 + \left(\frac{1}{ka}\right) = 4.91125 \qquad (3.7)$$

The actual value of the bandwidth is

$$BW = \frac{BW}{f_c} = 33.33\%$$

The approximate bandwidth for an RLC type circuit in terms of Q is:

$$BW = \frac{S-1}{Q * \sqrt{S}} \qquad (3.8)$$

Where, S is the Voltage Standing Wave Ratio (VSWR), BW is the Normalized Bandwidth

$$Let\ S = 2,\ then$$
$$BW = \frac{1}{\sqrt{2} * Q} = 10.18\% < 33.33\%$$

But this does not match with the actual percent bandwidth of 33.33%. So we need to find the value of Q that gives the actual bandwidth of 33.33%, from (3.8) we find Q_L=2.1213 for this bandwidth, then we need to find the value of (ka) that will give this Q_L from (3.7)

$$ka \approx 0.969$$
$$a = \frac{0.969}{0.0297} = 32.602\ mm$$

In practice, the gain of an electrically small antenna is bounded. This limitation has been expressed by Harrington [**72**] as

$$G = (ka)^2 + 2(ka) \qquad (3.9)$$

So, when (a=22.36 mm) we have a maximum gain of (G=1.74 dB) and when (a=32.602 mm) the maximum gain become (G=2.877 dB)

In some cases after matching, the impedance bandwidth would decrease or in some cases increase. A fundamental limitation on antenna size versus impedance bandwidth brings order to what can appear to be mysterious changes in antenna performance.

3.3 Parameters Variation

There are many parameters that need to be investigated in order to have a general view of the effect of every parameter and these parameters are:

3.3.1 Dielectric Permittivity (ε_r)

FR-4 glass epoxy is a popular and versatile high pressure thermoset plastic laminate grade with good strength to weight ratios. With near zero water absorption FR-4 is most commonly used as an electrical insulator possessing considerable mechanical strength. The material is known to retain its high mechanical values and electrical insulating qualities in both dry and humid conditions. These attributes, along with good fabrication characteristics, lend utility to this grade for a wide variety of electrical and mechanical applications.

Dielectric constant or permittivity($\boldsymbol{\varepsilon_r}$) for this material has a minimum value of (4.0) and a maximum value of (4.8). [**73**]

Table 5: Dielectric Permittivity Effect on the Design

ε_r	$f_c\ (GHz)$	$S_{11}\ (dB)$	$BW\ (MHz)$
4	0.78	-32.52	240
4.4	0.78	-30.9	260
4.8	0.77	-31.68	260

In Table 5 above, it shows different dielectric constant values for the same FR-4 material and the corresponding center frequency, reflection coefficient and bandwidth. We notice that the resonant frequency decreases as the dielectric constant increase.

3.3.2 Spacing Between MLA Arms

The spacing (W4 in figure 11) between two bends is very critical, where if the bends are too close to each other, then cross coupling will be more, which affects the polarization purity of the resultant radiation pattern.

In other case the spacing is limited due to the available array grid space and also the polarization of the radiated field will vary with the spacing between the bends, and the spacing between the microstrip lines. The present meander line structure is designed with liner polarization with less cross coupling between the bends, to fit within the available array grid size.

The following three figures show the effect of spacing on frequency, reflection coefficient and on bandwidth. We notice from figure 15 that as the spacing between meander line arms increased the center frequency will reduce, while figure 16 shows the effect of spacing on the reflection coefficient and we can see that as the spacing increased until a certain value the reflection coefficient will be further improved and if it is increased more than that the reflection will reduce but it is still gives a good reflection. Figure 17 shows the relationship between the spacing and bandwidth and it is obvious to notice that as the spacing increased the bandwidth will reduce, which is almost same relation as with the frequency.

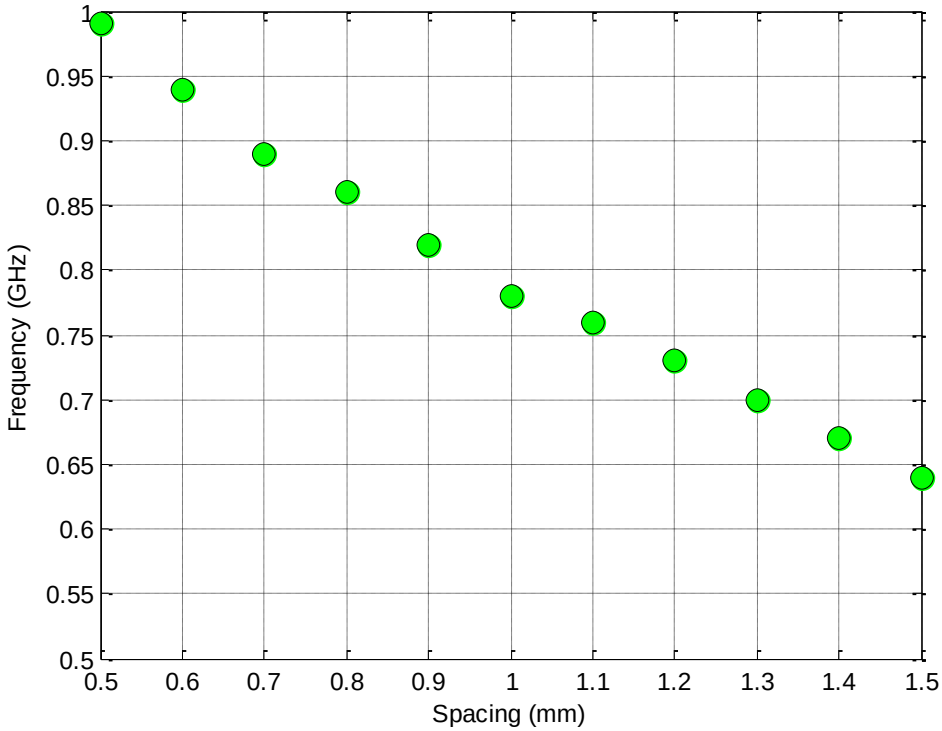

Figure 15: Effect of Spacing on Center Frequency

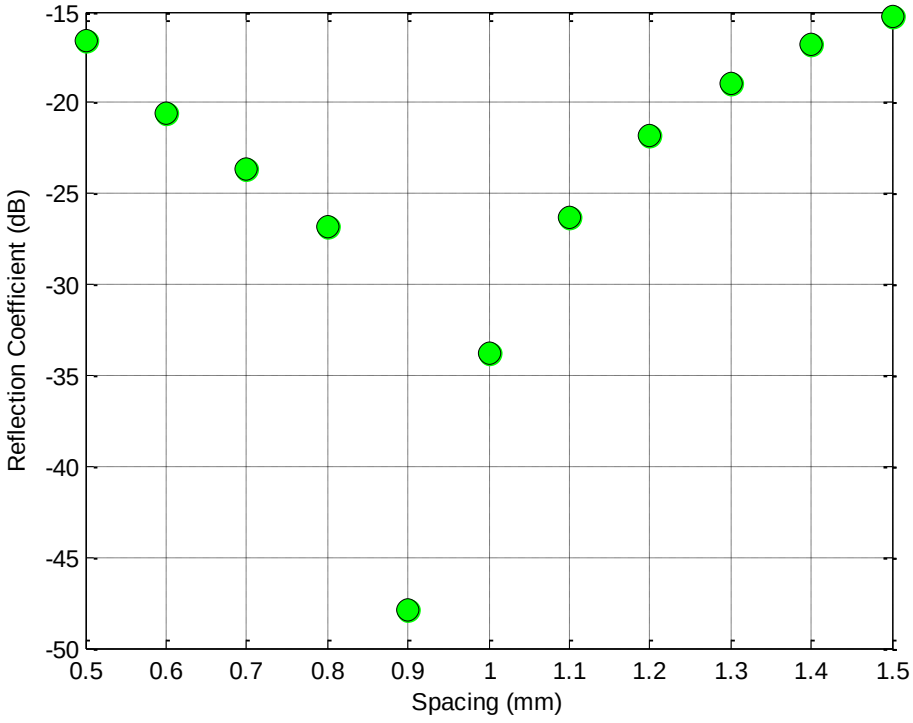

Figure 16: Effect of Spacing on Reflection Coefficient

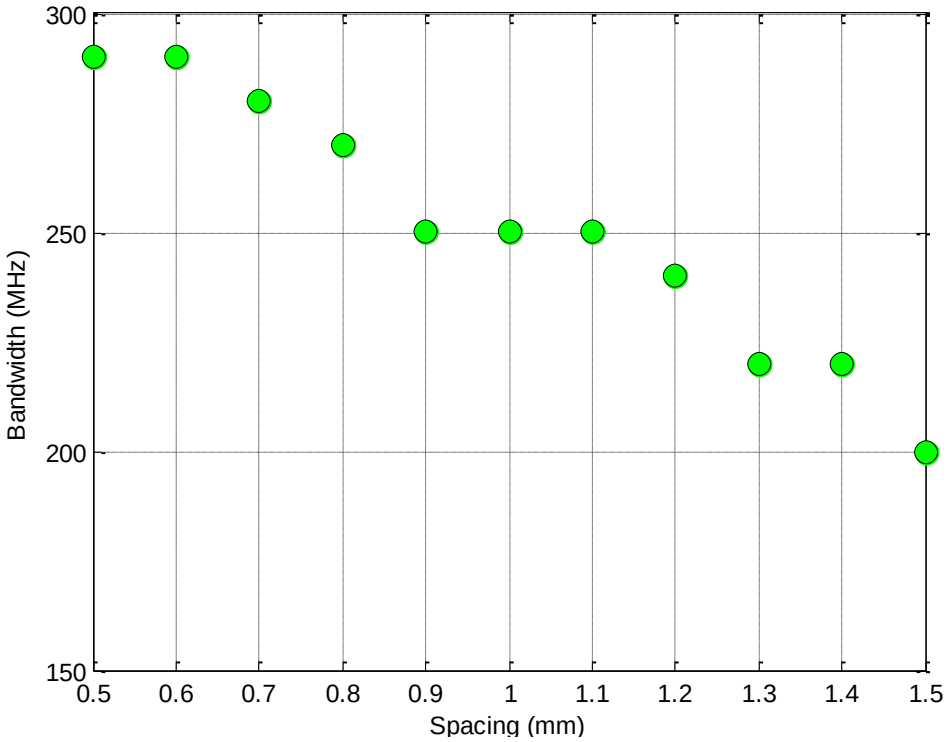

Figure 17: Effect of Spacing on Bandwidth

3.3.3 Width of the Meander Line Antenna

Now, we study the effect of varying the width of the meander line in our parameters.

The effect of MLA width (W5 in figure 11) on frequency as shown in Figure 18 and reflection coefficient in Figure 19 has the same effect of the spacing on these parameters, while the effect of the width of the mender on the bandwidth has different relation that if the width increased the bandwidth also increased which is a direct relationship (See Figure 20).

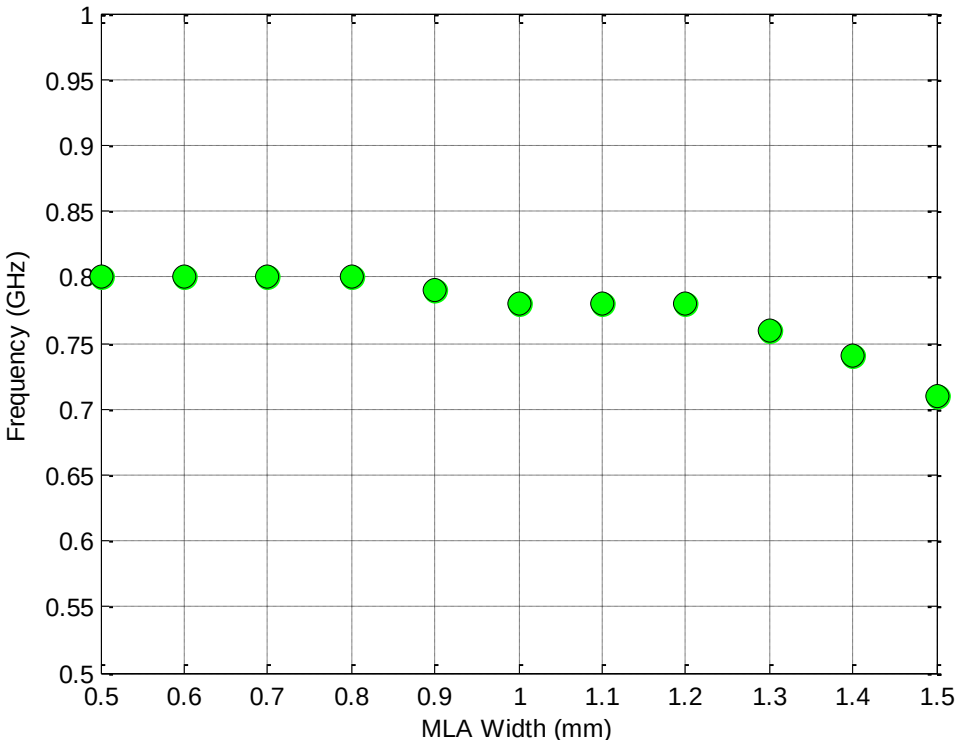

Figure 18: The effect of Varying the MLA Width on Frequency

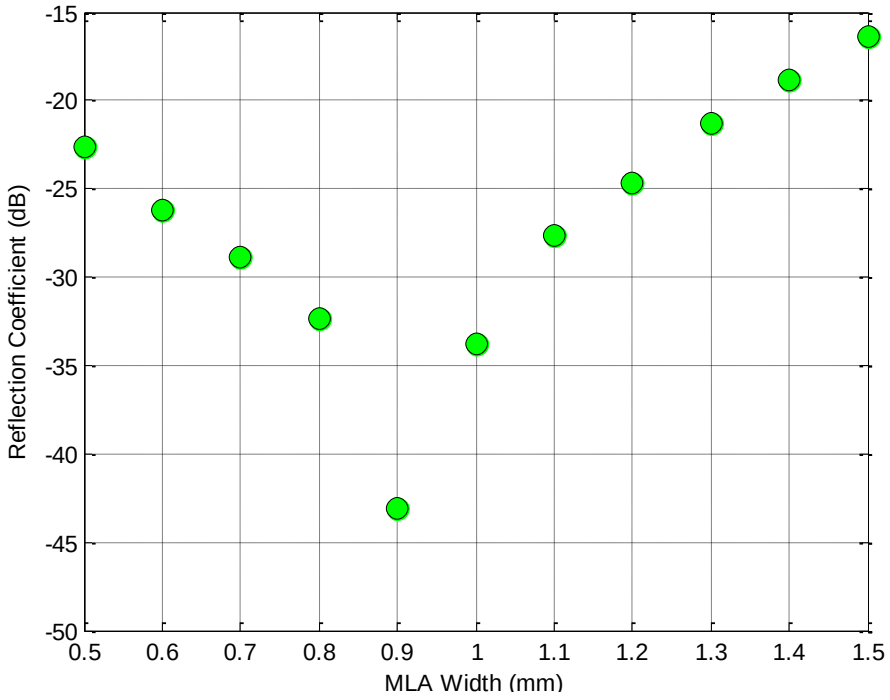

Figure 19: The effect of Varying the MLA Width on Reflection Coefficient

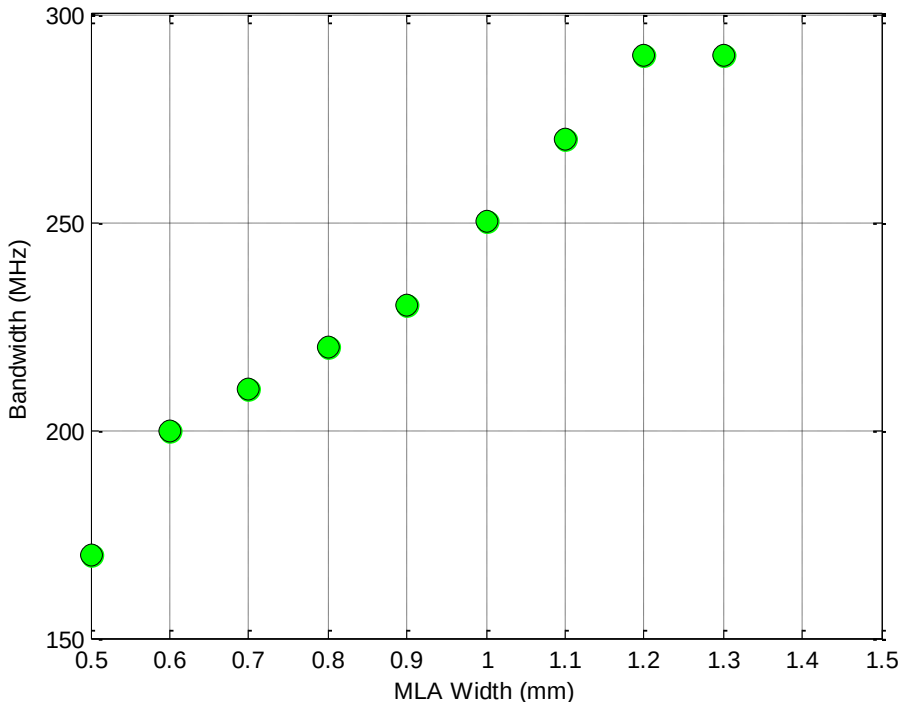

Figure 20: The effect of Varying the MLA Width on Bandwidth

3.3.4 Length of the Meander Line Antenna

The length of the mender line (S in figure 11) also has its effect on the design parameters, and this effect appears mainly on the frequency as illustrated in Figure 21 that the frequency goes down as the width of the mender line increases, but its effect on reflection coefficient and bandwidth is less obvious than the frequency but we can see that if the width increases the reflection coefficient increase (Figure 22) and the bandwidth will decrease (Figure 23).

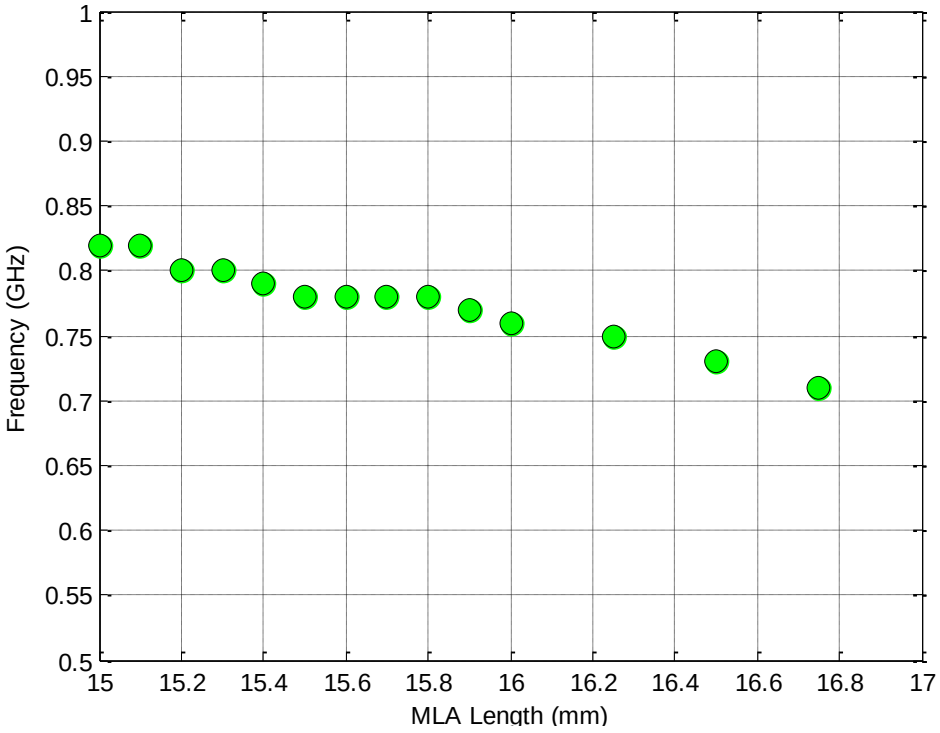

Figure 21: The effect of Varying the MLA Length on Frequency

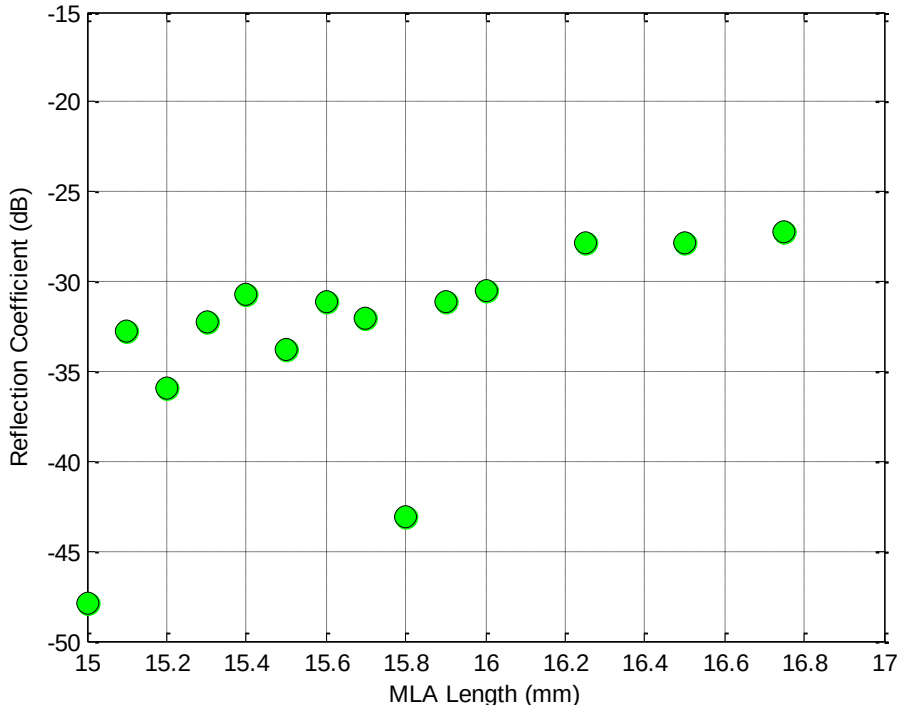

Figure 22: The effect of Varying the MLA Length on Reflection Coefficient

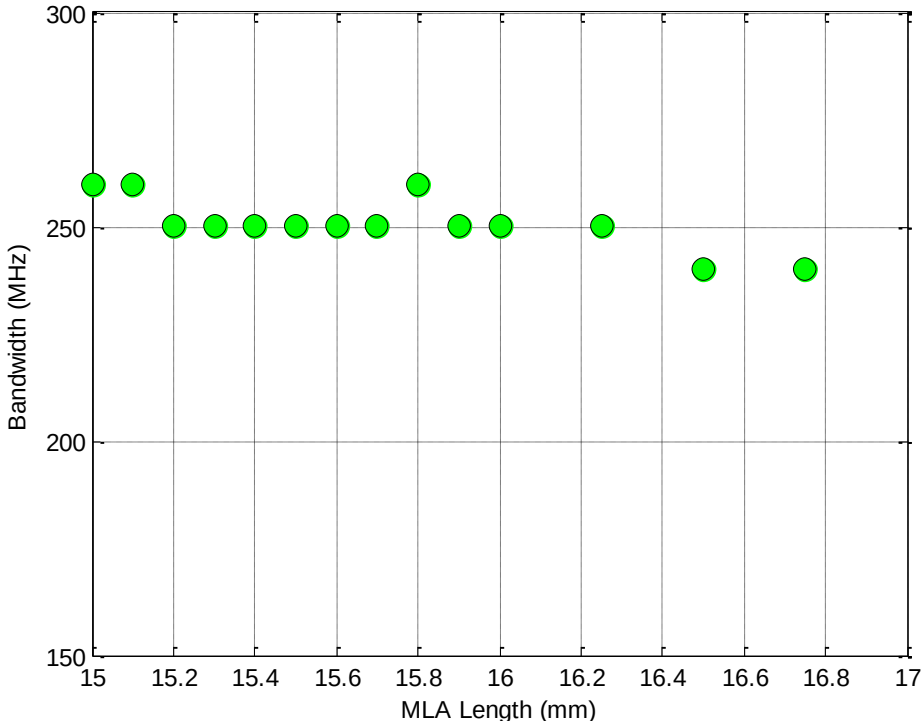

Figure 23: The effect of Varying the MLA Length on Bandwidth

3.3.5 Width of the Matching Line

The matching line (W3 in figure 11) that fed the meander line antenna effect has also been investigated and the results are shown below

As the width of the matching line increased more than (1mm) its effect on frequency becomes obvious but less than that it has no effect on the frequency that what we can say about Figure 24, also same thing that we can say about its effect on the bandwidth it has no effect if the width is lower than (1.2 mm) and more than that it will affect (See Figure 26), furthermore as the matching line increase the reflection coefficient will reduce but still gives an acceptable reflection as Figure 25 shows.

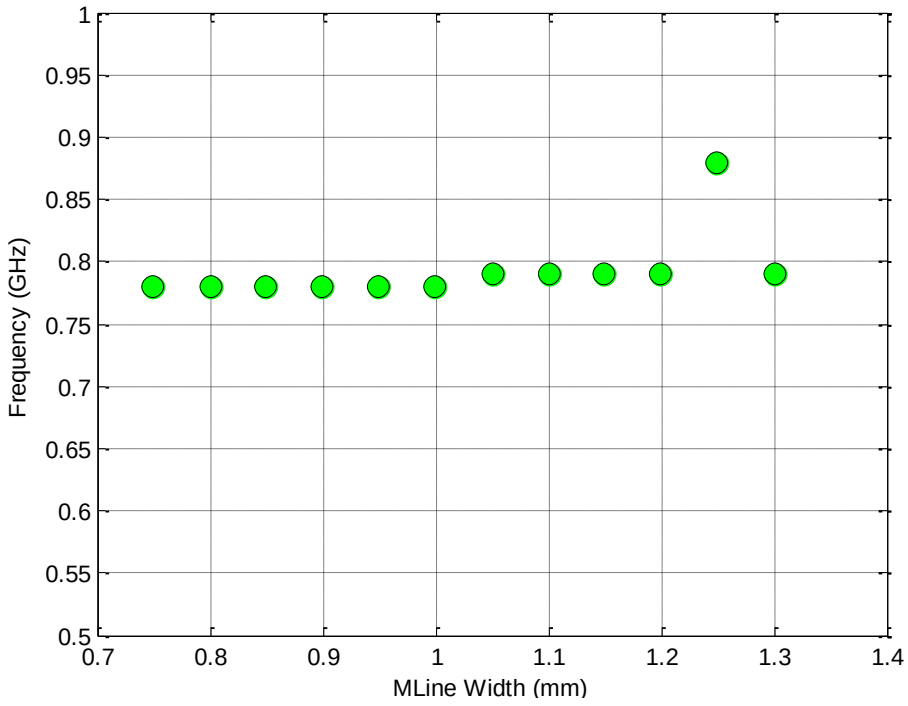

Figure 24: The effect of varying the Matching Line Width on Frequency

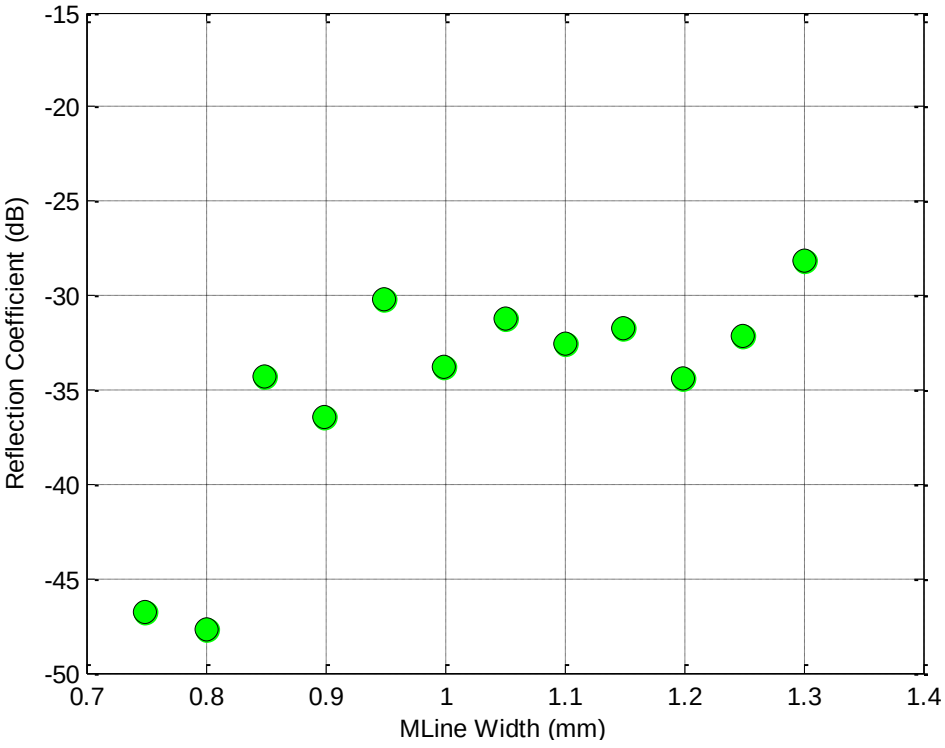

Figure 25: The effect of varying the Matching Line Width on Reflection Coefficient

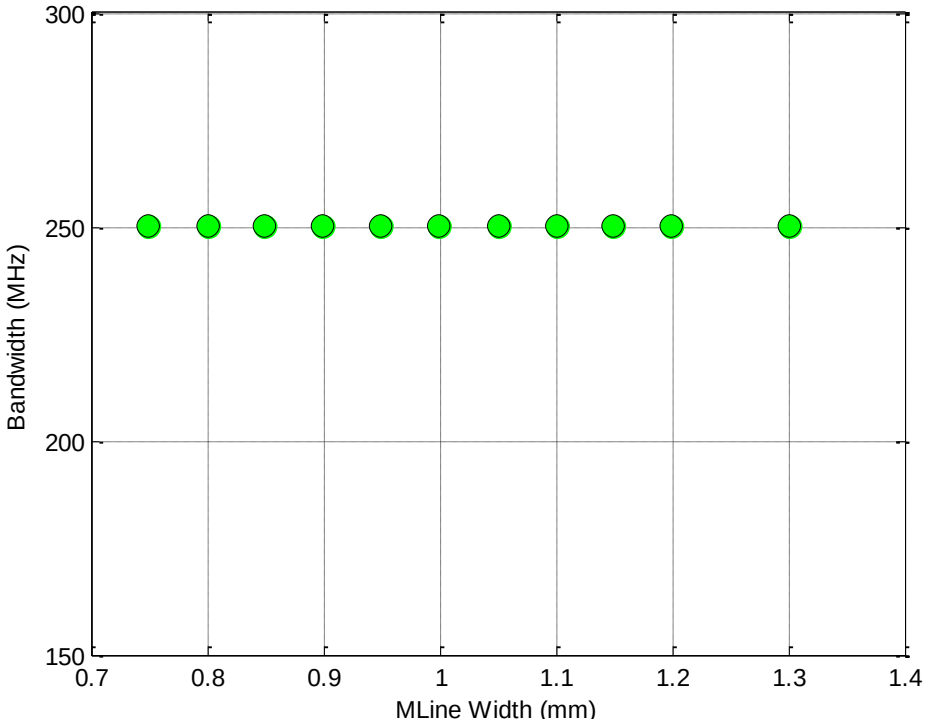

Figure 26: The effect of varying the Matching Line Width on Bandwidth

3.3.6 Length of the Ground Plane

The last parameter that has been investigated is the length of the ground plane (Lg in figure 11), and it has a direct relation effect on the frequency and bandwidth that means if the ground area increased both frequency and bandwidth will increase as Figures 27 & 29 illustrate, but the reflection coefficient becomes better as the ground length increased until a certain limit then the reflection will become higher but again it still less than -10 dB which could considered as a good reflection, as shown in Figure 28.

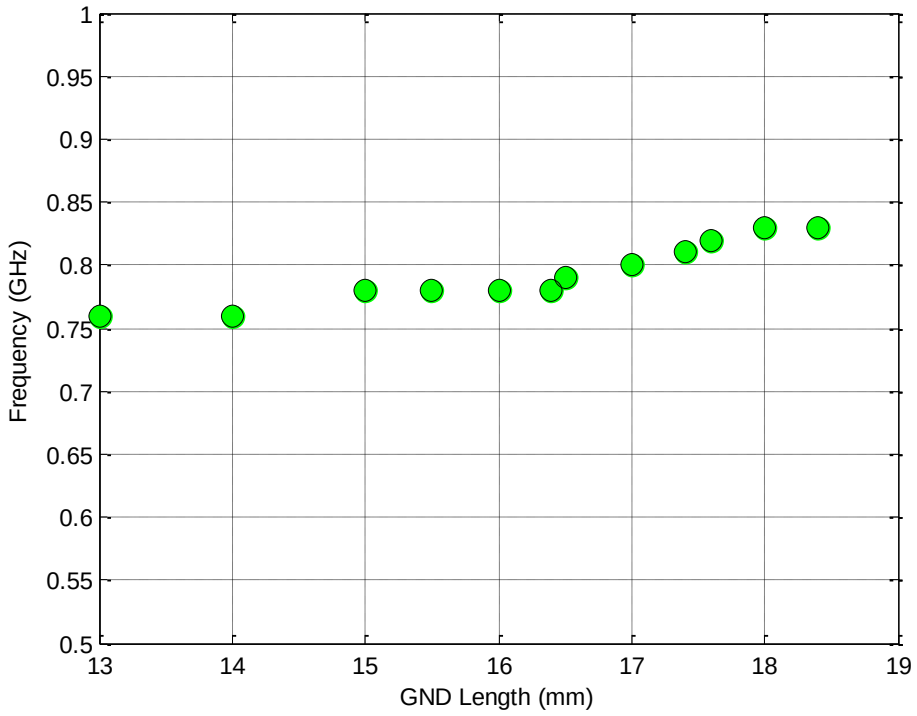

Figure 27: The effect of Varying the Ground Plane Length Width on Frequency

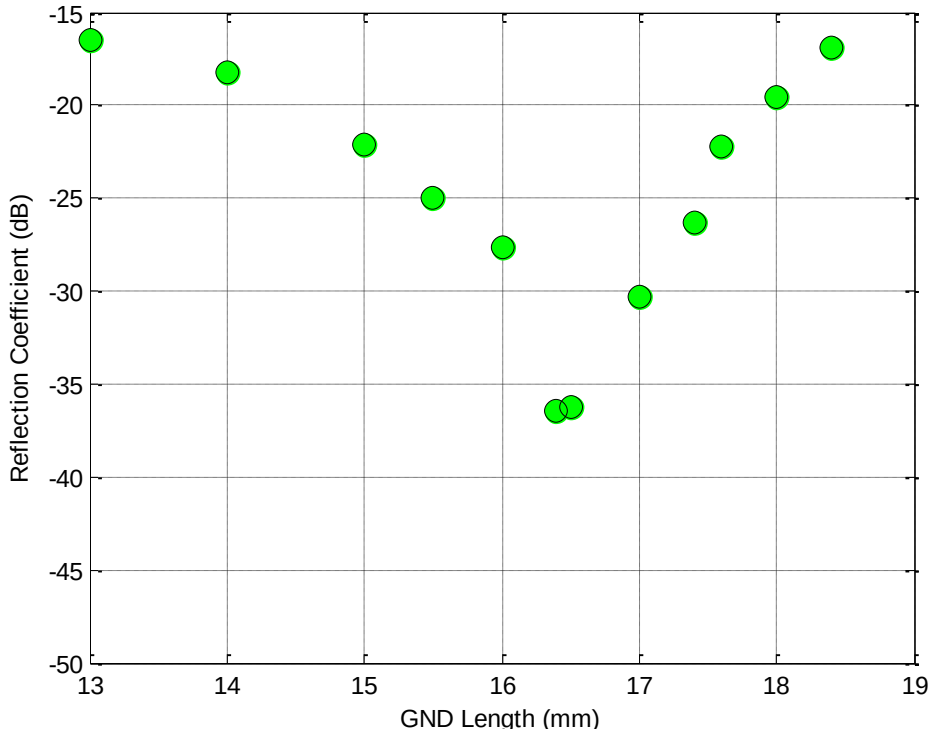

Figure 28: The effect of Varying the Ground Plane Length Width on Reflection Coefficient

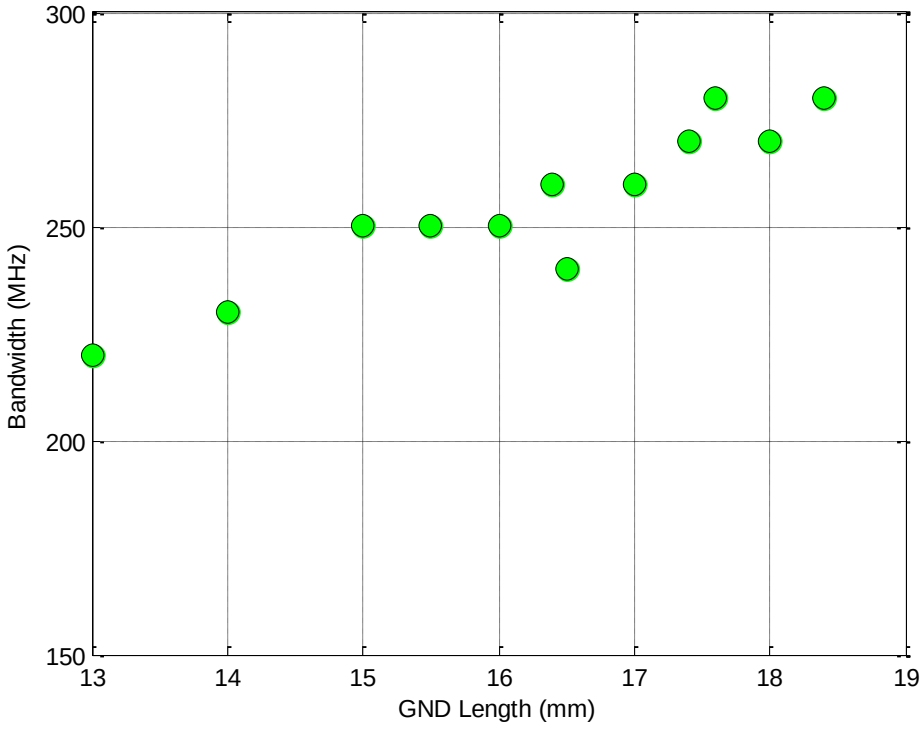

Figure 29: The effect of Varying the Ground Plane Length Width on Bandwidth

3.4 Planar Inverted F Antenna (PIFA)

Since PIFA are more commonly used in mobile phones due to many advantages mentioned before in 2.2.3, we design another antenna to meet the same specifications from the operating frequency point of view and to compare our design with this one from different aspect such as antenna size, Bandwidth, gain, radiation patterns, thickness of the substrate etc.

The HFSS designed model of the PIFA is shown in Figure 30 which consist from a substrate of FR-4 material which is the same material used in the previous design with a

dielectric constant of 4.4 and large ground plane with area of 30x80mm^2 and a patch antenna with area of 30x22mm^2 and a shorting pin and feeding point as shown in the figure. Table 6 summarizes the specifications for this antenna.

Figure 31 shows the reflection coefficient of this antenna that operates at our required frequency with a value of -22.59 dB and has a band width of 20 MHz, and the 3D radiation pattern is shown in Figure 32.

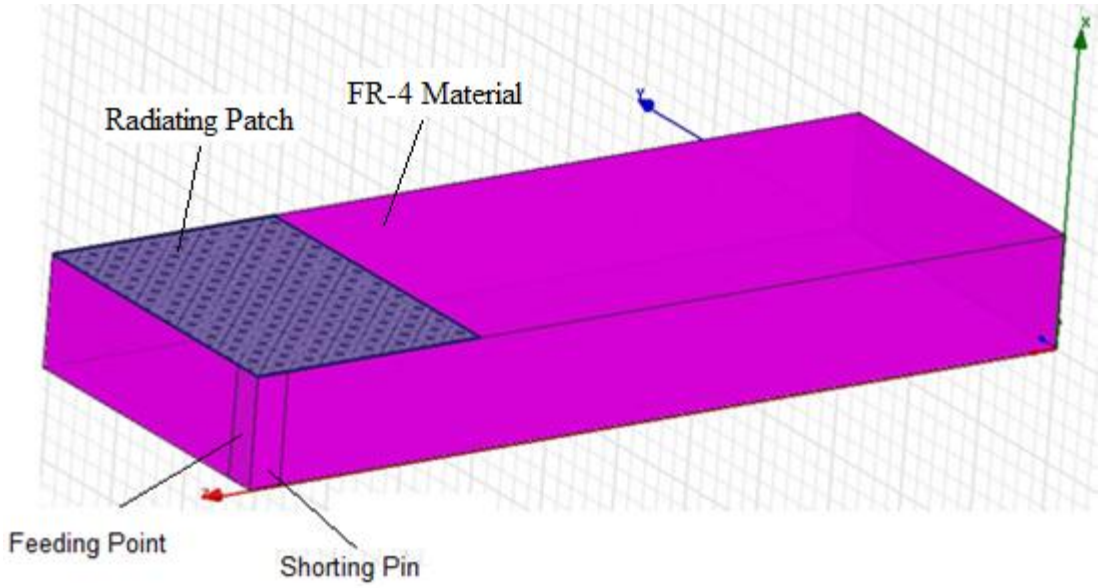

Figure 30: HFSS Model for the PIFA Antenna

Table 6: PIFA Specifications

Frequency	S_{11}	Bandwidth	Width	Length	Thickness
780 MHz	-22.59 dB	20 MHz	30 mm	80 mm	10 mm

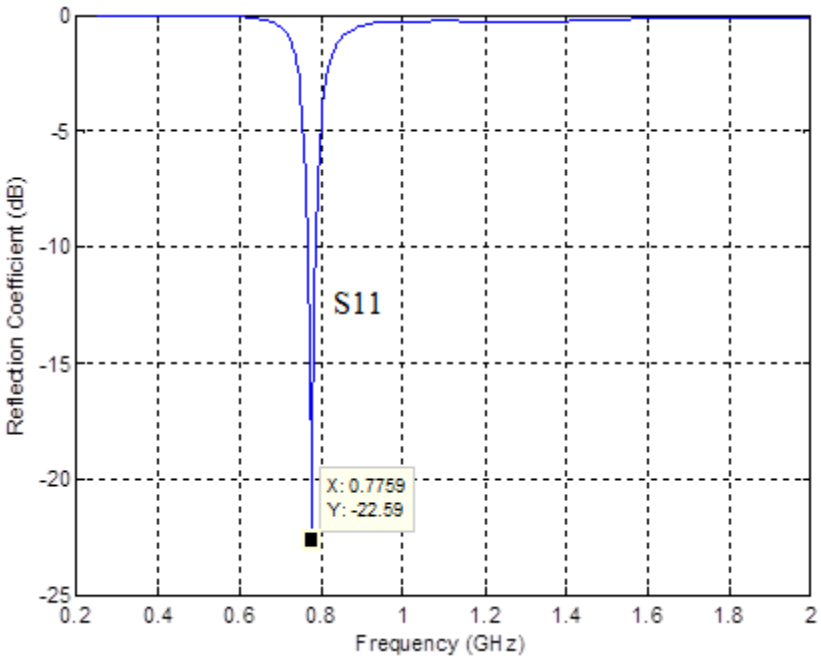

Figure 31: Reflection Coefficient for the PIFA Antenna

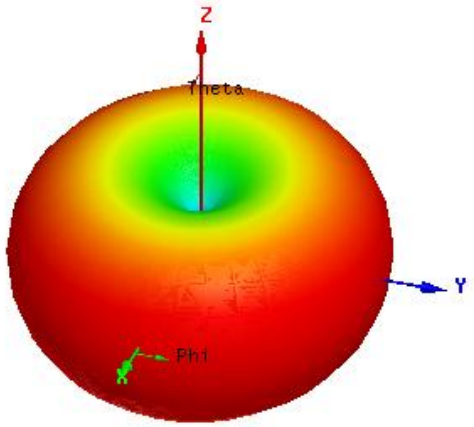

Figure 32: 3D Radiation Pattern for the PIFA Antenna

3.5 Conclusion

In this chapter we have presented three types of printed antennas, the first one it is based on empirical equation and it is seen that by theoretical calculation of meander line antenna parameter, the empirical relationship between dimension and various parameter of meander line antenna at desired frequency range can be calculated. The empirical relation obtained is useful for structuring the meander line antenna but it is not useful in our case.

Second one it is an electrically small antenna which has a huge reduction in terms of size compared to first designed antenna and the last antenna is a planar inverted F antenna that has a larger size and thickness compared with the electrically small antenna.

Table 7 summarizes the differences between the two designed antennas. It is evident that the ESA MLA antenna is more suitable for use due to its size is much less than PIFA.

Table 7: Differences between MLA & PIFA

	MLA	PIFA
Bandwidth	260 MHz	20 MHz
Length	40 mm	80 mm
Width	20 mm	30 mm
Thickness	1.6 mm	10 mm

CHAPTER 4

Design of a MIMO Antenna System

The design of a multiple input and multiple output (MIMO) antenna for LTE systems is presented here. The MIMO antenna comprises of a two element meander line linear array. The designed antenna is optimized using HFSS simulator and the mutual coupling between the antennas elements are improved using a novel technique. A detailed overview of a MIMO and array antenna is presented in section 2.4.

4.1 Design of a 2 Element MIMO Antenna System

The design procedure of a MIMO antenna is presented in this section. The designing consist of the 2 element meander line antenna (MLA), positioned reasonably apart to satisfy the limitation related to antenna size and mutual coupling between elements. The configurations of MIMO antennas investigated with four different arrangements of the meander line elements are shown in Figures 33(a) to 36(a). The reflection and isolation responses (S_{11}, S_{22} and S_{21}) of these configurations are plotted in Figures 33(b) to 36(b), respectively. Note that in Figure 33(b), the reflection responses (S_{11} and S_{22}) of the MIMO configuration #1 demonstrate an impedance bandwidth of

25% with mutual isolation -7.10dB. Although the reflection response is acceptable, but the isolation needed improvement.

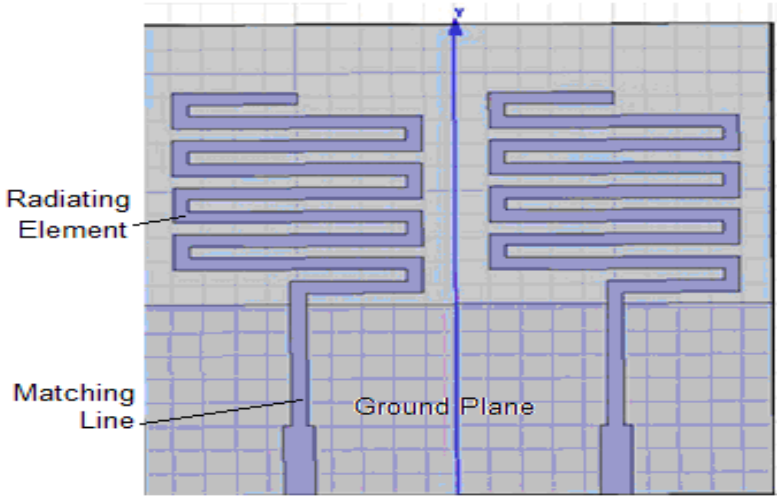

(a)

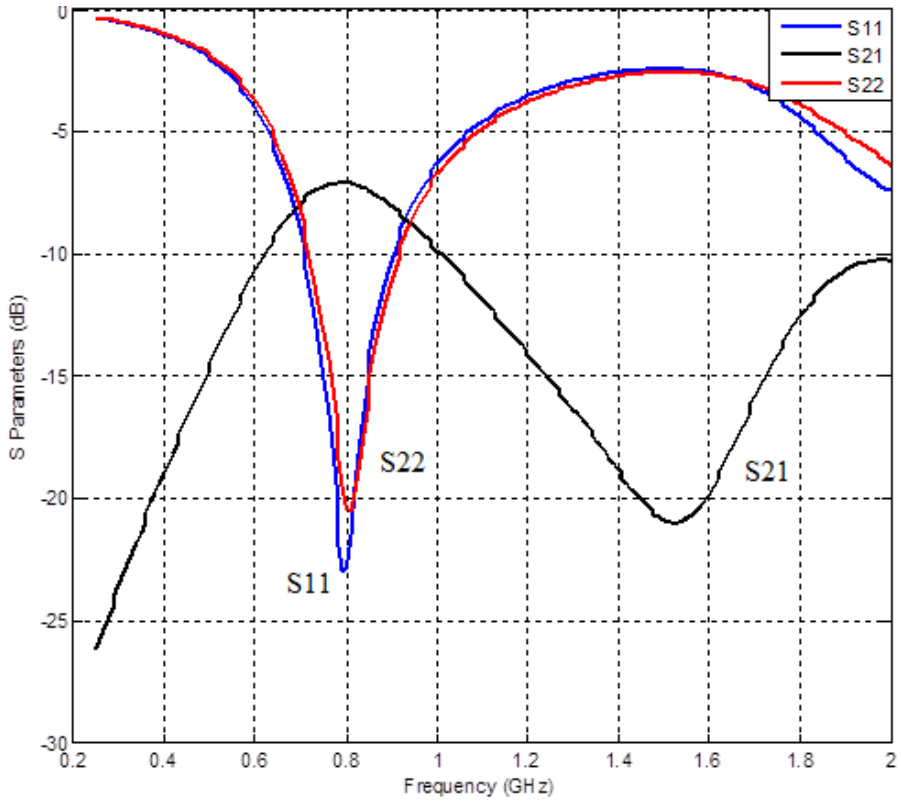

Figure 33: (a) MIMO antenna configuration-#1 (b) S-parameter Responses

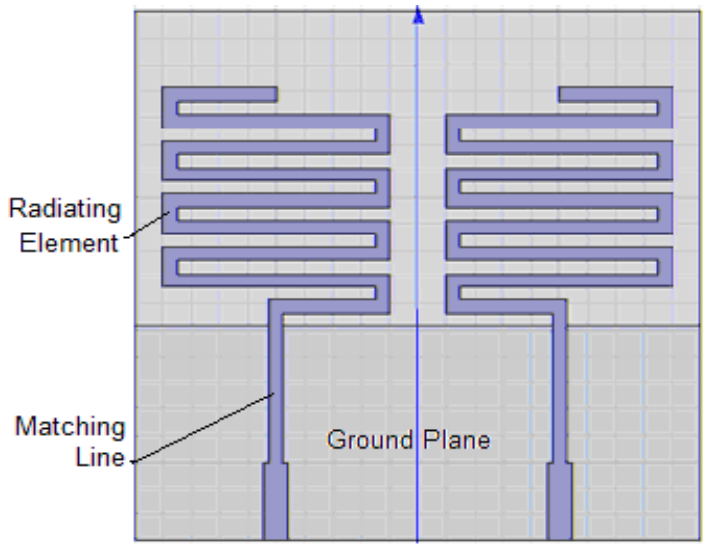

(a)

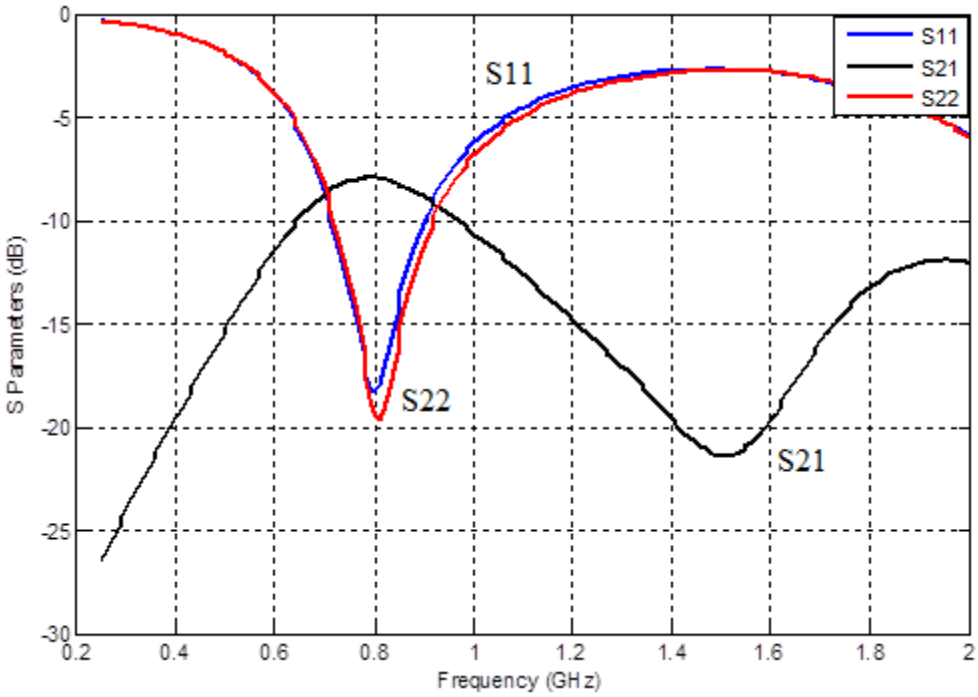

(b)

Figure 34: (a) MIMO antenna configuration-#2 (b) S-parameter Responses

So the meander line elements are placed as configuration #2, and the S-parameter response is shown in Figure 34(b). It is evident from this figure that the isolation has improved to -7.91 dB without affecting the reflection response. Then the meander line elements are poisoned in configurations #3 and #4, shown in figures 35(a) and 36(a). Note that the isolation responses (S_{21}) of figures 35(b) and 36(b) clearly indicate the improvement without affecting the reflection response. The resonant frequency and the dB values of the reflection and isolation responses related to these configures are tabulated in Table 8. Note that the best isolation achieved is -10.54 dB, and needs to be improvement to avoid cross talk between the antenna elements. Novel techniques employed for this purpose are discussed in the following sections.

Table 8: Summary for the Four Cases of MIMO Antenna

Configuration #	**Frequency**	**S11**	**S22**	**S21**
1	0.78 GHz	-23.13 dB	-20.49 dB	-7.10 dB
2	0.78 GHz	-19.39 dB	-19.39 dB	-7.91 dB
3	0.78 GHz	-27.79 dB	-31.33 dB	-9.78 dB
4	0.80 GHz	-26.07 dB	-28.71 dB	-10.54 dB

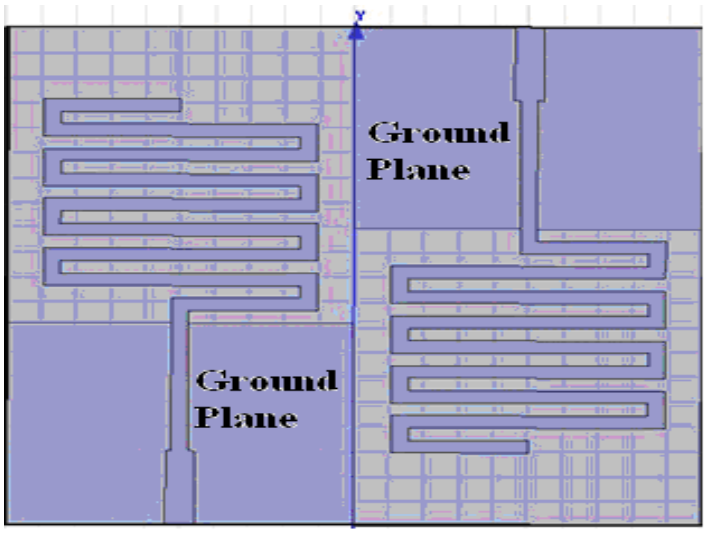

(a)

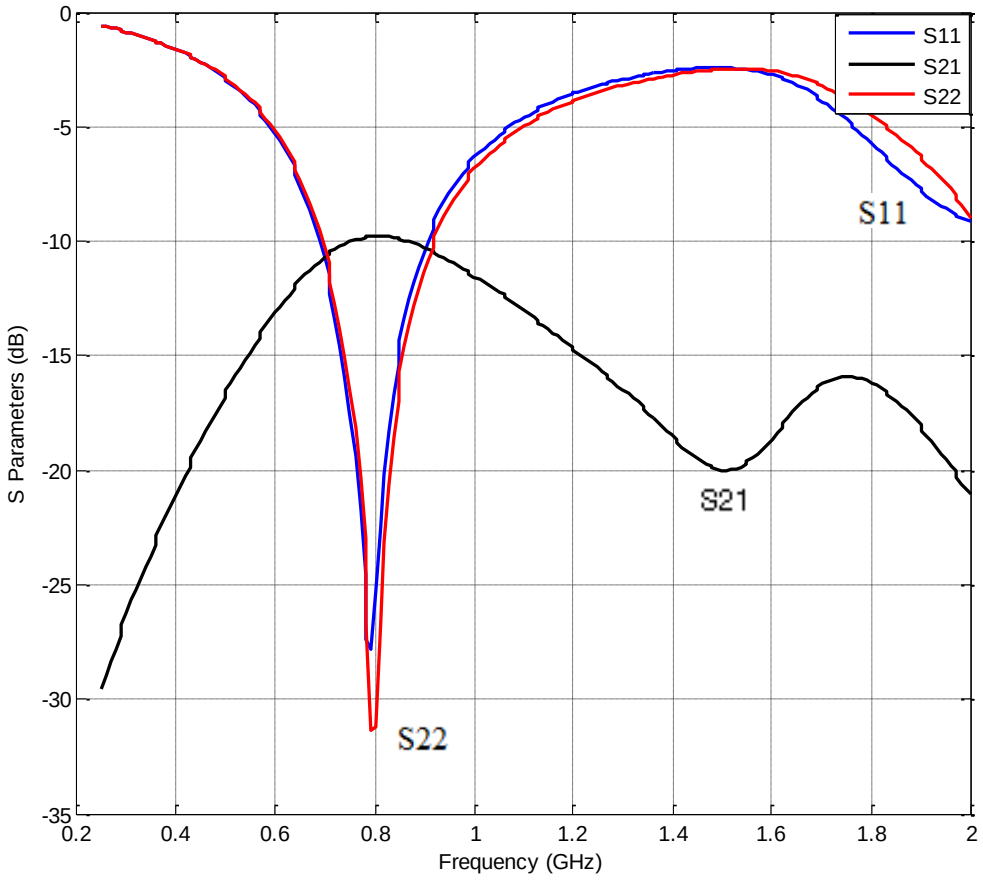

(b)

Figure 35: (a) MIMO antenna configuration-#3 (b) S-parameter Responses

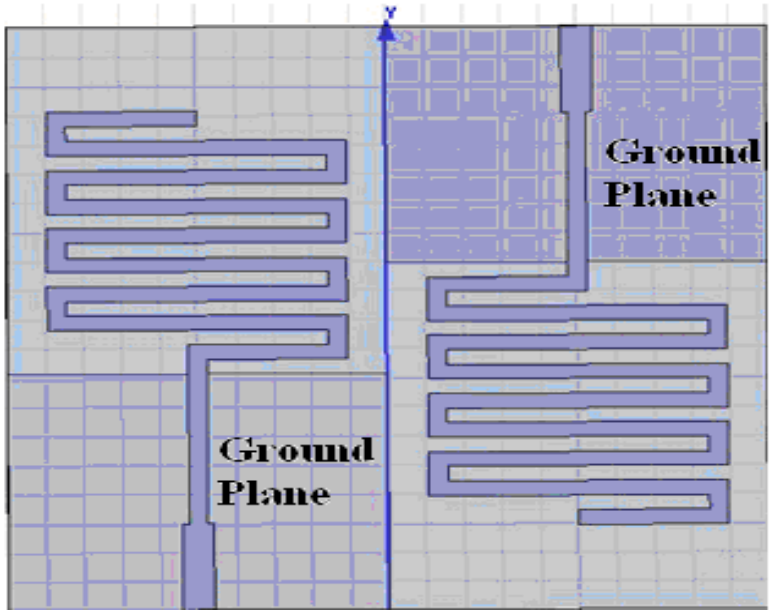

(a)

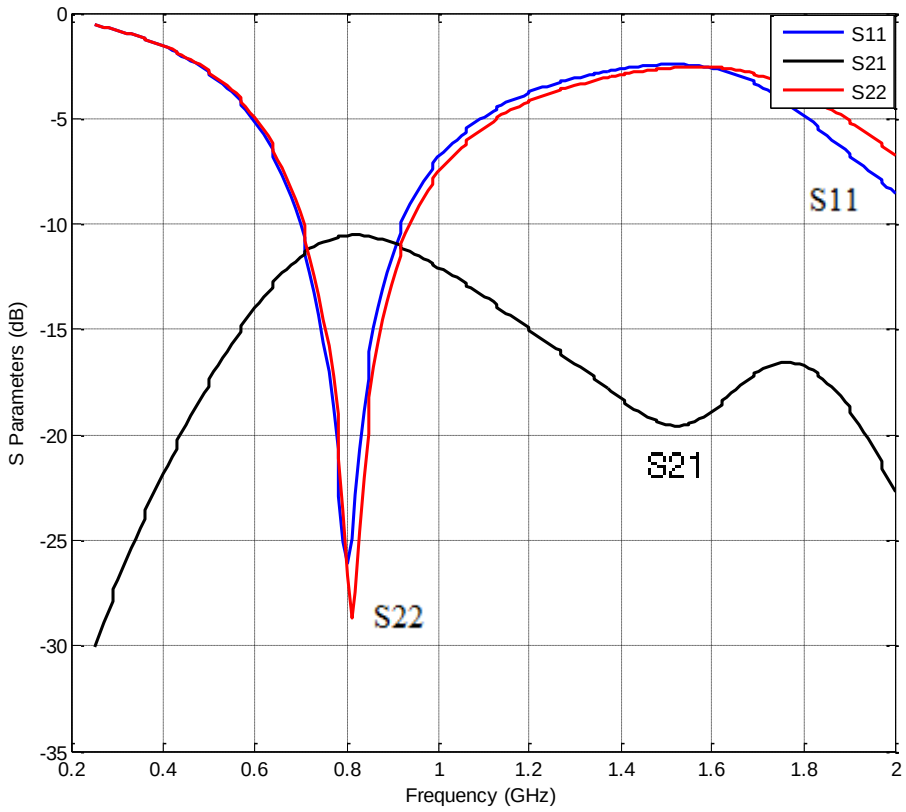

(b)

Figure 36: (a) MIMO antenna configuration-#4 (b) S-parameter Responses

4.2 Improving Isolation between Antenna Elements

Novel techniques are discussed here section to improve the isolation or correlation coefficient between the adjacent elements of the MIMO antenna. The first method adopted here to improve the mutual coupling increases the separation between the antenna elements. Figure 37 shows a MIMO antenna with antenna elements placed apart from each other to reduce the isolation or mutual coupling. Figure 38 plots the isolation with increasing substrate width, while the antenna elements are always placed at the center of each side of the substrate. Note that this technique allows us to improve the isolation up to -14.2dB. The improvement of isolation can be further improved by increasing the substrate, while keeping the distant between the antenna and the substrate edge constant. The isolation response for this case is shown in figure 39, where best possible isolation is -22dB. Note that in both above cases, the isolation is improved at the cost of the total size of the MIMO antenna, although they were kept within the limit of LTE specifications.

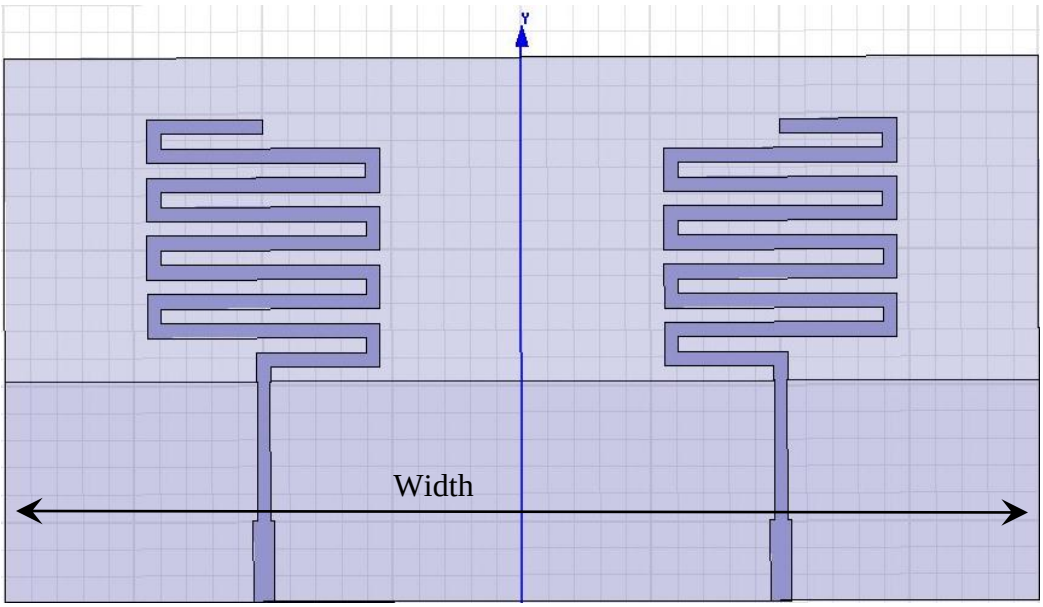

Figure 37: 4x8cm with Antenna being in the middle of each Half

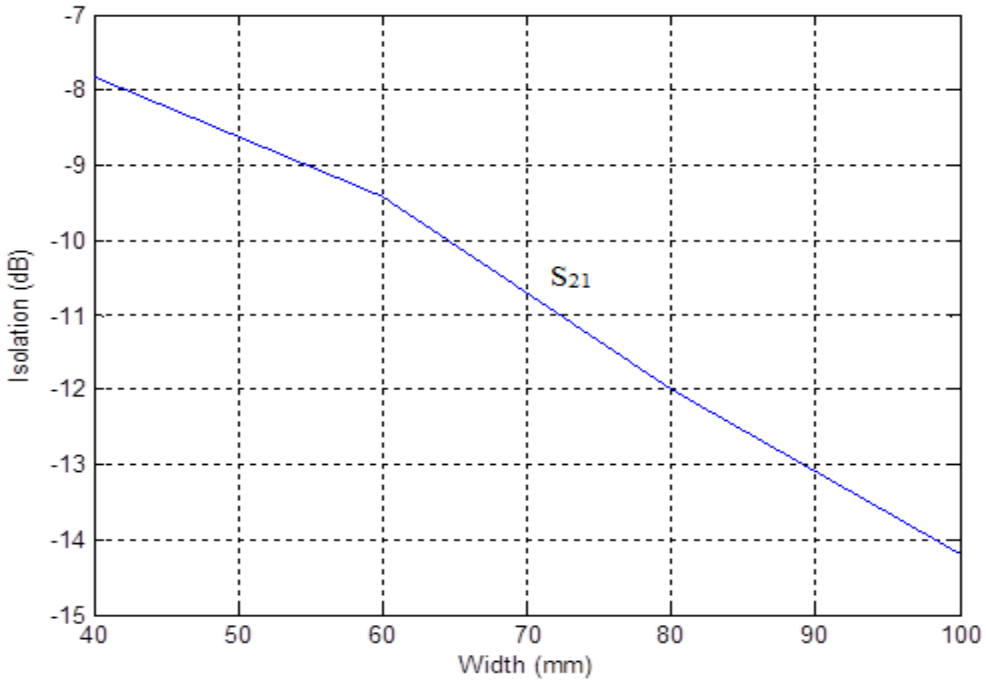

Figure 38: Isolation Reduction by Separation

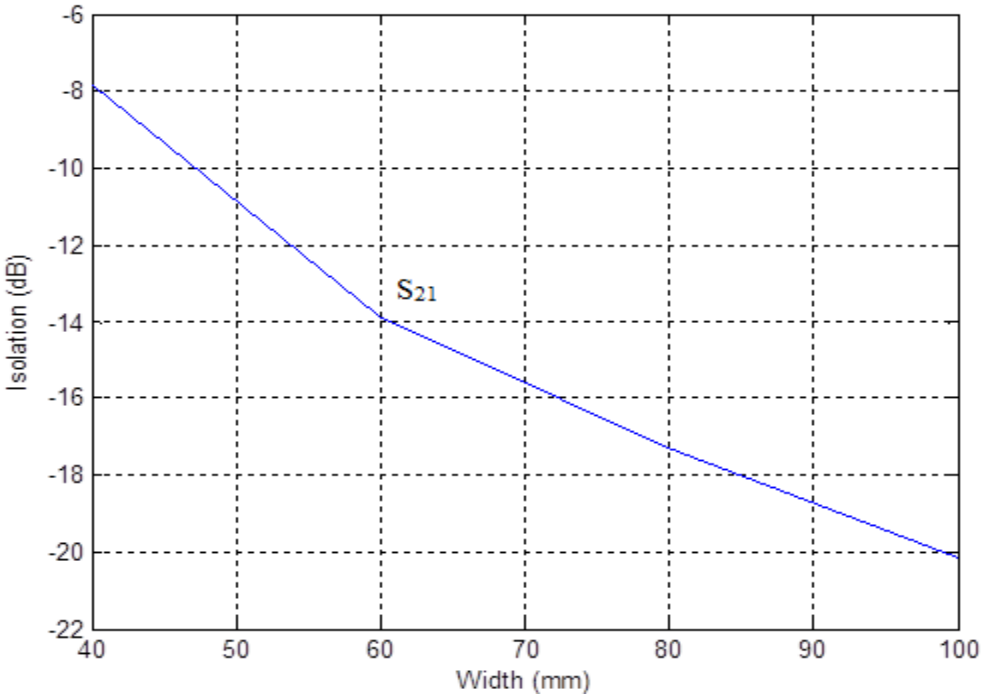

Figure 39: Isolation Reduction by Separation with the Distance between the Antennas and the Edge Being Fixed

The second method adopted here used a grounded metal strip to increase the isolation of the antenna elements. This configuration is shown in Figure 40. This method can give good results for isolation but unfortunately the reflection coefficient will go worst, so in this method the best value for the isolation we get with better reflection is $S_{21} = -9.27\ dB$ at the design frequency and it is shown in Figure 41 with the width and length of the ground metal strip as shown in Figure 40. The effect of changing the length and width of this ground strip element is shown in Figure 42. Note that with increasing width of the element the isolation will reduce and with increasing length it will also reduce.

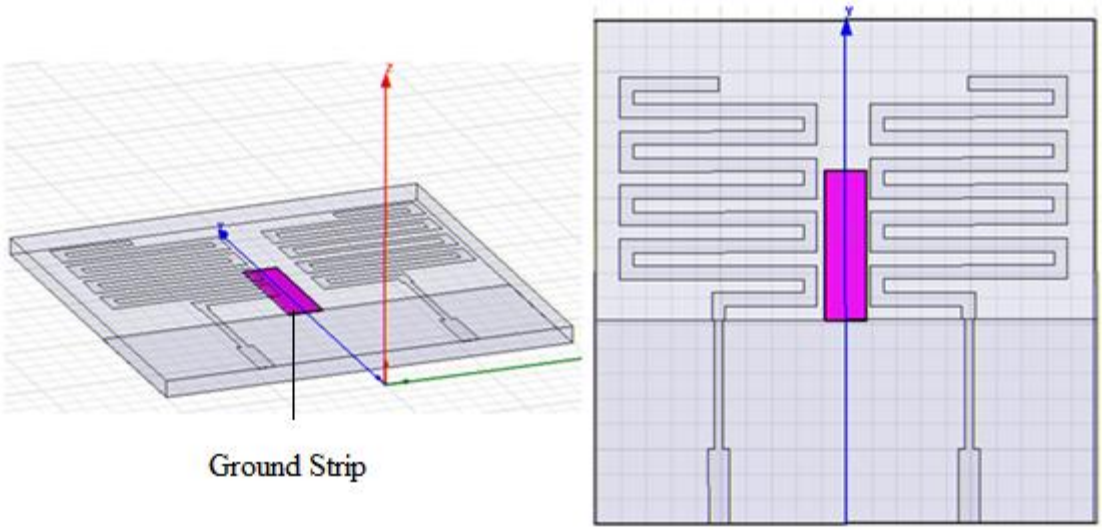

(a) (b)

Figure 40: Isolation Reduction by Inserting a Ground Strip (a) 3D view and (b) Top view

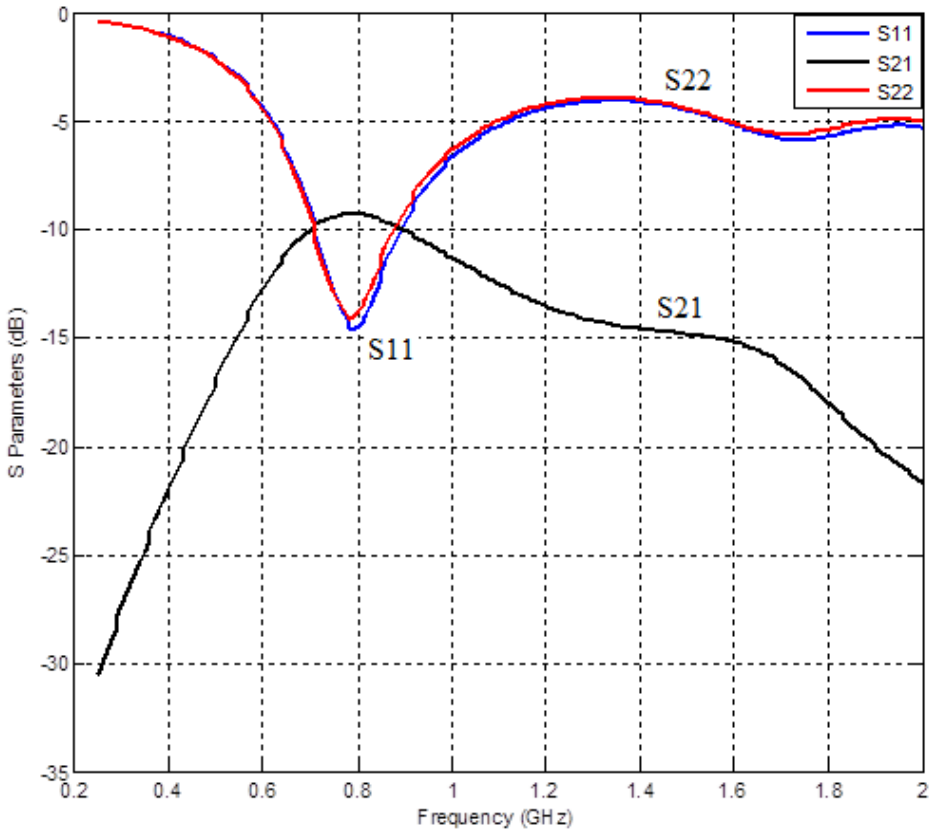

Figure 41: S-Parameter Responses of the MIMO Antenna with Ground Strip

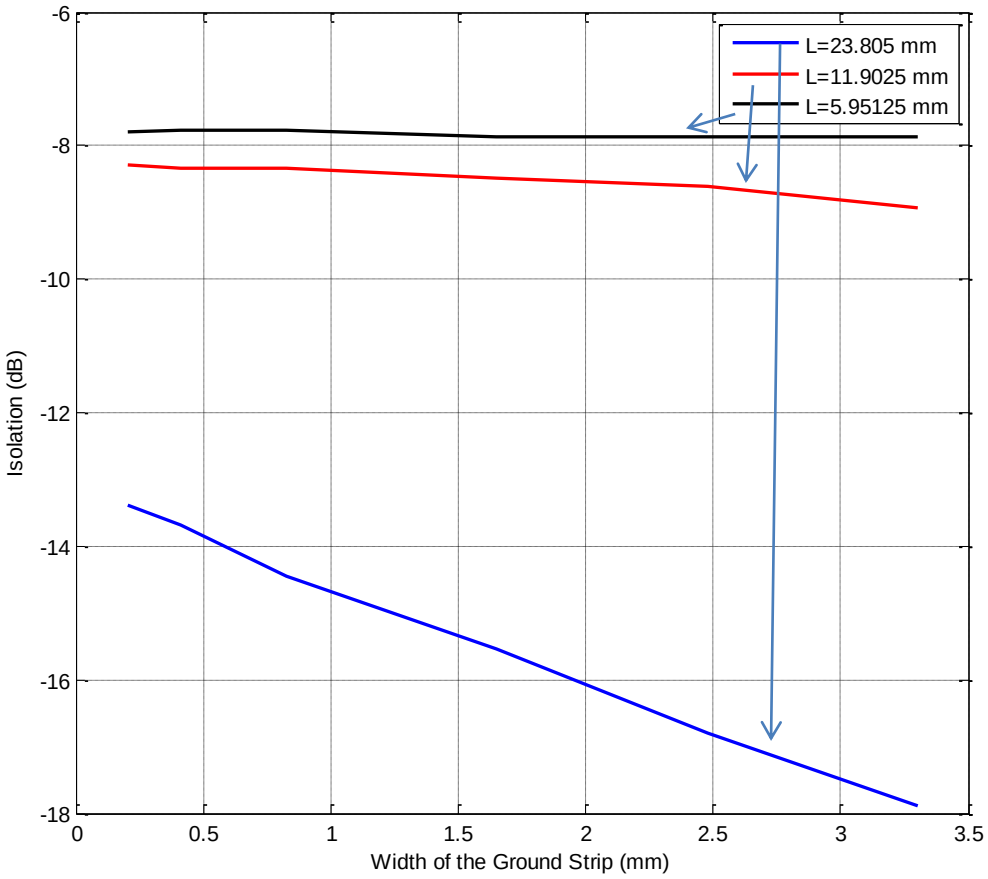

Figure 42: Isolation verses width and Length of the Ground Strip

The third method to reduce isolation combined the first and second method. In this method the separation between the edges of the antenna elements are varied in addition to introducing a parasitic element between them. This antenna is shown in Figure 43. The simulated reflection (S_{11}, S_{22}) and isolation (S_{21}) responses are plotted in Figure 44. Note that the isolation demonstrate by this configuration is -11.14 dB with an impedance bandwidth of 27.71%.

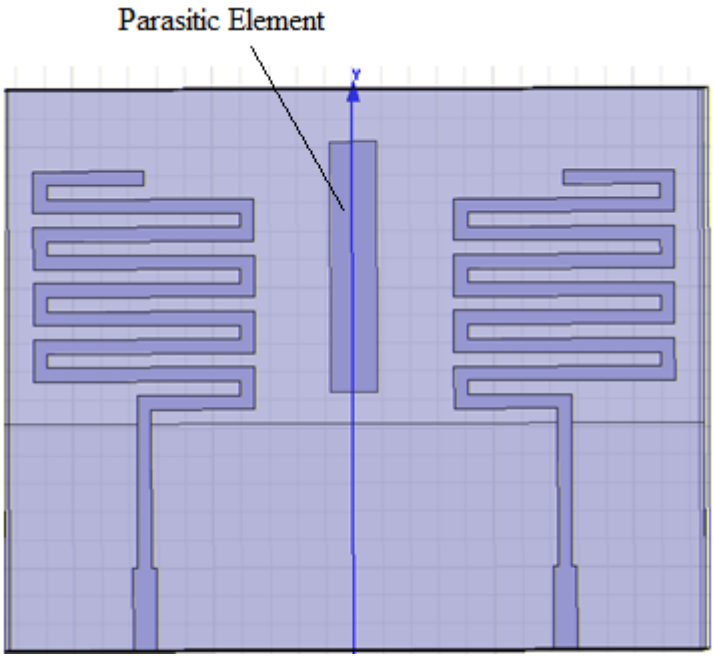

Figure 43: Isolation Reduction by Inserting a Parasitic Element

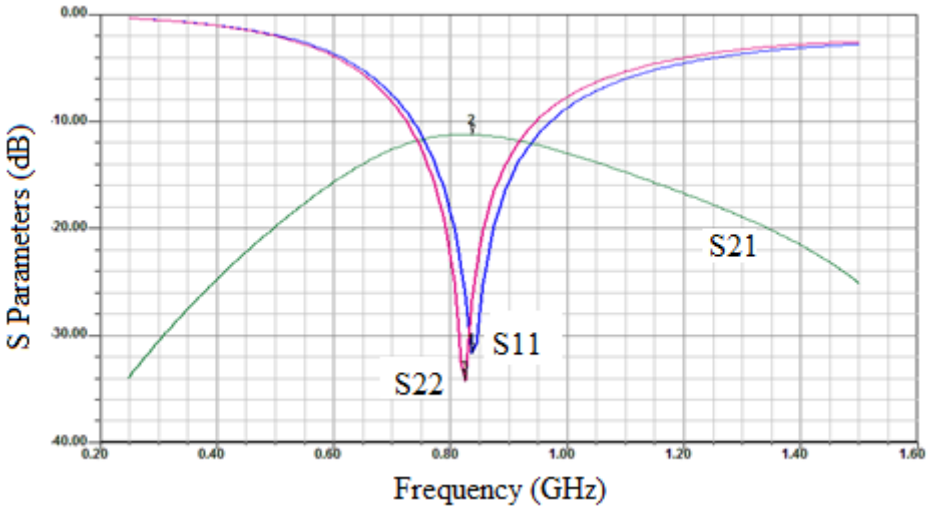

Figure 44: S-Parameter Responses of the MIMO Antenna with Parasitic Element

Next the configuration used to limit the mutual coupling combined configurations shown in Figures 40 and 43. This configuration of MIMO antenna is illustrated in Figure 45, where the isolation metal strip consisted of grounded and parasitic parts. The measured reflection and isolating response for this configuration is plotted in Figure 46. To reduce the surface waves, varying lengths of the copper strips and variable gaps are related to this antenna is also investigated.

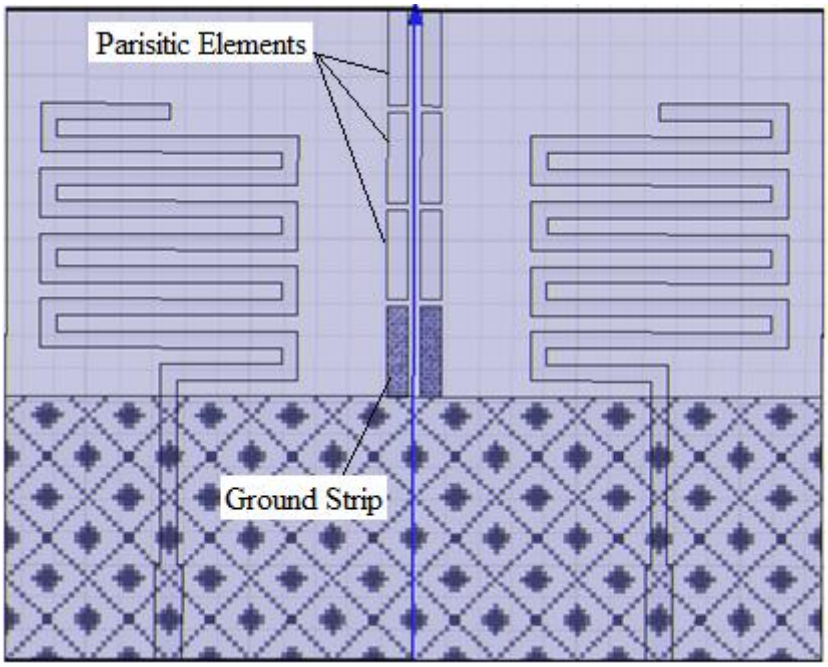

Figure 45: Antenna elements separated by segmented metal grounded and parasitic strips

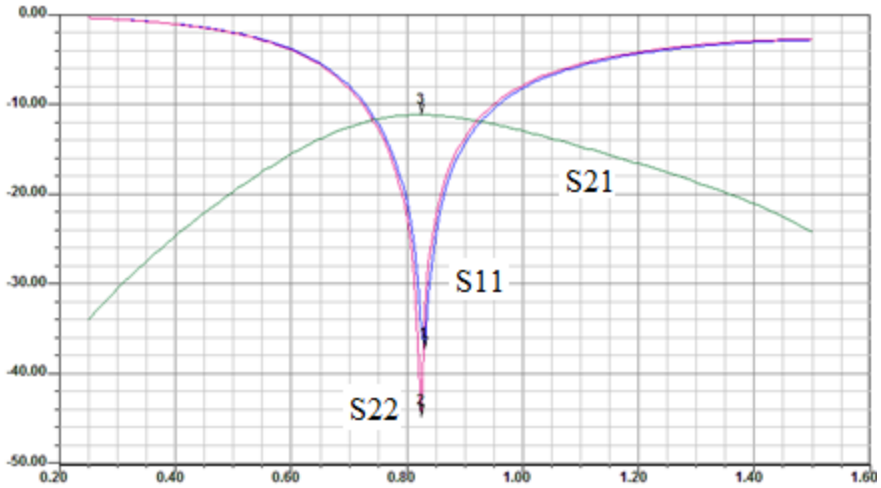

Figure 46: S-parameter responses of the MIMO antenna of figure 45.

The final novel method investigated here to reduce the isolation evolved from above investigation and employed an L-shaped ground conductor for each meander line antenna element. This configuration is shown in Figure 47 and demonstrates the expected isolation between the antenna elements. The simulated s-parameters of this configuration are plotted in Figure 48. Note that the isolation exhibited by this MIMO antenna is -20 dB and with impedance bandwidth of 23%. The radiation response of this antenna is also simulated and plotted in Figure 49. Note that the 3D radiation plot in Figure 49(a) clearly illustrates the doughnut shaped radiation pattern, as expected from this class of antenna. The elevation and azimuth plane plots of this antenna are also shown in this figure. Note that isolation between the antennas elements can further improved by superimposing the separation technique illustrated in Figure 40 with the allowable antenna size of 40x100 mm^2. The s-parameters of the design are tabulated in Table 9.

Table 9: Specification for the Two Element MIMO Antenna

Frequency	S_{11}	S_{22}	S_{21}
0.78 GHz	-16.02 dB	-16.11 dB	-19.89 dB

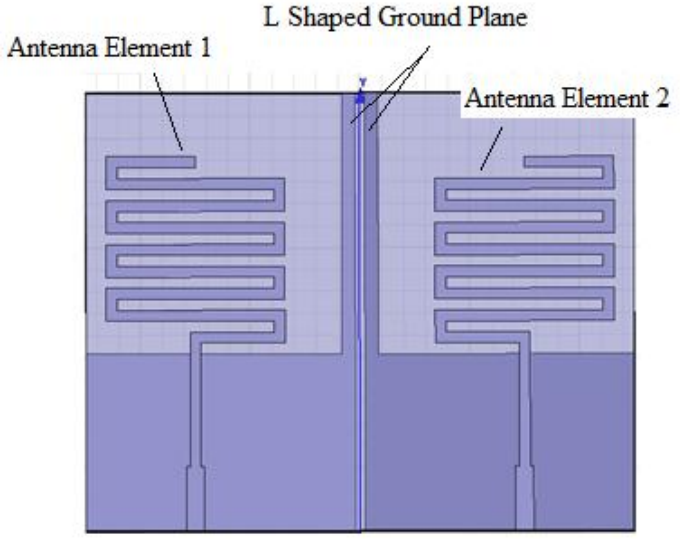

Figure 47: HFSS Model for MIMO Antenna with Two L Shaped Ground Plane

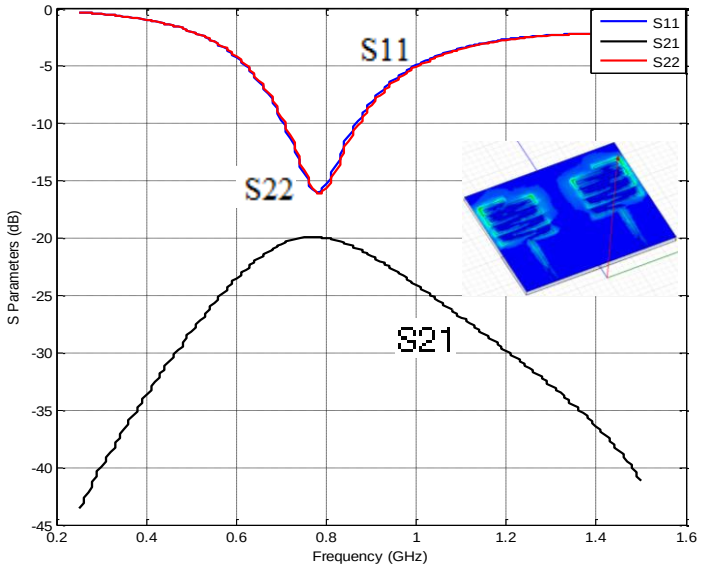

Figure 48: S Parameters for the MIMO Antenna with Two L Shaped Ground Plane

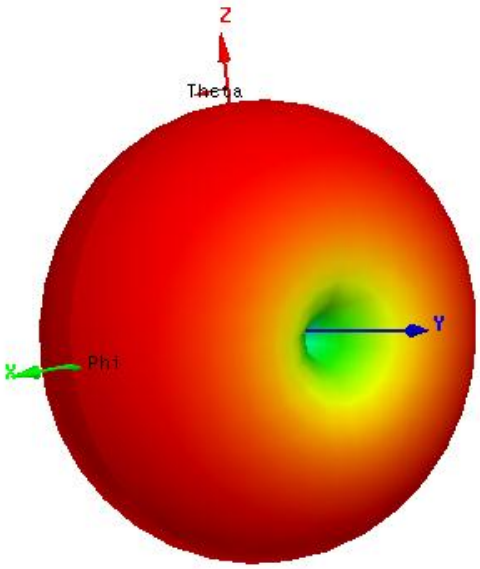

(a)

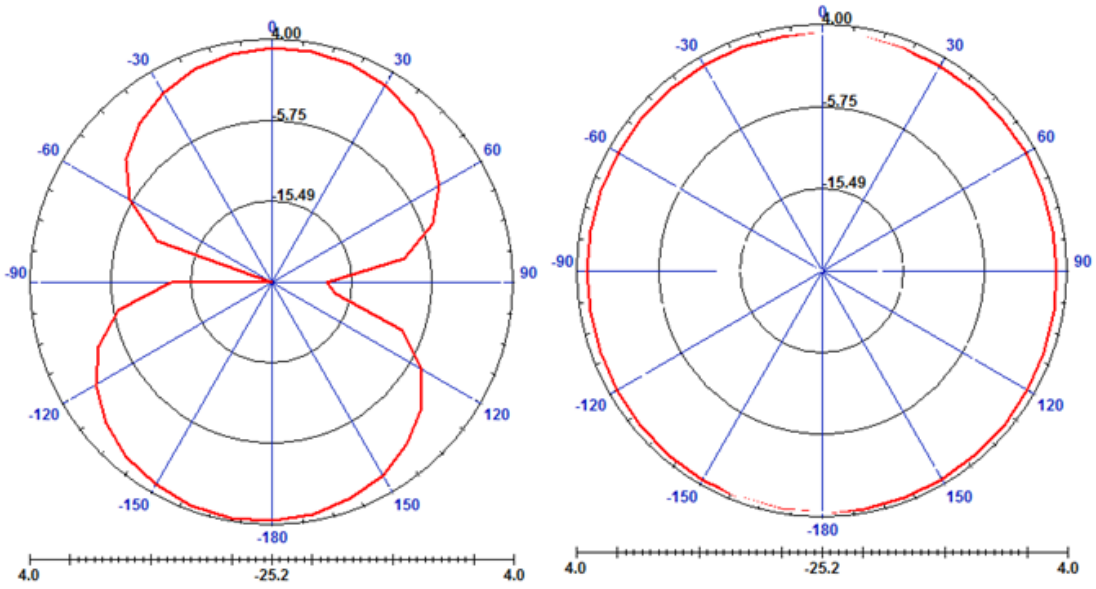

(b) (c)

Figure 49: Radiation pattern of the antenna shown in figure 4.14 (a) 3D plot (c) Elevation plane (phi=90^0) plot (b) Azimuth plane (phi=0^0) plot

The correlation coefficient for the optimum (latest) design is analyzed using MATLAB program based on equation (1.12), shown below:

$$|\rho_{12}|_{\max} = \frac{-S_{11}^{*}S_{12} - S_{21}^{*}S_{22}}{\sqrt{\left(1-|S_{11}|^2-|S_{21}|^2\right)\left(1-|S_{22}|^2-|S_{12}|^2\right)\eta_1\eta_2}} + \sqrt{\left(\frac{1}{\eta_1}-1\right)\left(\frac{1}{\eta_2}-1\right)}$$

The derivation for this equation is in chapter 1. The antenna radiation efficiency and scattering parameter were extracted from simulated results are used for this calculation. The radiation efficiency for both antennas was found to be 0.8761; the correlation coefficient with respect to frequency is shown in Figure 50 with a maximum value of 0.3366 and it is equal to 0.1758 at our design frequency.

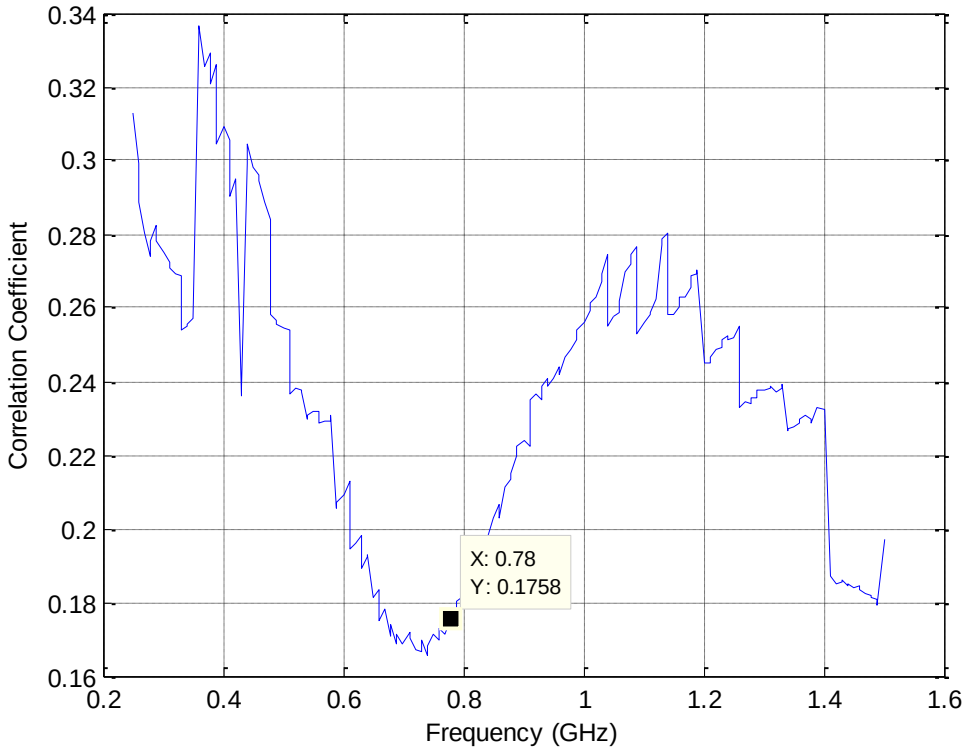

Figure 50: Correlation Coefficient

4.3 Design of Array Feeder

Often the multiple antenna elements of a MIMO antenna needs to be fed through a single connector and requires integrating array feeder. In this work a corporate feed network is used to feed the antenna elements. This feeding technique allows the radiating elements to be excited with microwave signals having same or progressive amplitude and phase. Since this application of this linear array configuration is to enhance the gain of the antenna, a corporate feed network is designed here to send/receive power with equal phase and magnitude. Figure 51(a) illustrates a 4-element linear antenna fed by a simple corporate power divider and Figure 51(b) schematically shows the designed power divider. The related dimensions are listed in Table 10.

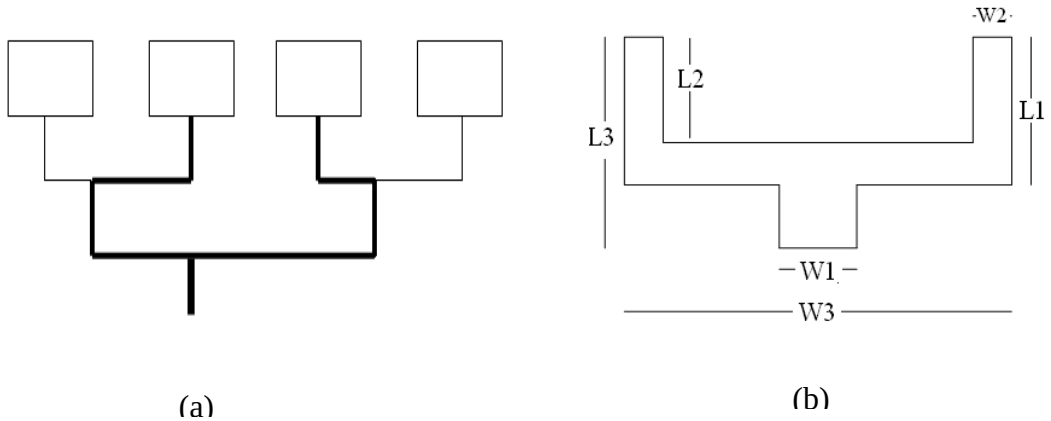

Figure 51: Schematic diagram of corporate feeder (a) 4-way (b) 2-way

The simulated reflection (S_{11}) and transmission (S_{31} and S_{21}) responses of the designed power divider are shown figure 52. Note that the at the design frequency band of 700 MHz, the values of S_{11} is around -20 dB and S_{21} & S_{31} are very close to -3 dB.

Table 10: Dimensions of the two way Power Divider of figure 4.5 (a)

W1	W2	W3	L1	L2	L3
5.36 mm	1.651 mm	21.651 mm	6 mm	4.349 mm	10 mm

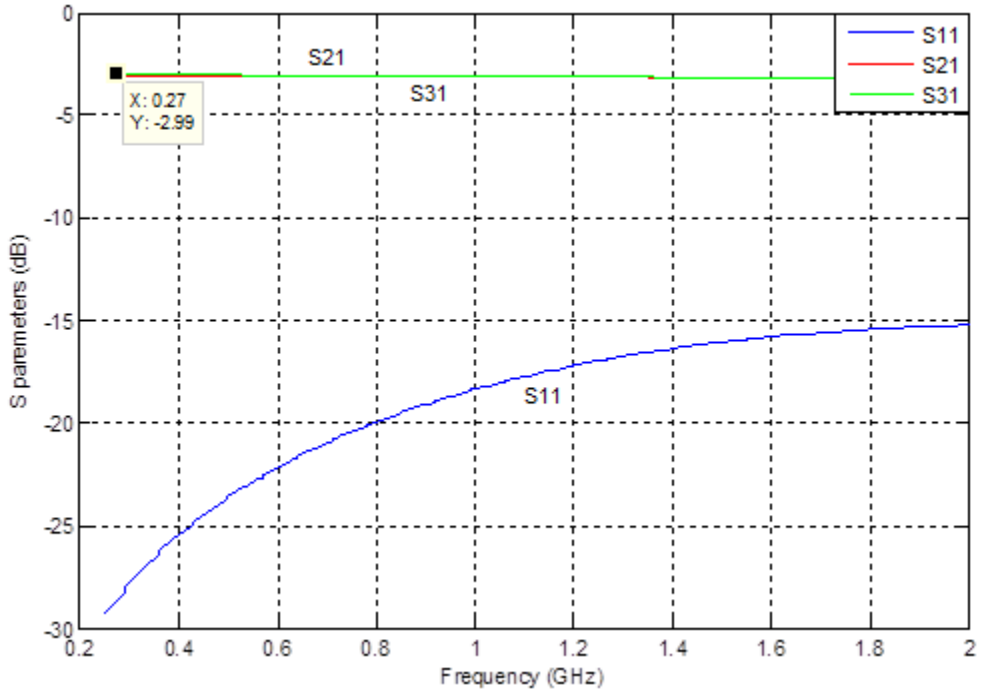

Figure 52: S Parameters for the Two Port Power Divider

4.4 Design of a Two-Element MIMO Antenna Array

To reducing the multiple-access interference, MIMO antennas often employ beam-forming technique. Using this technique the antenna gain can be increased in the direction of the desired user, whilst reducing the gain towards the interfering users. Although investigating this technique is not the objective of this research work, a simple

linear antenna with two meander line elements are presented here. The antenna array is shown in Figure 53. Note that using same method discussed in section 4.2, isolation between the meander lines elements can be improved up to -20dB. Improvement in the array feeder, designed in section above, is achieved by introduce compensated bends and impedance transformers. The simulated result for this antenna array is plotted in Figure 54. Note that the array design is optimized to achieve the best reflection response $S_{11} = -31.54\ dB$ at the design frequency of 780MHz.

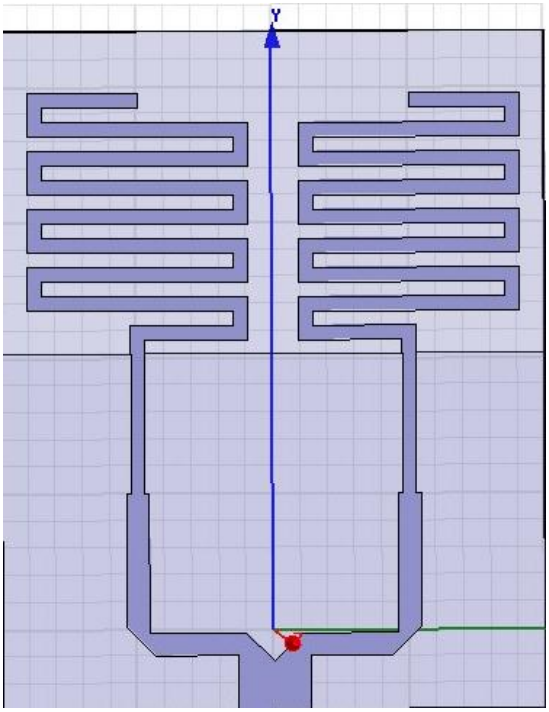

Figure 53: HFSS Model for MIMO Antenna System

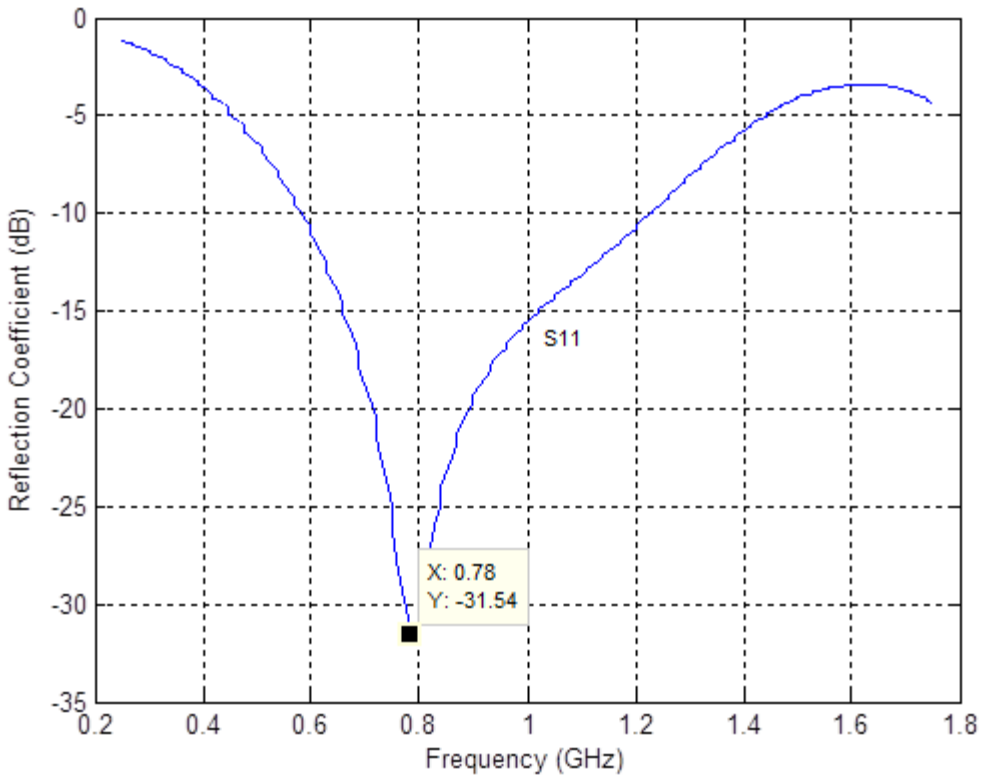

Figure 54: Reflection Coefficient for the MIMO Antenna

4.5 Conclusion

This chapter discusses the design process of a 40x50mm^2 MIMO antennas with two meander line radiating elements and acceptable isolation properties. Two main methods are demonstrated to improve isolation between antenna elements, of which the novel technique of introducing L-shaped ground plane produced the desired isolation response of -19dB. Extracted values from the simulation response is used in a MATLAB program to study the frequency dependence of the Correlation Coefficient related the designed MIMO antenna.

CHAPTER 5

EXPERIMENTAL RESULTS

This chapter describes the fabrication and experimental results for the single and dual element antenna for LTE handsets.

5.1 Experimental Setup

S-parameter measurements:

Since HP 8510 Vector Network Analyzer allows the measurement of reflection and transmission relate S-parameter, it a very popular tool in measuring active and passive microwave devices [**74**]. A network analyzer is used in this study to measure the scattering parameters of the designed antennas.

Radiation measurements:

The radiation characteristics of the antennas were measured using the antenna training and measurement system (ATMS) available at the KFUPM laboratory. Figure 55 shows the setup used for this purpose. The distance d was about 1.5 m.

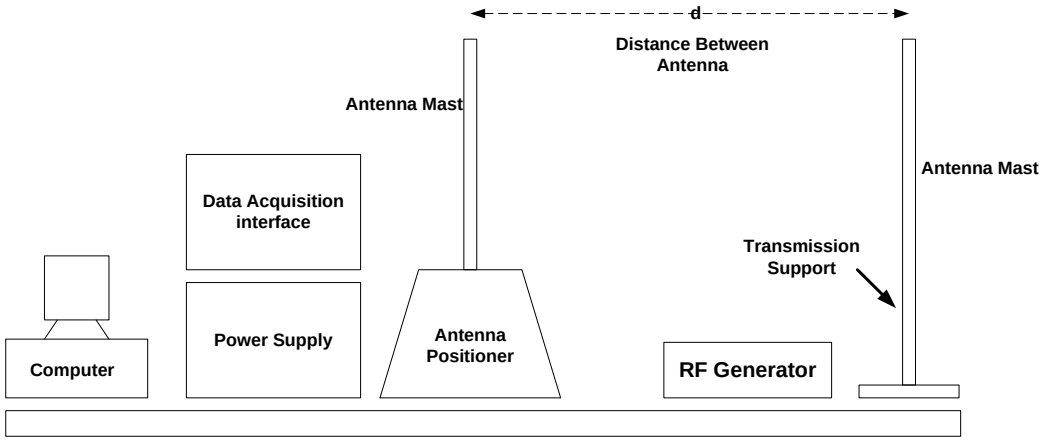

Figure 55: Experimental Set-up of ATMS

The RF generator was used to generate a single tone of the designed center frequency. External voltage was used to tune the original supply frequency of 1 GHz and we found that by applying a 2 volt the RF generator will transmit at 800MHz which is a very close frequency to what we need. A Yagi-antenna was used to transmit the signal. Initially a dipole antenna is used to obtain the reference radiation pattern before using the meander line antennas with single and dual elements. The receiving antenna positioner was controlled by the PC to collect the complete radiation patterns.

5.2 Single LTE Antenna

Two sample prototype antennas were built to verify repeatability of the results obtained.

Figure 56 shows one sample of these prototypes with front and back views of single meander line antenna which has been manually designed by using a FR-4 material

and copper tape. The copper tape was laid on a FR-4 material and then the sheet is etched out according to the antenna geometry. Finally, a 50Ω SMA connector is connected to the input of the antenna.

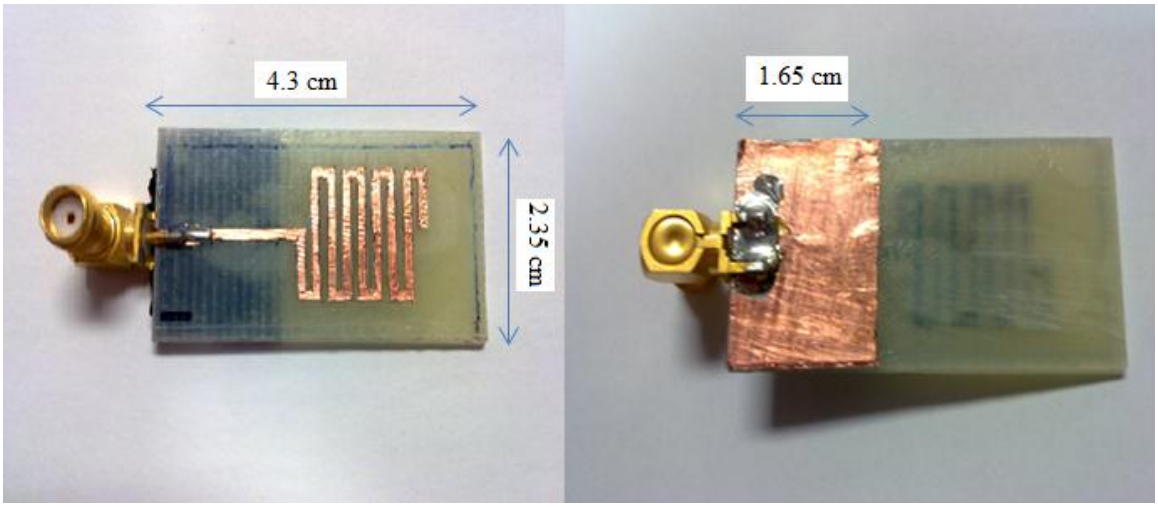

(a) Front View (b) Back View

Figure 56: The Fabricated Sample, (a) Front View (b) Back View

The experimentation started with the measurement of the antenna reflection response (S_{11}) using the network analyzer. The need, method of calibration and working principle of the network analyzer are presented in Appendix A. Since the antennas are designed to operate at a frequency of 780 MHz, the reflection response of the device was observed for a frequency range of 0.5 to 2 GHz. Figure 57 plots the reflection response (S_{11}) of the single antenna. From the figure, it is evident that the antenna is resonating at 897 MHz, which is relatively close to our operating frequency. Also the $|S_{11}|$ = -32.67 dB

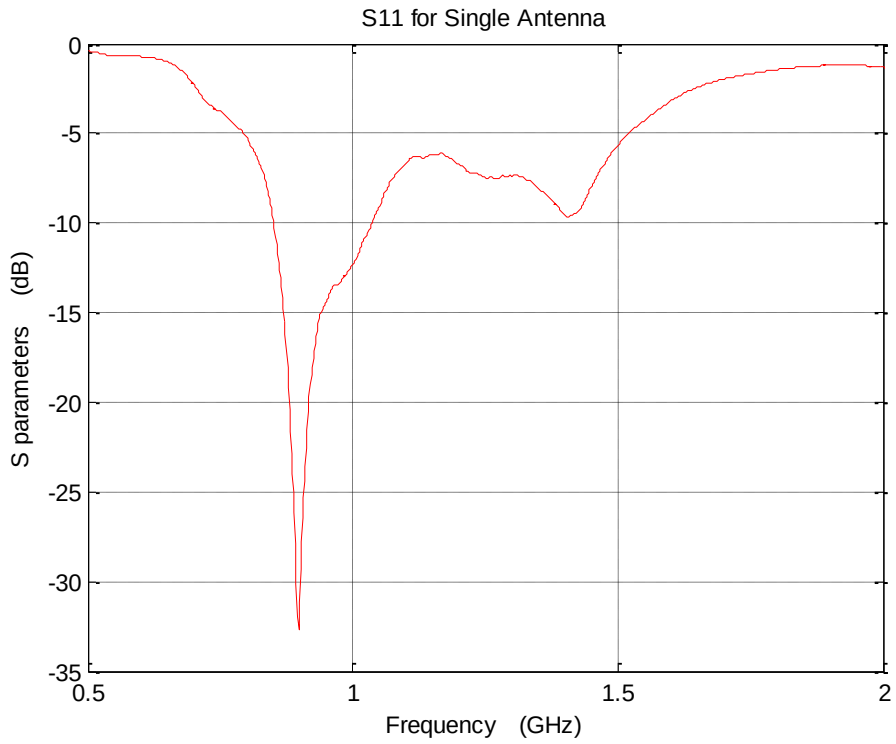

Figure 57: Experimental Reflection Coefficient for the Single Antenna

Figure 58 shows the reflection coefficient of the simulated and measured single meander line antenna for an LTE handset. The behavior of both curves is in agreement. A slight shift in the result frequency and measurement bandwidth was obtained from measurement due to imperfect fabrication process. Table 11 summarizes the result of Figure 58.

Table 11: Simulated and Experimental Results for Single MLA Antenna

	Frequency	Reflection Coefficient	Bandwidth
Theoretical	780 MHz	-30.9	260
Experimental	897.5 MHz	-32.67	185.4

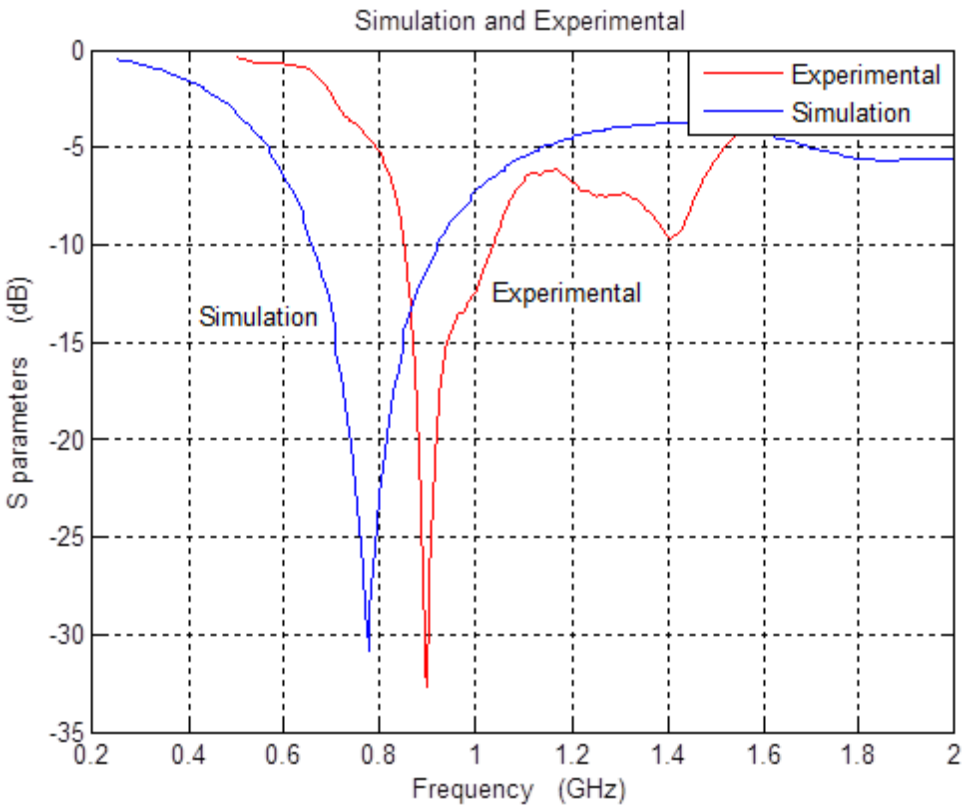

Figure 58: Simulation and Experimental Reflection Coefficient for the Single Antenna

The single antenna radiation pattern was obtained using the "ATMS" antenna measured system at KFUPM microwave laboratory with the setup shown in Figure 55.

Figure 59 and Figure 61 shows the E-plane of sample antenna 1 and 2 respectively with reference to the E-plane of the dipole and Figures 60 and 62 shows the H-plane of sample antenna 1 and 2 respectively with reference to the H-plane of the dipole at 1 GHz. Figure 63 and 64 shows the comparison between E-plane and H-plane for sample 1 and 2 respectively operating at 800 MHz and as we mention before we get this frequency by applying an external voltage to RF generator.

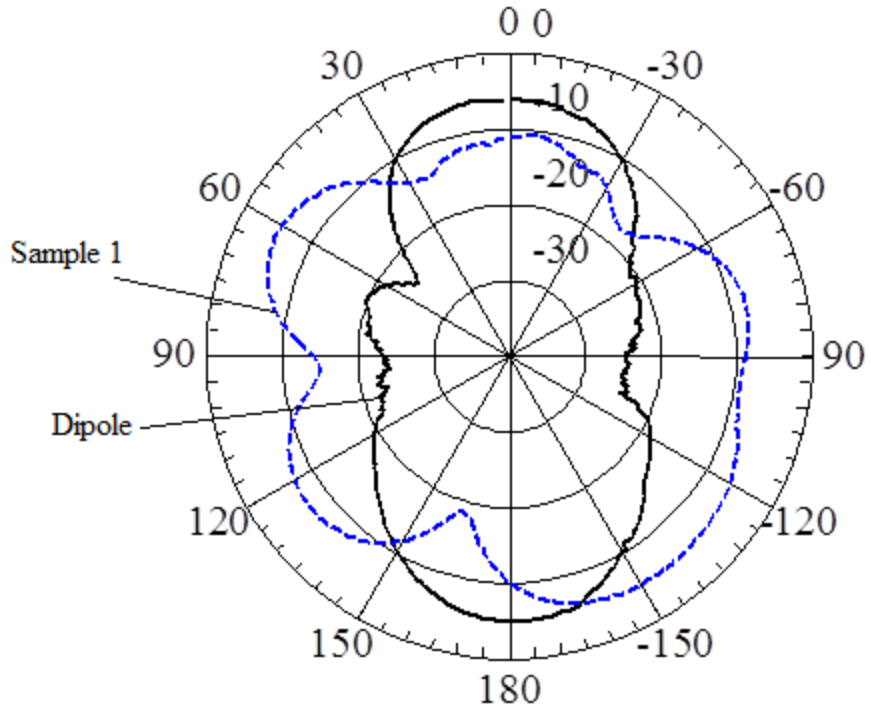

Figure 59: Comparison between the E-Plane of the Reference Antenna and Sample 1 Operating at 1 GHz

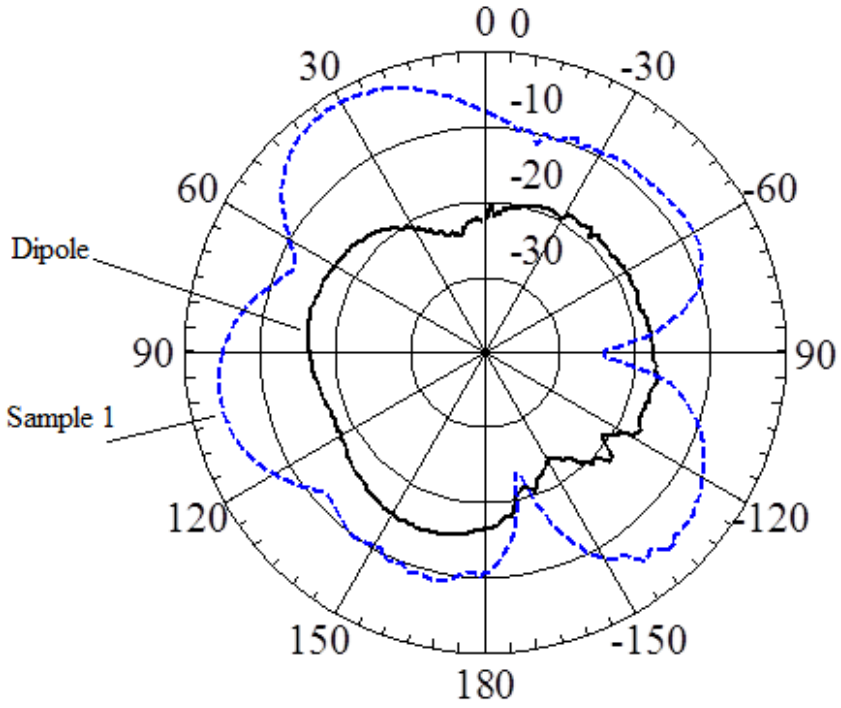

Figure 60: Comparison between the H-Plane of Reference Antenna and Sample 1 Operating at 1 GHz

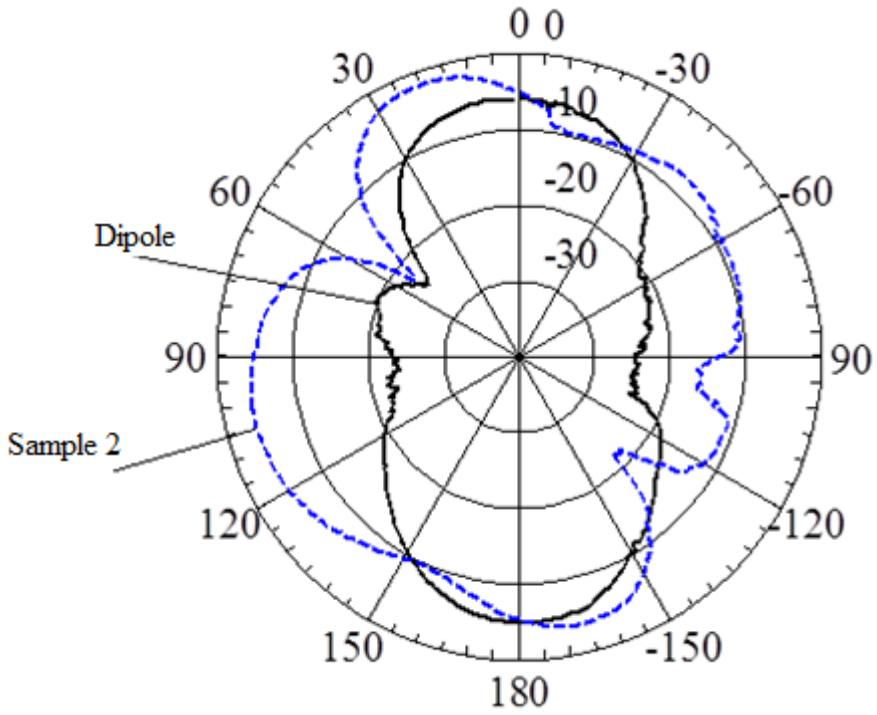

Figure 61: Comparison between the E-Plane of Reference Antenna and Sample 2 Operating at 1 GHz

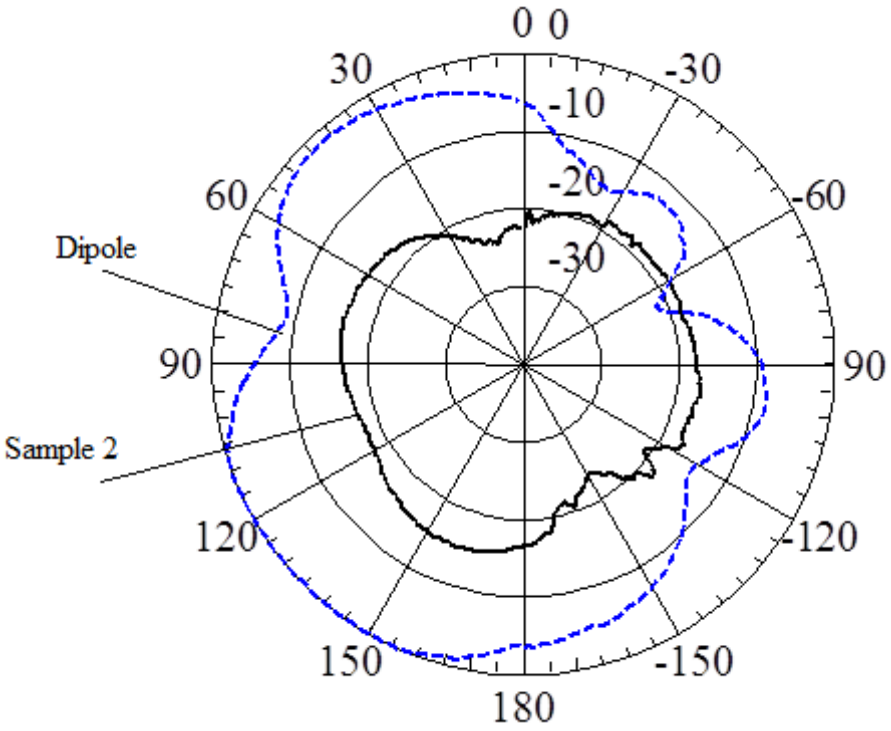

Figure 62: Comparison between the H-Plane of Reference Antenna and Sample 2 Operating at 1 GHz

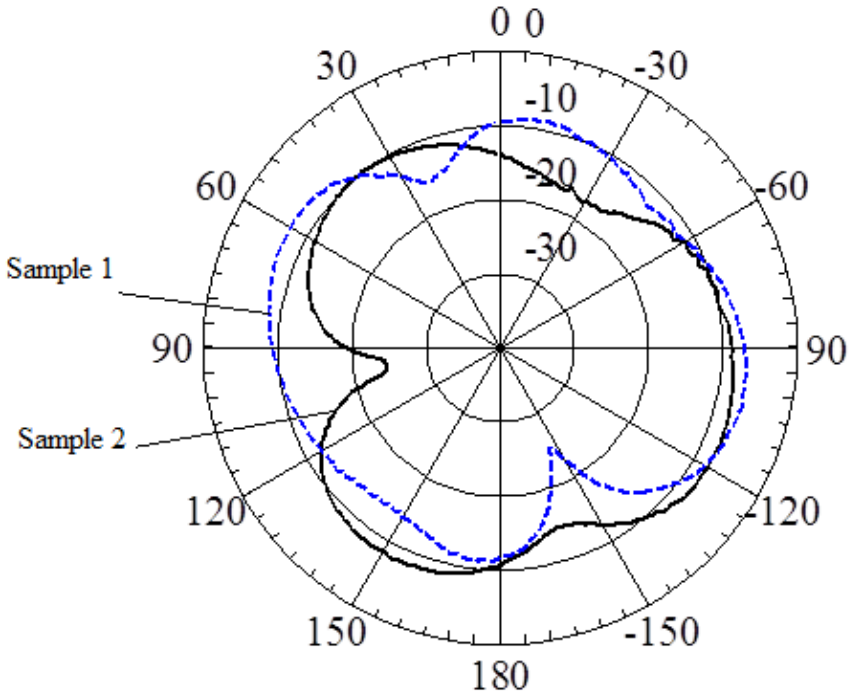

Figure 63: Comparison between the E-Plane of Sample 1 and Sample 2 Operating at 800MHz

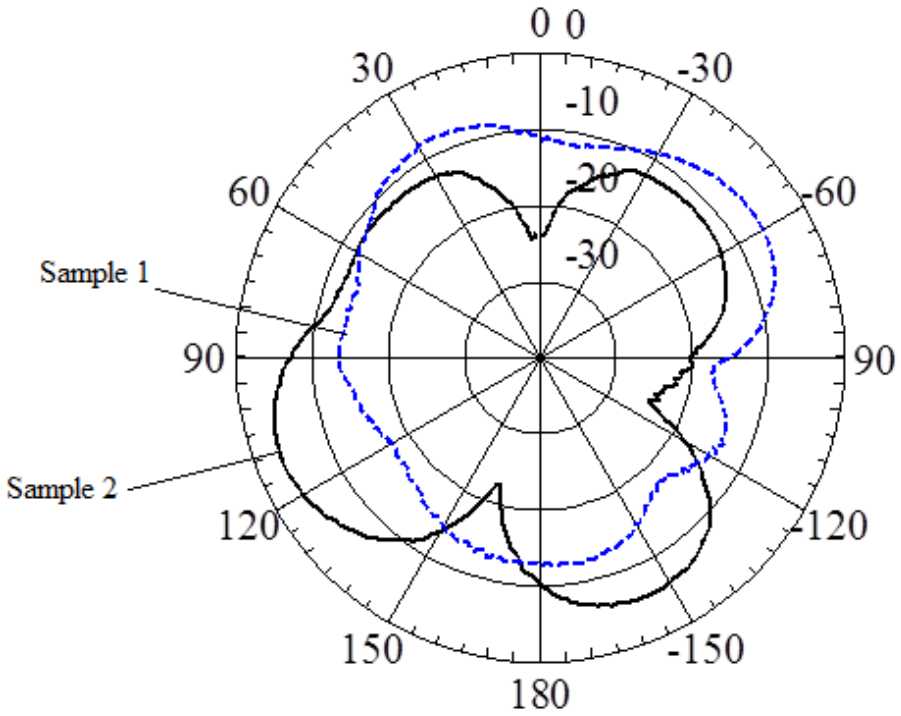

Figure 64: Comparison between the H-Plane of Sample 1 and Sample 2 Operating at 800MHz

5.3 MIMO Antenna System

The dual element MIMO antenna system with the geometry showing in Figure 47 is implemented as shown in figure 65.a (front view) and figure 65.b (back view) and it was tested using a VNA (Vector Network Analyzer).

The measurement process for this MIMO antenna starts by applying a signal through a network analyzer to one of the antennas and terminating the second by using 50 ohm terminating load and measure for S_{11}. Then we interchange the terminating end and network analyzer and measure for S_{22}. Then we connect the two end of the network analyzer to both of the antennas and measure S_{21}. The simulated and experimental results for S_{11}, S_{22} and S_{21} with the process mentioned above were conducted and the results are shown in Figures 66, 67 and 68 respectively. It was found that there is a 150-200 MHz frequency shift between the simulated and experimental results. This can be due to many reasons and some of them are:

- Since the antenna is fabricated manually it does not have an absolute structure as desired.
- The network analyzer was not perfectly calibrated especially for two ports.
- The third reason is error in the connectors and cables used.

We notice from Figure 68 that the experimental S_{21} (isolation) gives a good isolation of less than -15 dB around 870 MHz which is the same frequency where both S_{11} and S_{22} are resonating around.

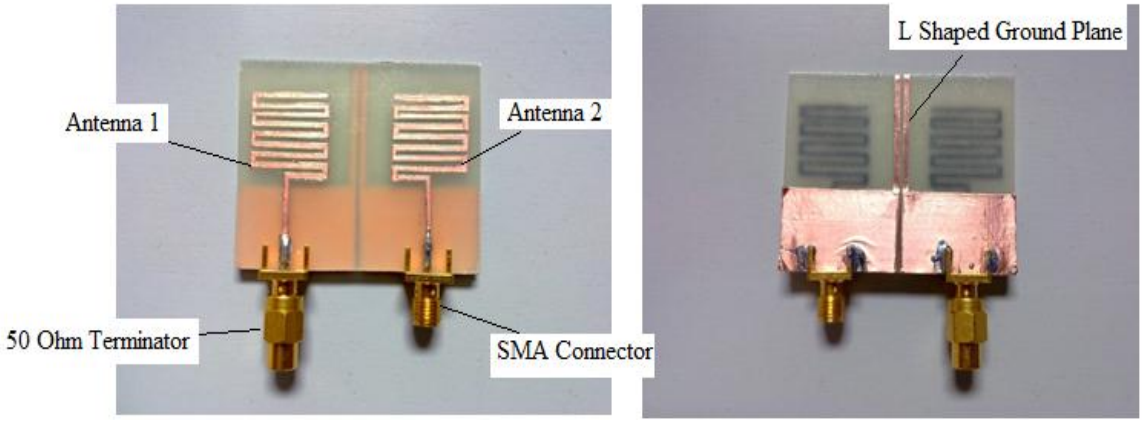

Figure 65: A prototype of the MIMO Antenna (a) Front View (b) Back View

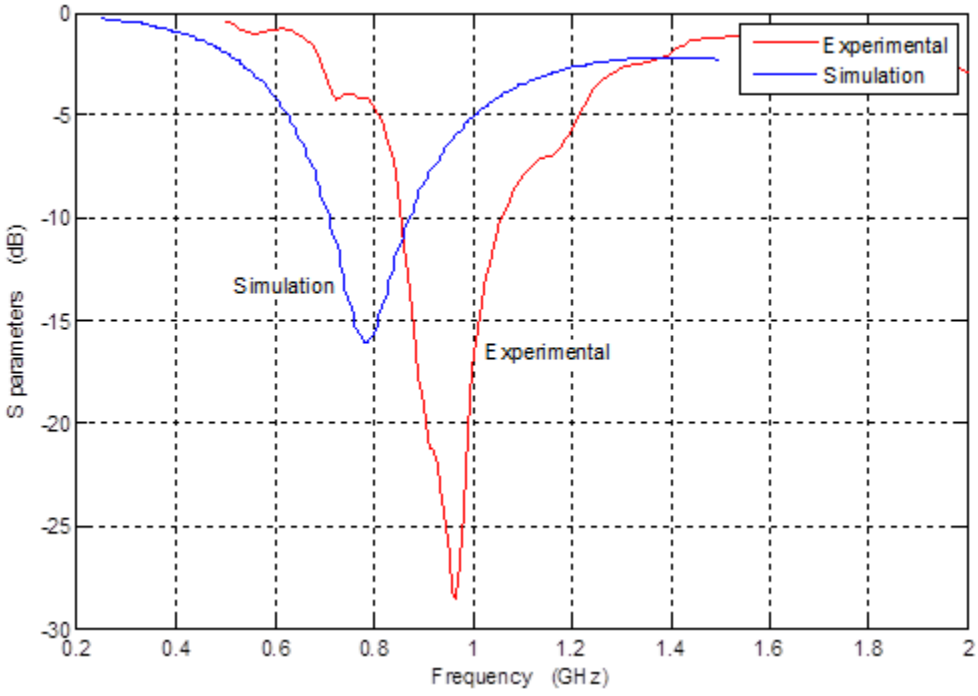

Figure 66: Simulated and Measured S_{11} for MIMO Antenna

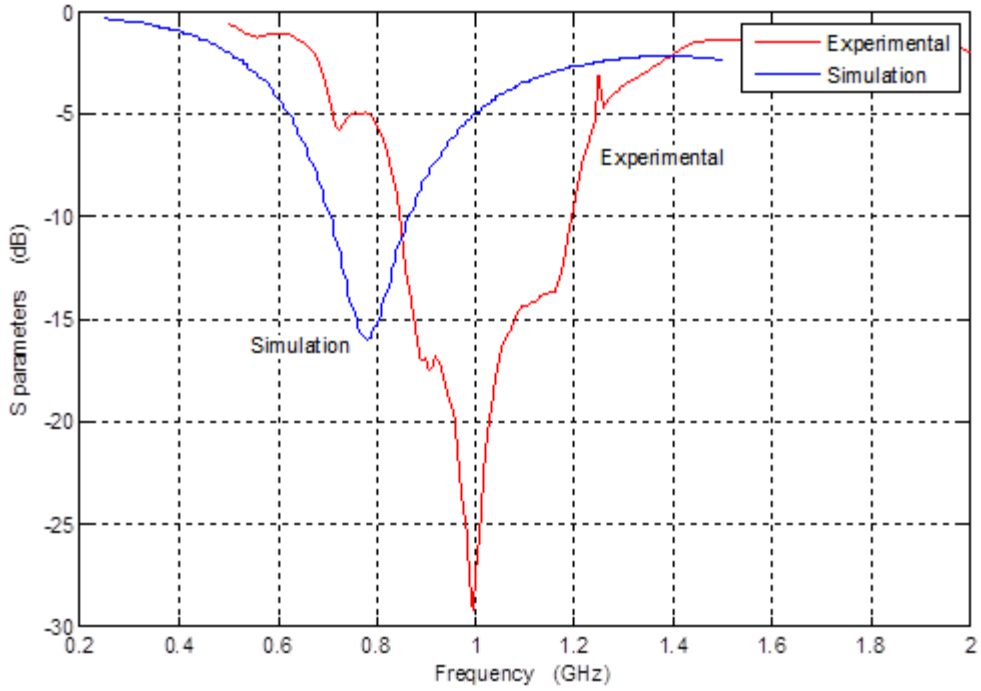

Figure 67: Simulated and Measured S_{22} for MIMO Antenna

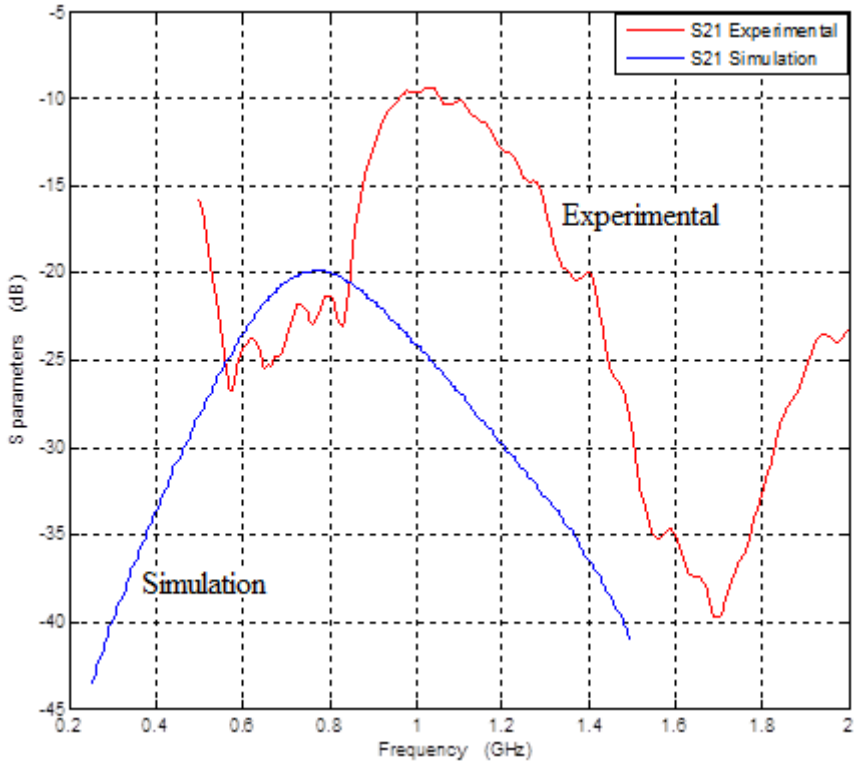

Figure 68: Simulated and Measured S_{21} for MIMO Antenna

Figure 69 and Figure 70 shows the E-plane and H-plane of antenna 1 and 2 of the MIMO system with the transmitted signal from yagi antenna at 1 GHz while Figure 71 and Figure 72 shows the E-plane and H-plane of antenna 1 and 2 of the MIMO system with the transmitted signal being tuned by an external voltage to get 800 MHz frequency.

Now we want to compare E-plane and H-plane of the MIMO system with the single antenna's sample 1 and 2. In Figure 73 and 74 E-plane of antenna 1 and 2 of the MIMO system are compared to the E-plane of sample 1. In Figure 75 and 76 the E-plane of antenna 1 and 2 are compared to the E-plane of sample 2.

It is evident that the single antenna has more radiation when horizontally polarized while it's cross polarization is high (vertical polarization). Also, it is clear that sample 2 has a better radiation and coverage in the azimuth plane than sample 1 at 1 GHz. The patterns obtained at 800 MHz for both samples have close trends, with sample 2 gives better results. The large deviations are obtained to the fabrication process and the primitive radiation measured equipment where measured were conducted in an open environment.

For the MIMO system, the behaviors of the two antennas were close in terms of the trends of the radiation patterns. A shift in the min-max position is easily observed but this can be attributed to a slight angle shift in the antenna positioner (about 30 degrees).

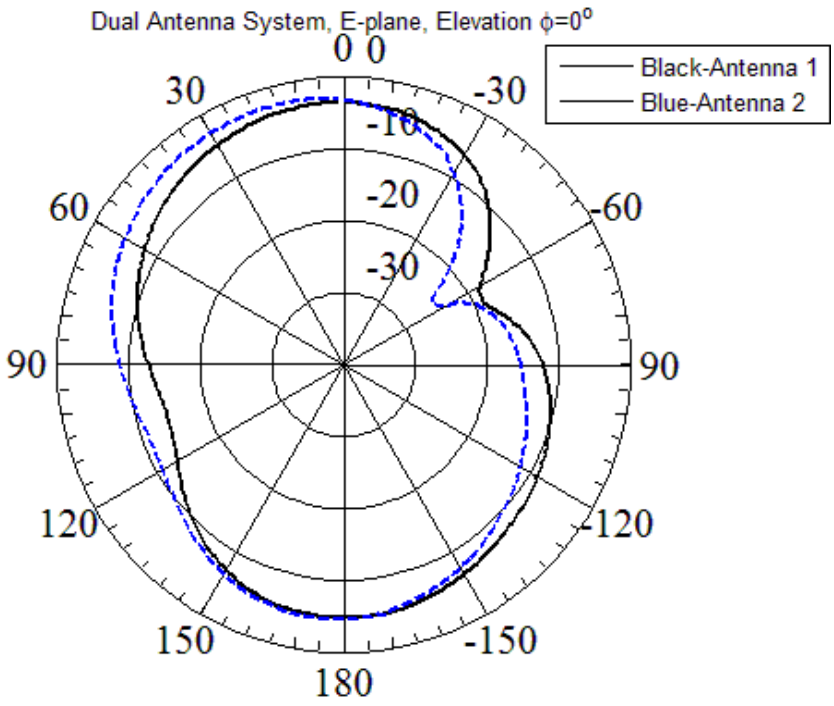

Figure 69: Comparison between the Elevation Plane (phi=0^0) of Antenna 1 and Antenna 2 for MIMO System Operating at 1 GHz

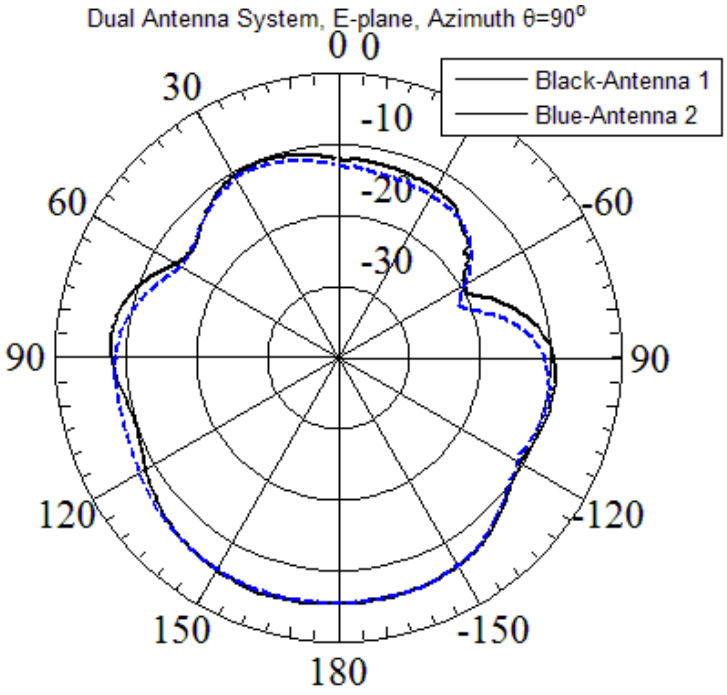

Figure 70: Comparison between the Azimuth Plane (theta=90^0) of Antenna 1 and Antenna 2 for MIMO System Operating at 1 GHz

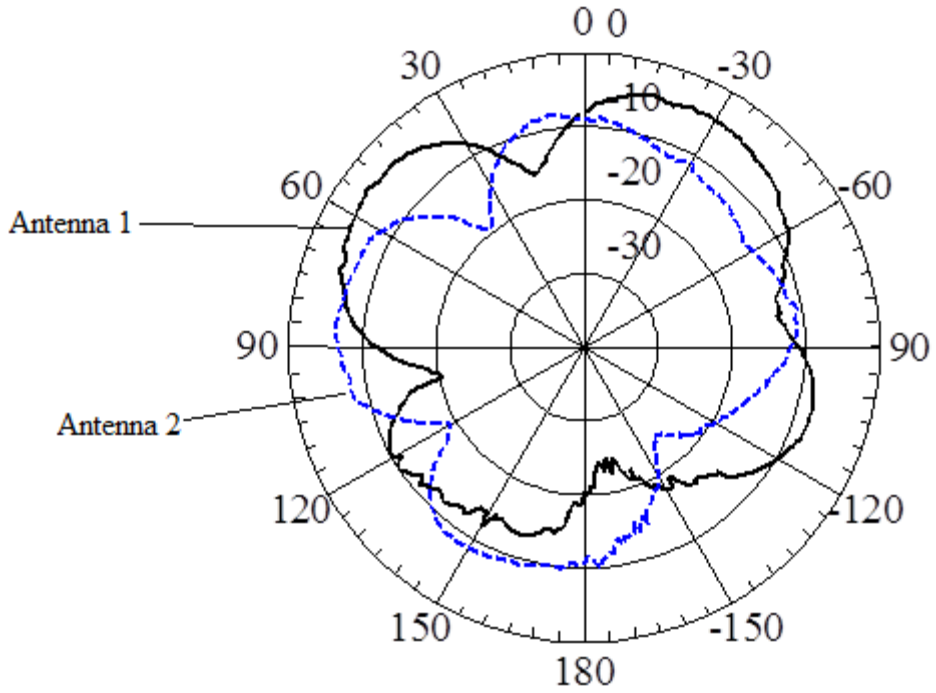

Figure 71: Comparison between the E-Plane of Antenna 1 and Antenna 2 for MIMO System at 800MHz

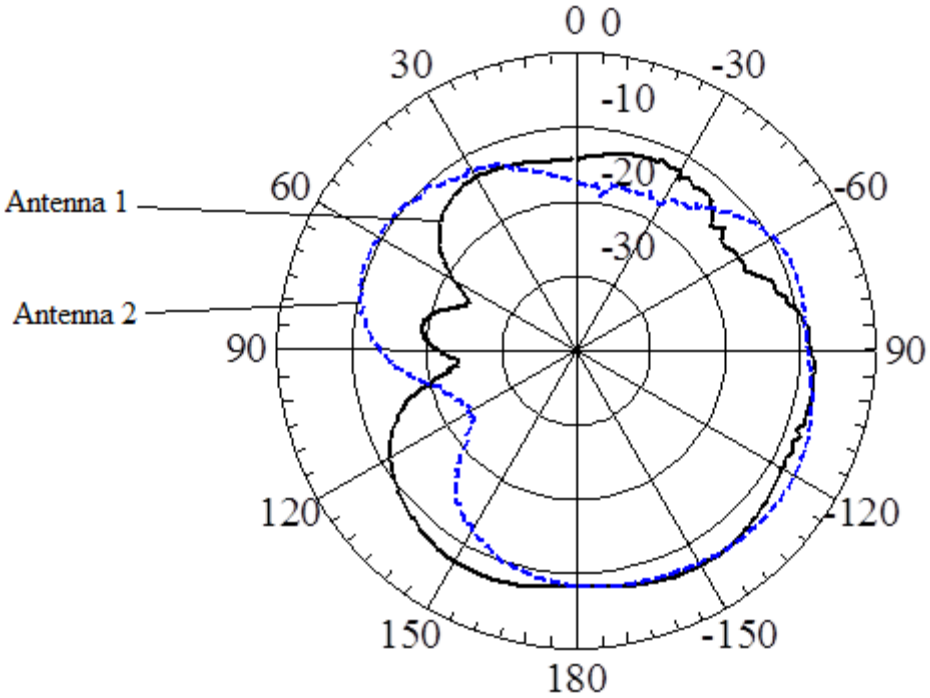

Figure 72: Comparison between the H-Plane of Antenna 1 and Antenna 2 for MIMO System at 800MHz

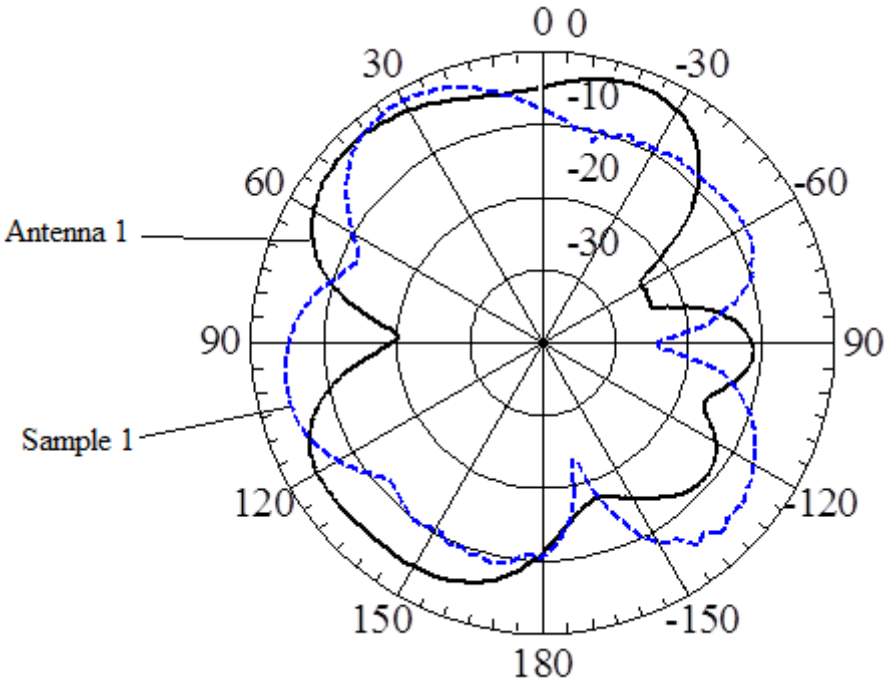

Figure 73: Comparison between the E-Plane of Antenna 1 for MIMO System and Sample 1 for the Single Antenna Operating at 1 GHz

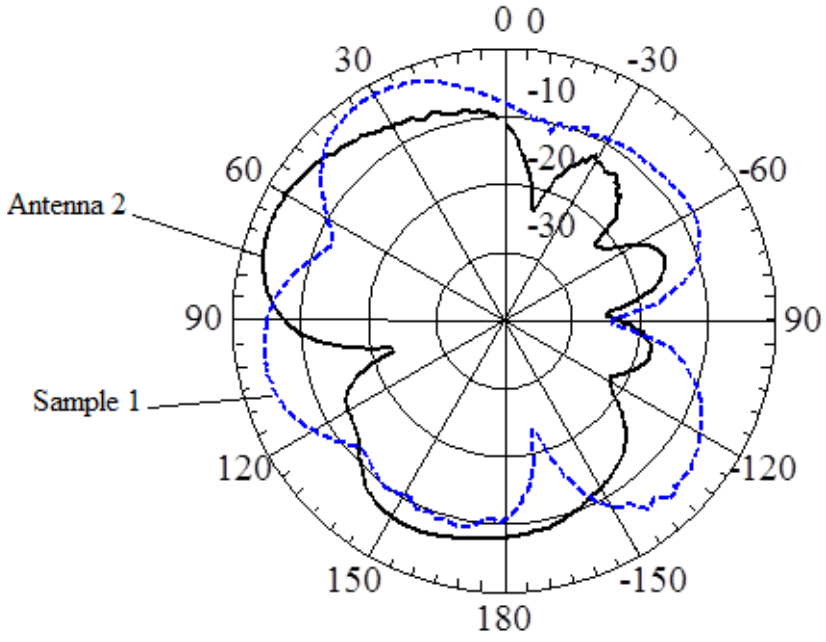

Figure 74: Comparison between the E-Plane of Antenna 2 for MIMO System and Sample 1 for the Single Antenna Operating at 1 GHz

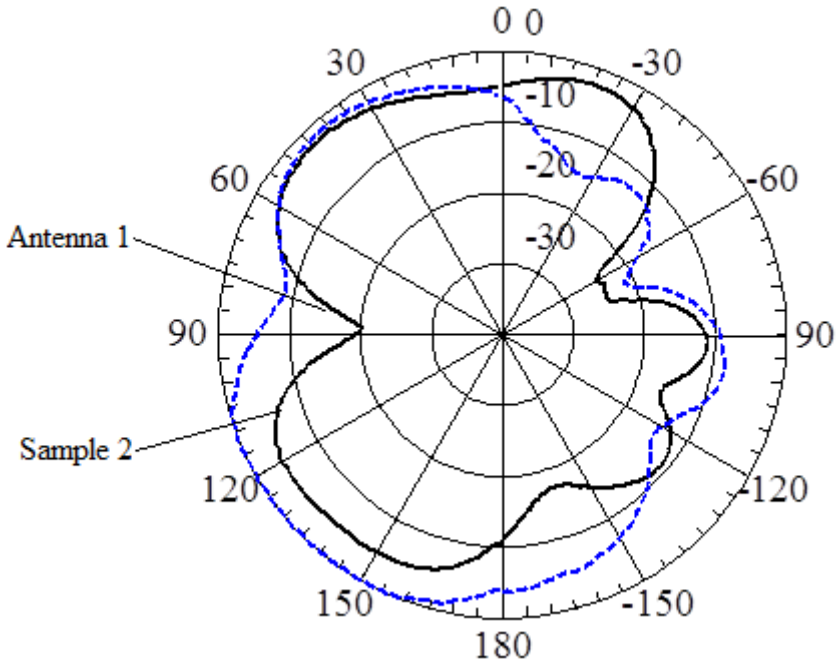

Figure 75: Comparison between the E-Plane of Antenna 1 for MIMO System and Sample 2 for the Single Antenna

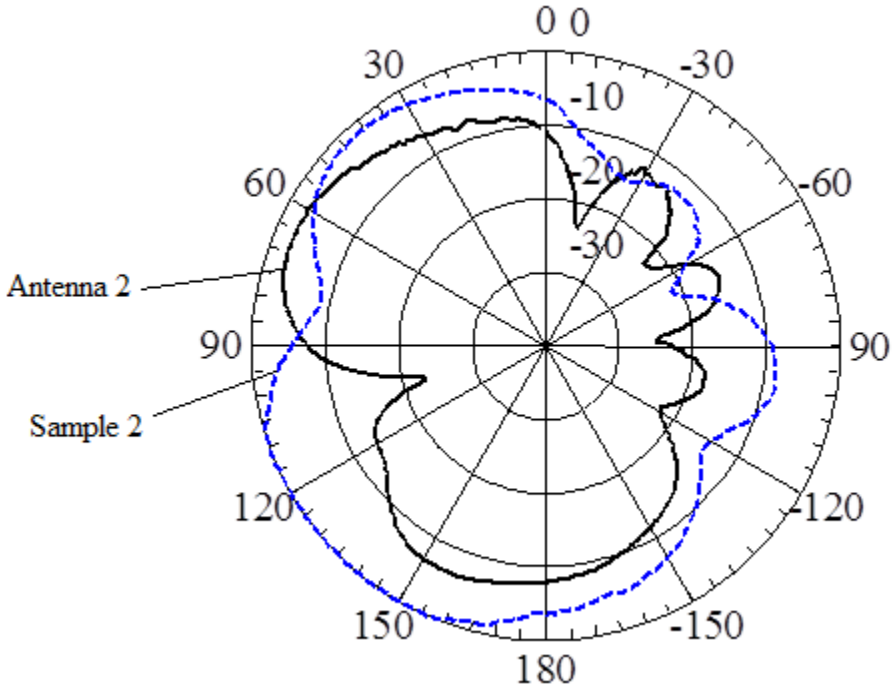

Figure 76: Comparison between the E-Plane of Antenna 2 for MIMO System and Sample 2 for the Single Antenna

5.4 Conclusion

In this chapter we had an overview of the fabrication and experimental process for both single element and MIMO antenna system. We have compared between simulated and experimental results for each of these antennas and found that there are some variations since we are dealing with antenna with many bends. The percentage of error in the resonant frequency was 19.17% in the dual antenna and 13.09% in the single antenna. Also, the radiation patterns were examined. A noticeable variation was observed between the two samples, but general trends look alike. The antennas fabricated worked around 1 GHz.

CHAPTER 6

CONCLUSION

6.1 Contribution

In this research work, a printed antenna is designed using meander line technique to demonstrated lager impedance bandwidth for considerably small dimensions, as tabulated in the conclusion section of chapter 3.

The 2nd contribution of this research work is to design and implement a printed MIMO antenna with two meander line radiating elements for LTE mobile handsets. A novel technique is adopted to improve the isolation between the two elements by introducing an L-shaped ground plane. This reduced the simulated isolation response of the antenna to less than -15 dB at 870MHz. Due to the size limitation of the LTE antennas, standard techniques for reducing the mutual coupling were not acceptable. End size requirement of the antenna (40x50mm^2), isolation was better than -19dB. MATLAB codes were written to investigate the frequency dependence of this Correlation Coefficient related to the MIMO antenna.

The final contribution of this research work is to experimental verification of the simulated results. Although HFSS is well-accepted software, the accuracy of the simulated results always depends on the experience of the user. A minor disagreement

between the simulated and experimental results (see conclusion of chapter 5) were due to the inaccuracy of the in house fabrication process.

6.2 Future Work

- Use Meta-material based substrates to further reduce the antenna size and introduce external control.

- Design and implement 4x4 MIMO antenna systems for LTE standards of mobile phones with reduced correlation coefficient. This is particularly challenging due to the size limitations and usage of 700 MHz band for this system.

Appendix A

Experimental Process

After we fabricate the antennas we need to test it in order to verify the simulation results, we start by testing the operating frequency of the antenna and the reflection coefficient and the bandwidth using network analyzer but before using it we need to calibrate it and test that calibration in order to eliminate any errors my caused by calibration, cables and connectors and the following topic is how to calibrate the network analyzer.

Network Analyzer Calibration

1. Turn on the power. You will turn on four "Line/Power" buttons.
2. Attach connectors and extra cables to the network analyzer as needed. Be careful with the network analyzer cables. Do not over bend them.

Calibrate the network analyzer (S11 or S22 Reflection Measurements only).

a. Choose a calibration kit for the type of connector you are using.
b. Set your frequency range. Press start and type the frequency you want to start. Do the same for the stop frequency.

c. On the MENUS control, press CAL. Delete a calibration set to make empty slot for yours. Do these by pressing MORE on the soft menu on the screen, then DELETE CAL SET, then choose a number.
d. Select a calibration type. Generally this is the type of cable connected to the network analyzer.
e. Choose S11-1 port or S22- 1 port (depending on which cable you want to use).
f. You will be prompted to put calibration standards on the end of your cable. They are in the wooden box.

    1. Start with the short (it is labeled). Connect the short, press the soft key SHORT, and when it is done measuring (quickly) it will underline the SHORT. Take it off, put the plastic cover back on the standard, and find the open.
    2. Open. It is the same length as the short, but with a smaller radius and a hole in the end. Press OPEN, wait until open is underlined, remove the open and replace the plastic cover.
    3. Find the load standard. They are the long, sliding cylinders in the box. Connect it, and press LOAD. Then BROADBAND. Then DONE LOADS. We are assuming our load is accurate over the whole frequency range of calibration and is therefore "broadband." Replace the plastic cover; put all the standards back in the box.

a. Press SAVE 1-port CAL. Press the number where you want to save the calibration settings. It should say "Correction ON"

b. Test your calibration. The worst is usually the open. Test the short and load the same way. IF these are not "clean", redo the calibration. Factors that can affect your calibration: tightness of cables and connectors, between elements and to the network analyzer.
c. If your calibration is good. PUT THE BOX of standards back in the closet. [**75**]

After the calibration is ready we can now take the results.

Appendix B

Simulator Software Used

B.1 What is HFSS?

HFSS is a commercial finite element method solver for electromagnetic structures from Ansoft Corporation. The acronym originally stood for **h**igh **f**requency **s**tructural **s**imulator. It is one of the most popular and powerful applications used for antenna design and the design of complex RF electronic circuit elements including filters, transmission lines, and packaging. It was originally developed by Professor Zoltan Cendes and his students at Carnegie Mellon University. Prof. Cendes and his brother Nicholas Cendes founded Ansoft and sold HFSS stand-alone under a 1989 marketing relationship with Hewlett-Packard, and bundled into Ansoft products. [**76**]

The power of HFSS (Version 12 the one we have) software comes from many research and development innovations, which have made i t the most widely used software for solving 3-D full-wave electromagnetic field simulations. The invention of tangential vector basis functions enabled the highly accurate finite element method for electromagnetic field solution. The transfinite element method allowed the 3-D finite element solution to couple to port solutions for fast and accurate multi-mode s-parameter extractions. Finally, the development of automatic mesh generation and adaptive refinement was a key innovation for reliable, repeatable and efficient results. [**77**]

B.2 Error Analysis

In order to have some reliability towards the simulator software used (HFSS) since we have a little differences between the simulated and experimental results we will introduce here a microstrip patch antenna that has been designed by a professional engineer and being perfectly implemented and analyzed

This microstrip patch antenna has been designed using HFSS simulation and it confirmed a resonance of 2.37 GHz with a return loss less than -10 dB, then the microstrip patch antenna was realized by photolithography. Figure 77 shows the realized microstrip patch antenna with a 3.5 mm SMA female connector compared with the HFSS model. The comparison of the numerical and experimental return loss is shown in Figure 78. Good agreement can be seen between HFSS and the measured results. [**78**]

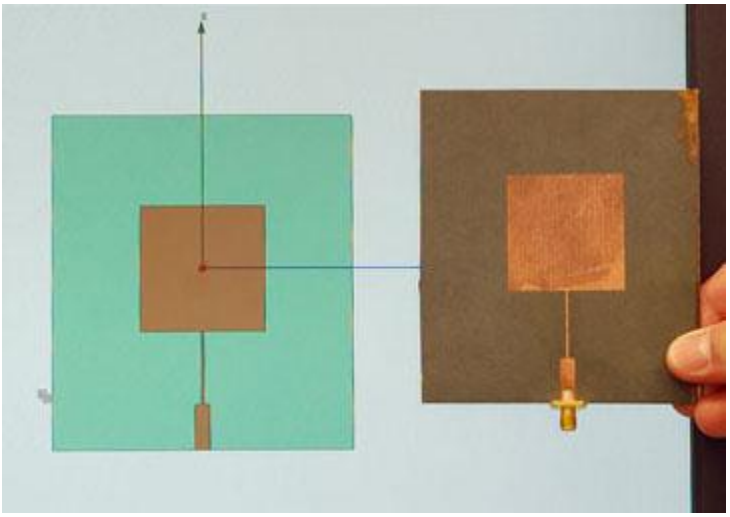

Figure 77: Microstrip patch antenna: Model versus Reality [78**]**

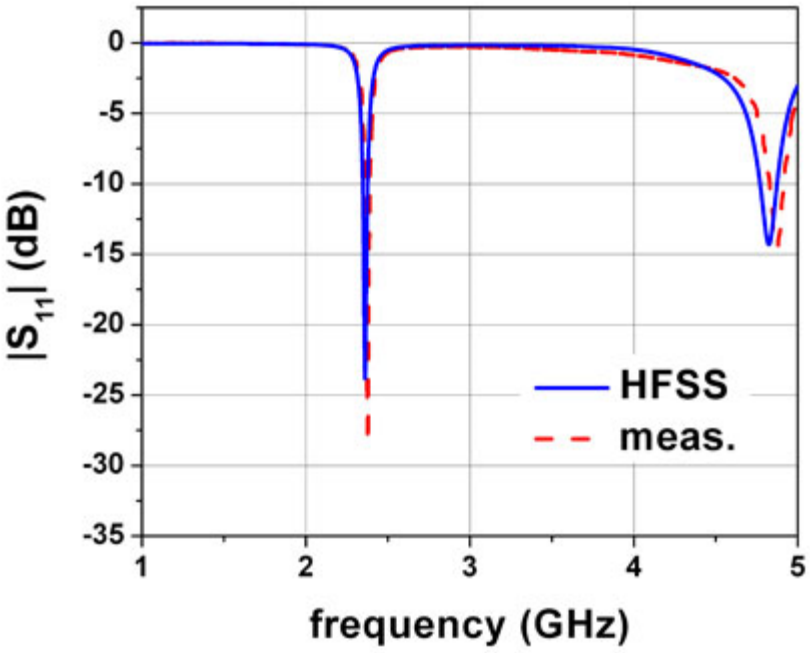

Figure 78: Return loss of the microstrip patch antenna [78]

B.3 Ansoft HFSS Tutorial: Dipole Antenna

This tutorial introduces the interface of Ansoft's HFSS, and walks the student through an example problem of creating, simulating and evaluating the response of a standard stripline structure. [**79**]

1. HFSS Interface

The main HFSS interface is shown in Figure 79, which illustrates the main components of the GUI (Graphical User Interface). They are summarized as follows:

• **3D Modeler Window** This is the area where you create the model geometry. This window consists of the model view area (or grid) and the history tree as shown in Figure

80. The history tree documents the actions that have been taken in the model view area, and provides an alternative way to select objects in the model view area.

• **Project Manager with Project Tree** The project manager window displays details about all open HFSS projects. Each project ultimately includes a geometric model, its boundary conditions and material assignments, and field solution and post processing information. An expanded view of the project manager is shown in Figure 81.

• **Properties Window** The properties window consists of two tabs. The command tab displays information about an action selected in the history tree that was performed to either create an object or modify an object. The attribute tab displays information about the material and display properties of a selected object.

• **Progress Window** This window is used when a simulation is running to monitor the solution's progress.

• **Message Manager** This window displays messages associated with a project's development (such as error messages about the design's setup)

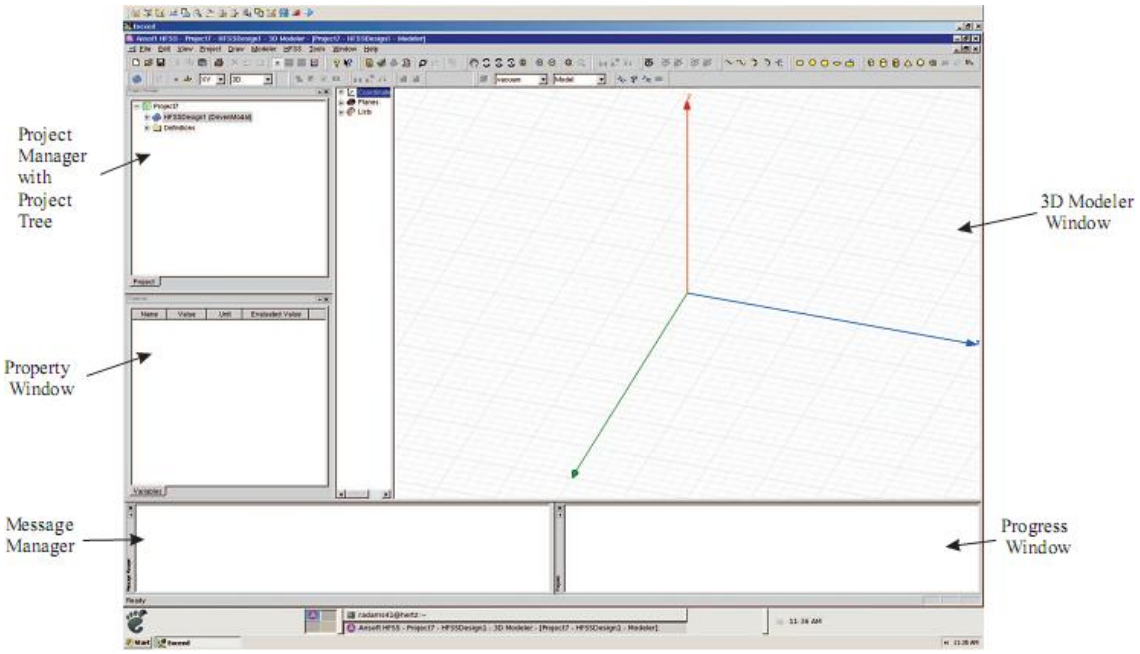

Figure 79: Main screen of HFSS.

2. *Setting up HFSS*

Before you can use HFSS for the first time, there are a couple of items that need to be configured for efficient and accurate operation.

1. On the Tools menu, select Options => General Options, click the Default Units tab and ensure that Length is set to mm. Click OK.

2. On the Tools menu, select Options => HFSS Options..., ensure the Include ferrite materials check box is checked. Click the Solver tab; set the number of Processors to 2 and Desired RAM Limit (MB) to 4000 (the Maximum RAM Limit (MB) should remain unchecked). Click OK. You should now be ready to use HFSS.

3. *Example: Dipole Antenna*

To begin to appreciate the functionality of this simulation tool, we will create and simulate a simple loop antenna. Before we can begin to work through the simulation though, we need to design the antenna on paper. This design will consist of a half-wave dipole antenna with center frequency of 300MHz. At this frequency, the wavelength in free-space is

$$\lambda = \frac{c}{f} = \frac{3*10^8}{300*10^6} = 1m$$

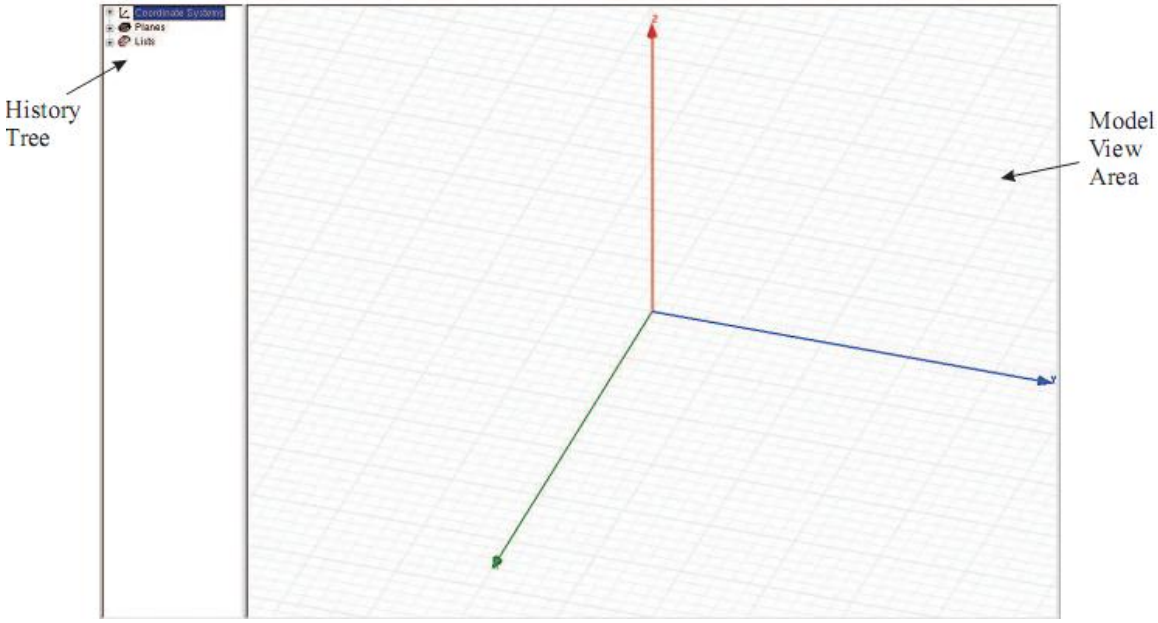

Figure 80: 3D Modeler Window, which consists of the model view area and the history tree

So, the total antenna length should be $\ell = \lambda/2 = 0.5$ m. Now, the only items remaining are the radius of the wires and the gap between the wires at the feed point. These items are difficult to determine analytically, so we will simply define them to be (r = 0.1 mm), and (g = 20 mm). With these choices, we expect to have an omnidirectional pattern in the far field.

3.1 Creating the Antenna

Now it's time to build this model in HFSS. We'll begin with the radiating structure itself. To do so, we'll create a series of cylindrical shapes by selecting Draw => cylinder in the file menu. To make the cylinder the correct size, you can either

1. Input the x, y, z coordinates of the center point, radius and height of the cylinder into the appropriate fields at the bottom of the 3D model window, or

2. Click randomly in the 3D model window three times to create a cylinder and edit the size in the properties box. To do this, click the command tab in the properties box and input the correct center point, radius and height for our cylinder.

For this design, we'll choose the center point to be placed at the location 0,0,10 mm, the radius should equal 0.1mm and the height should be 240mm. Next, we'll create the other half of the radiating element. This will be another cylinder with center point at 0,0,-10 mm, radius 0.1mm and height of -0.240mm.

Next we need to create the feed structure. To do so, we need to create two more cylinders, and two spheres. The cylinders will occur in the zx–plane, so we need to change the desired plane accordingly in the pull-down menu. Then, we create two cylinders,

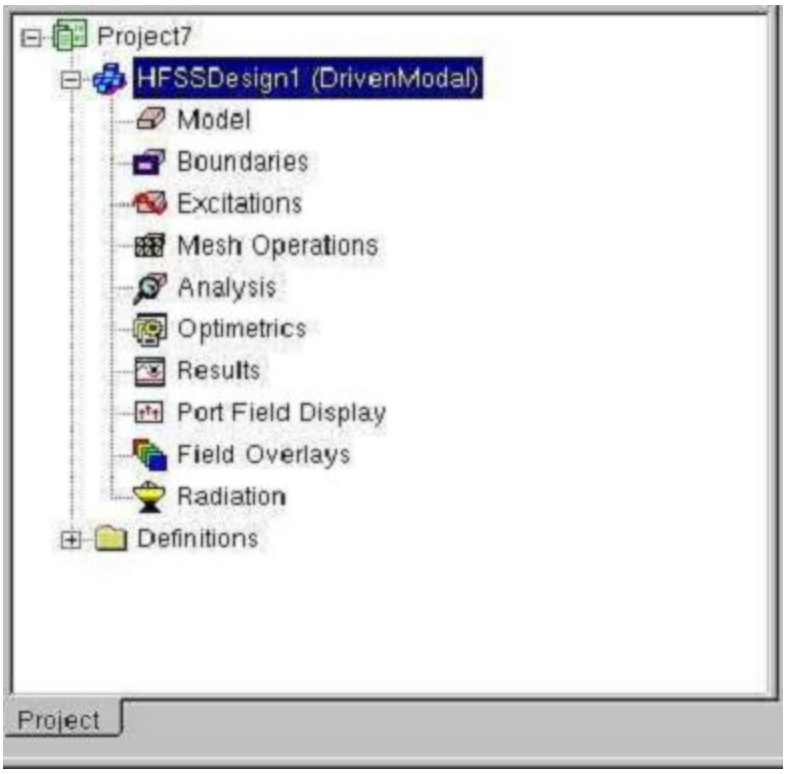

Figure 81: Project Manager Window illustrating the boundary conditions, excitation, etc. of the current model

• The first with center at 0,0,10 mm, radius = 0.1mm, and height = 250mm

• The second with center at 0,0,-10 mm, radius = 0.1mm, and height = 250mm

Now, we have an incomplete connection between the feed wires and the radiating wires. To complete this connection, we'll add two spheres at the junction.

• The first with center at 0,0,10 mm, and radius = 0.1mm

• The second with center at 0,0,-10 mm, and radius = 0.1mm

Now select all items that you have drawn so far and select Modeler => Boolean => Unite.

Finally we will identify the resulting geometry as a perfect electric conductor (PEC) by right clicking in the geometry window and selecting Assign Material. In the resulting window, select PEC and click OK.

3.2 Creating the radiation box

Now, we need to establish a box around the antenna in which we will compute the fields, and from which we will calculate the far-field response. To assure good far-field calculations, the box should extend at least $\lambda/4$ away from all radiating surfaces. We will choose the box to be centered on the antenna and $\lambda/2$ wide, so that all surfaces are at an adequate distance from the antenna.

To draw the radiation box, select Draw => box and input the following parameters for the box:

• Beginning point: -250mm, -250mm, -510mm

• The Cartesian sizes are: X size = 500mm, Y size = 500mm, and Z size = 1020mm

Now select the attribute tab and do the following:

• Ensure that the material is vacuum. If it is not, click the button next to material and select vacuum as the material.

• Click the button next to transparent and set the transparency to 0.95.

Now, the model is complete.

3.3 Boundary Conditions

The following items need to be setup to assure a good simulation:

1. Mesh Operations: To ensure we receive a good quality far field calculation, we need to ensure that the mesh is generated with sufficient accuracy on the outer boundary of the domain. According to Ansoft, we can achieve sufficient accuracy if the following rules of thumb are followed:

(a) The outer boundary must be at least $\lambda/4$ away from every radiating surface

(b) The mesh length must be constrained to be no greater than $\lambda/6$ on the boundary

The wavelength at 300 MHz in free space is $\lambda = 1$m, so the maximum length of elements on the boundary is $\ell max = 0.16$m.

To limit the mesh to this value, perform the following steps:

(a) Highlight the vacuum box

(b) Right click in the 3D modeler window and select Assign Mesh Operation => On Selection => Length Based

(c) Set the maximum length of elements to 160mm

(d) Click OK

2. Radiation Boundary: To compute the radiated fields, we need to establish a radiation boundary on all surfaces of the vacuum box. Do this, we right click in the drawing window and click select faces. Then, click on each face of the vacuum box while holding

the control key. Once all faces are selected, right click again in the drawing window and click assign boundary => Radiation.... Use all defaults on this boundary.

3. Far Field Calculation: To compute the radiated fields in the far-field, we need to tell HFSS what level of granularity we want on the far-field sphere. To do so, right-click radiation in the project tree and select Insert Far Field Setup => infinite sphere; use the defaults for this sphere.

3.4 Excitations

We will create a "WavePort" excitation at the feed lines of the antenna. To do so, we perform the following steps:

1. Create a rectangle in the zx-plane with first point (-25mm, 250mm, -24.85mm) and axis = Y, X size = 50mm, Z size = 50mm

2. Select the resulting rectangle

3. Right-click in the 3D modeler window and select Assign Excitation => Wave Port.

4. Click Next

5. Under "Integration Line," click the word None, and select New Line...

6. In the 3D modeler window, click the center of the bottom wire

7. Click the center of the top wire

8. Click Next

9. Click Finish

3.5 Analysis

Perform the following steps to set up the analysis options:

1. Right click on Analysis in the Project Tree, and select “Add Solution Setup”

2. Under the General tab:

(a) Set the solution frequency to 300 MHz

(b) Set the maximum number of passes to 30

(c) Set maximum Delta S to 0.01

3. Under the Options tab:

(a) Set the Maximum Refinement per pass to 20 %

(b) Set the Order of Basis Functions to First Order

4. Under the Advanced Tab, check the box titled Use Radiation Boundary on Ports

5. Click OK

Perform the following steps to set up a frequency sweep (if desired):

1. Under the Analysis item in the Project Tree, right-click on Setup1

2. Select Add Frequency Sweep...3. Set start frequency to 20 MHz

4. Set stop frequency to 300 MHz

5. Set step size to 20 MHz

6. Click OK

3.6 Final Checks and Running the Simulation

Select HFSS => Validation Check... to ensure the project is prepared for simulation (click close).

Save the project by clicking on the save icon at the top of the screen. Right-click setup1 under Analysis in the project tree, select Analyze to begin the simulation. At this point the progress window should show the progress of the simulation, beginning with the mesh generation.

3.7 Simulation Results

To view the far-field results of the simulation, perform the following steps:

1. Right click on the results item in the Project Tree

2. Click Create Far-Fields Report => 3D Polar Plot

3. Under the trace tab, select Gain

4. Add trace by clicking the Add Trace button

5. Click Close

To view the impedance results of the simulation, perform the following steps:

1. Right click on the results item in the Project Tree

2. Click Create Modal Solution Data Report => Rectangular Plot

3. Under the trace tab, select Z-Parameter, Z(1,1), highlight re and im with the control key

4. Add traces by clicking the Add Trace button

5. Click Close

Bibliography

[1] Kevin Peter. Analysis and Comparison of 1G , 2G , 3G ,4G and 5G Telecom Services. [Online]. http://hubpages.com/hub/3G-and-4G-Mobile-Services

[2] ITU. (2002) Mobile cellular, subscribers per 100 people. [Online]. http://www.itu.int/ITU-D/ict/statistics/at_glance/cellular02.pdf

[3] Y., Jeong, B.J., Chung, J., Hwang, C., Ryu, J.S., Kim, K., Kim, Y.K. Kim, "Beyond 3G: Vision, Requirements, and Enabling Technologies," pp. 120-124, March 2003.

[4] 2G – 3G Cellular Wireless data transport terminology. [Online]. www.arcelect.com/2G-3G_Cellular_Wireless.htm

[5] Mohammad S. Sharawi, "RF Planning and Optimization for LTE Networks," in *Evolved Cellular Network Planning and Optimization for UMTS and LTE*, Lingyang Song Jia Shen, Ed.: CRC Press, To appear 2010, ch. 11, pp. 399-432.

[6] Vasco Pereira and Tiago Sousa, "Evolution of Mobile Communications: from 1G to 4G," Department of Informatics Engineering of the University of Coimbra,.

[7] Christian Papassarandis, "Introduction to LTE," in *LTE Workshop*, KFUPM, Dhahran, 2010.

[8] NOKIA. LTE - Delivering the optimal upgrade path for 3G networks. [Online]. http://www.nokia.com/NOKIA_COM_1/Press/Press_Events/Nokia_Technology_Media_Briefing/LTE_Press_Backgrounder.pdf

[9] Motorola. TECHNICAL WHITE PAPER: Long Term Evolution (LTE): A Technical Overview. [Online]. www.motorola.com/lte

[10] J. B. Andersen, J. P. Kermoal and P. Mogensen K. I. Pedersen, "A Stochastic Multiple-Input-Multiple-Output Radio Channel Model for Evaluation of Space-Time Coding Algorithms," *Proceedings of IEEE Vehicular Technology Conference*, pp. 893-897, 2000.

[11] Ko S. C. K. and Murch D., "Compact Integrated Diversity Antenna for Wireless Communications," *IEEE Transaction on Antennas and Propagation Letters*, vol. 9, pp. 954-960, June 2001.

[12] Paul Hallbjörner, "Antennas, The Significance of Radiation Efficiencies When Using S-Parameters to Calculate the Received Signal Correlation From Two," *IEEE ANTENNAS AND WIRELESS PROPAGATION LETTERS*, vol. 4, pp. 97-99, 2005.

[13] Salonen I. and Vainikainen P., "Estimation of Signal Correlation in Antenna Arrays," *Proc. JINA Int. Symp. Antennas*, vol. 2, pp. 383-386, Nov 2002.

[14] J. Romeu, and I. Corbella S. Blanch, "Exact representation of antenna system diversity performance from input parameter description," *IEE Electron. Lett*, vol. 39, no. 9, pp. 705–707, May 1 2003.

[15] V. Plicanic, T. Bolin, G. Kristensson, and A. Derneryd Z. Ying, "Characterization of multi-channel antenna performance for mobile terminal by using near field and far field parameters," *presented at the COST 273 TD(04)(095)*, June 7–9 2004.

[16] D. M. Pozar, "Microwave Engineering," *Addison Wesley*, pp. 220-226, 1990.

[17] D. M. Pozar, "Microwave Engineering," *Addison Wesley*, pp. 228-230, 1990.

[18] Wikipedia. [Online]. http://en.wikipedia.org/wiki/700_MHz_wireless_spectrum_auction

[19] Constantine A Balanis, *Antenna theory-Analysis and Design*, 2nd ed.: John Wiley & Sons Ltd, 1997.

[20] S Taylor., J Simkin, J M Oakley., C Emson and M J Lancaster H Y Wang, "SIMULATION OF MICROSTRIP SMALL ANTENNAS ," *Vector Fields Limited*.

[21] Alok Singh, Amit Kumar Singh, Sandeep Kumar, Triloki Kumar O P N Calla, "Empirical Relation for Designing the Meander Line Antenna," in *International Centre for Radio Science, Jodhpur-342003, Shobhit Institute of Engg & Technology*, Meerut, 2008.

[22] I. A. Salamat, M. F. Abdul Kadir, M. R. Che Rose, M. S. R. Mohd Shah, D. Misman, "The Effect of Conductor Line to Meander Line Antenna Design," in *ASIA-Pacific Conference on Applied Electromagnetic Proceedings*, 2007.

[23] Randy Bancroft, "Fundamental Dimension Limits of Antennas," Westminster, Colorado, White paper, Centurion Wireless Technologies.

[24] Hing Kiu Kan and Rod B. Waterhouse, "Shorted Spiral-Like Printed Antennas," *IEEE TRANSACTIONS ON ANTENNAS AND PROPAGATION*, vol. 50, no. 3,

March 2002.

[25] Rod B. Waterhouse, "Small microstrip patch antenna," *Electron. Lett.*, vol. 31, pp. 604-605, April 1995.

[26] Y. Hwang, E. K. W. Lam, and B. Lee T. K. Lo, "Miniature aperture coupled microstrip antenna of very high permittivity," *Electron. Lett.*, vol. 33, pp. 9-10, Jan 1997.

[27] K.-L. Wong and Y. F. Lin, "Small broadband rectangular microstrip antenna with chip-resistor loading," *Electron. Lett.*, vol. 33, pp. 1593–1594, Sept 1997.

[28] H. K. Kan and R. B. Waterhouse, "Size reduction technique for shorted patches," *Electron. Lett.*, vol. 35, pp. 948–949, June 1999.

[29] D. J. Kim and Y. M. Moon K. S. Min, "Improved MIMO Antenna by Mutual Coupling Suppression between Elements," *Proceedings of the IEEE European Conference on Wireless Technology*, pp. 125-128, 2005.

[30] K. L. Wong, *Planar Antennas for Wireless Communications*.: Wiley, 2003.

[31] P. S. Hall, and D. Wake Z. D. Liu, "Dual-frequency planar inverted F antenna," *IEEE Trans. Antennas Propagat*, vol. 45, pp. 1451-1458, Oct 1997.

[32] C. R. Rowell and R. D. Murch, "A compact PIFA suitable for dual-frequency 900/1800-MHz operation," *IEEE Trans. Antennas Propagation*, vol. 46, pp. 596-598, April 1998.

[33] F. R. Hsiao and K. L. Wong, "A shorted patch antenna with an L-shaped ground plane for internal mobile handset antenna," *Microwave Opt. Technol. Lett.*, vol. 33, pp. 314-316, May 2002.

[34] Ansoft Corporation, "HFSS Online Help," V. 9.2,.

[35] Freescale Semiconductor. (2006, July) Compact Integrated Antennas Application Note.

[36] R., Bhartia, P., Bahl, I. Garg, *Microstrip Antenna Design Handbook*.: Artech House, Inc, 2001.

[37] G., and Ray, K.P. Kumar, *Broadband Microstrip Antennas*.: Artech House, Inc, 2003.

[38] B. R. Waterhouse, *Microstrip Patch Antennas: A Designer's Guide*.: Kluwer Academic Publishers, 2003.

[39] P. S. Nakar, *Design of a compact Microstrip Patch Antenna for use in Wireless/Cellular Devices*.: Masters Thesis report, 2004.

[40] Frank M. Caimi. (2002) SkyCross, Inc.

[41] Z. Du, Q. Wang and K. Gong F. Wang, "Enhanced-bandwidth PIFA with T-shaped ground plane," *Electronic Letters*, vol. 40, no. 23, pp. 1504 – 1505, Nov 2004.

[42] J. Hoon and H. Choi B. Kim, "Small wideband PIFA for mobile phones at 1800

MHz," , vol. 1, May 2004, pp. 27-29.

[43] H.A. Wheeler, "Fundamental Limits of Small Antennas," *Proceedings of The I.R.E. (IEEE)*, pp. 1479-1484, Dec. 1947.

[44] L. J. Chu, "Physical Limitations of Omni-Directional Antennas," *Journal of Applied Physics*, vol. 19, pp. 1163-1175, Dec. 1948.

[45] R.C. Hansen, "Fundamental Limitations in Antennas," *Proceedings of the IEEE*, vol. 69, no. 2, pp. 170-182, Feb 1982.

[46] A. Henderson, K. Hirasawa and J.R. James K. Fujimoto, *Small Antennas*.: John Wiley & Sons Inc., 1987.

[47] J. McLean, "A Re-Examination of the Fundamental Limits on the Radiation Q of Electrically Small Antennas," *IEEE Transactions on Antennas and Propagation*, vol. 44, no. 5, pp. 672-675, May 1996.

[48] H. Wheeler, "Small Antennas," in *Antenna Engineering Handbook*, R. Johnson, Ed., 1993, ch. 6.

[49] Sumeet Sandhu. [Online]. http://www.comsoc.org/oeb/Past Presentations/Sumeet June04.pdf

[50] I. E. Telatar, "Capacity of Multi-Antenna Gaussian Channels," *European Transactions on Telecommunications*, vol. 10, pp. 585–595, 1999.

[51] S. Al-Ghadhban, "Multi-Layered Space Frequency Time Codes," Virginia Polytechnic Institute and State University, Virginia, USA, PhD thesis Nov. 2005.

[52] J. Salz, "Digital transmission over cross-coupled linear channels," *At&T Technical Journal*, vol. 64, no. 6, pp. 1147-1159, July-August 1985.

[53] O. Alamri,M. El-Hajjar, andN.Wu L.Hanzo, *Near-CapacityMulti-Functional MIMO Systems*. UK: Wiley Press, 2009.

[54] "Applications of Antenna Arrays to Mobile Communications Part I: Performance Improvement, Feasibility, and System Considerations," *Proceedings of the IEEE*, vol. 85, pp. 1029–1030, July 1997.

[55] L. Godara, "Application of Antenna Arrays toMobile Communications. Part II. Beam-Forming and Direction-of-Arrival Considerations," *Proceedings of the IEEE*, vol. 85, pp. 1195–1245, Aug 1997.

[56] Christian Wolff. Phased Array Antenna. [Online]. http://www.radartutorial.eu/06.antennas/an14.en.html#this

[57] J. Litva and T. K. Lo, *Digital Beamforming in Wireless Communications*. Boston, London: Artech House Publishers, 1996.

[58] T. Haynes, "A Primer on Digital Beamforming," *Spectrum Signal Processing*, March 1998.

[59] T. H. Ismail and M. M. Dawoud, "Null Steering in Phased Arrays by Controlling the

Element Positions," *lEEE Transactions on Antenna and Propagation,* vol. AP-39, no. 11, pp. 1561-1566, Nov 1991.

[60] M. M. Dawoud T. H. Ismail, ""Experimental Verificatoin of Null Steering by Element Position Perturbations," *IEEE Transactions on Antennas and Propagation*, vol. AP40, no. 11, pp. 1431-1434, Nov 1992.

[61] M. M. Dawoud, A. P. Anderson A. Tennant, "Array Pattem Nulling by Element Position Perturbation using a Genetic Algorithm," *Electronic Letters*, vol. 30, no. 3, pp. 174-176, February 1994.

[62] M. M. Dawoud, "Null Steering in Scanned Linear Arrays by Element Position Perturbations," *International Journal of Electronics*, vol. 78, no. 4, pp. 743-757, 1995.

[63] M. J. Mismar and T. H. Ismail, "Null Steering using Minimax Approximation by controlling only the Current Amplitudes," *International Journal of Electronics,* vol. 78, no. 2, pp. 409-415, February 1995.

[64] W. P. Liao and F. L. Chu, "Null Steering in Planar Arrays by controliing only Current Amplitudes using Genetic Algorithms," *Microwave and Optical Technology Letters*, pp. 97-103, 1997.

[65] W. P. Liao and F. L. Chu, "Application of Genetic Algorithms to Phase only Null Steering of Linear Arrays," *Electromagnetics,* pp. 171-183, 1997.

[66] T. H. lsmail and M. J. Mismer, "Null Steering with Arbitmy Phase Perturbations using Dual Phase Shiffers," *Journal of EIectromagnetic Woes and Applications*, vol. 13, no. 8, pp. 1021-1029, 1999.

[67] H. Steyskal, "Simple Method for Pattern Nulling by Phase Perturbations," *IEEE Transactions on Antennas and Propagation*, vol. AP-31, pp. 163-166, January 1983.

[68] L. Zheng and D. N. C. Tse., "Diversity and multiplexing: A fundamental tradeoff in multiple antenna channels," *IEEE Transactions on Information Theory*, vol. 49, pp. 1073–1096, May 2003.

[69] V. Erceg, D. Gesbert, and R. W. Heath Jr. S. Catreux, "Adaptive modulation and MIMO coding for broadband wireless data networks," *IEEE Communications Magazine*, vol. 40, no. 6, pp. 108-115, June 2002.

[70] V.V. Swarte,. Dehli: New Age International Limited, 1993, Reprint-2006, pp. 396, 397.

[71] Arto Hujanen, and Paivi K. Koivisto Johan C.—E. Sten, "Quality Factor of an Electrically Small Antenna Radiating Close to a Conducting Plane," *IEEE Transactions on Antennas and Propagation*, vol. 49, no. 5, p. 829—837, May 2001.

[72] Roger F. Harrington, "Effect of Antenna Size on Gain, Bandwidth, and Efficiency," *Journal of Research of the National Bureau of Standards—D, Radio Propagation*, vol. 64D, no. 1, p. 1—12, January-February 1960.

[73] TACONIC. FR4 Processing Guide, Synthane-Taylor Laminates.

[74] N. Hercovici, "CAD of aperture coupled microstrip transmission lines and antennas: software and user's manual," Artech House, 1996.

[75] COE Department in UTAH University. Calibration and S-parameter Measurements with the Network Analyzer. [Online]. http://www.coe.utah.edu/~cfurse/Tutorials/hp8510c/network%20analyzer.html

[76] Q&A With Zoltan Cendes, Founder, Chairman, And CTO Of Ansoft Corporation, By Jim Pomager, Editor in Chief, RF Global Net.

[77] Director, Ansoft Product Management, ANSYS, Inc. By Larry Williams. (2009) ANSYS Advantage. [Online]. http://www.ansys.com/magazine/issues/vol4-iss1-2010/hfss.pdf

[78] EM Talk. [Online]. http://www.emtalk.com/mwt_mpa.htm

[79] Dr. Ryan S. Adams. (2009, September 8) Ansoft HFSS Tutorial: Dipole Antenna.

Vitae

NAME: Yanal Shaher Al-Faouri

BIRTH: 13th July, Amman, JORDAN

EDUCATION: BACHELOR OF ENGINEERING (BSc)

Electrical Engineering,

University of Jordan,

Amman, JORDAN.

MASTER OF SCIENCE IN ELECTRICAL ENGINEERING

Department of Electrical Engineering

King Fahd University of Petroleum & Minerals

Dhahran, K.S.A.

CONTACT: y_faouri@yahoo.com